

Image-based Condition Assessment for Concrete Bridge Inspection

Ram Sebak Adhikari

A Thesis

In The Department of Building, Civil, and Environmental Engineering

Presented in Partial Fulfillment of the Requirements for the Degree of Doctor of

Philosophy at Concordia University

Montreal, Quebec, Canada

July 2014

© Ram Sebak Adhikari, 2014

CONCORDIA UNIVERSITY
SCHOOL OF GRADUATE STUDIES

This is to certify that the thesis prepared

By: Ram Sebak Adhikari

Entitled: Image-based Condition Assessment for Concrete Bridge
Inspection

and submitted in partial fulfillment of the requirements for the degree of

DOCTOR OF PHILOSOPHY

complies with the regulations of the university and meets the accepted standards with respect to originality and quality.

Signed by the final examining committee:

| | |
|-------------------------------|---------------------|
| <u>Dr. W. Fang Xie</u> | Chair |
| <u>Dr. Simaan M. AbouRizk</u> | External Examiner |
| <u>Dr. Amin Hammad</u> | External to Program |
| <u>Dr. Khaled E. Galal</u> | Examiner |
| <u>Dr. Tarek Zayed</u> | Examiner |
| <u>Dr. Osama Moselhi</u> | Thesis Supervisor |
| <u>Dr. Ashutosh Bagchi</u> | Thesis Supervisor |

Approved by _____
Chair of Department or Graduate Program Director

_____ 2014 _____

Dean of Faculty

Abstract

Image-based Condition Assessment for Concrete Bridge Inspection

Ram Sebak Adhikari, Ph.D.

Concordia University, 2014

The following approaches are usually taken for the condition assessment and performance evaluation of civil infrastructure: visual inspection, structural response measurement due to loads, and sensing based inspection of bridge structures. This thesis concentrates on the last alternative using remote sensing for condition assessment of concrete bridge structures. Focusing on defect quantification problems for condition assessment of bridge structures, remote sensing techniques based on digital images provides superior result over conventional visual inspection-based methods. The aim of this thesis is to develop digital image-based condition assessment tools and techniques, which can be integrated with existing bridge management systems (BMSs) in order to enhance the reliability of current inspection practices.

The methodology of this research divides the entire task of bridge inspection into two modules. The first module develops quantification models based on the extent and severity of defects, and the second module develops a change detection model defined as change in element condition state over times. For defect quantification, three fundamental concrete defects such as cracks, spalling, and scaling have been considered. To illustrate the proposed methodology, digital images are acquired from laboratory experiments during the testing of reinforced concrete beams in flexure, and from field visits of bridges in Montreal,

Quebec using portable digital cameras. This research contributes in the development of crack quantification model based on the corresponding crack skeleton which takes consideration of crack tortuosity for retrieving of crack properties. The output of the crack quantification model is validated by capturing the crack properties using a crack scale. In addition, an automated model for estimating the condition rating and related computational algorithms for bridge inspection are developed using the guidelines of the Ontario Structure Inspection Manual. The developed algorithms for mapping of condition ratings are based on the supervised training of back propagation neural networks. Recognizing the importance of 3D visualization, which can mimic the on-site visual inspection, 3D visualization model is developed using ordinary digital images by manually projecting images on the 3D model of the bridge being inspected.

The second module proposes a novel approach for periodic detection of defects in concrete bridges based on a set of dimensionless metrics pertinent to spectral and fractal analyses of the captured images. The fractal analysis of digital images is described by fractal dimension (FD) using Box Counting algorithms. Similarly, the method of spectral analysis requires digital images to be translated from spatial domain to Fourier domain, and then finds one dimensional signatures to quantify change detection. The developed algorithm for change detection demonstrates superior results and eliminates the limitations of traditional approach of change detection based on image subtraction. The developed image-based models can either be applied as standalone condition assessment and rating applications or integrated with existing systems such as PONTIS (a Bridge Management System in USA) in order to enhance the reliability of visual inspection.

Acknowledgements

It is impossible to teach someone until a favorable teaching environment is available to someone's inner world where learning can happen automatically. Once a favorable learning cosmic space is available, it is sure that he/she will be near to experience success in no time. I heartily thank my supervisors: Dr. Osama Moselhi and Dr. Ashutosh Bagchi for helping me in catching up the abundant available cosmic energy where success is always going to flourish. I am indebted to my supervisors for such a precious gift in my life.

I thank for valuable comments and information about condition of bridges in Quebec provided by Mr. Adel Zaki, Chief Engineer (Roads and Bridges), SNC Lavalin Inc., and special thanks to Dr. Arash Rahmatian for providing me access to acquire digital images from flexural tests of reinforced concrete beams. I would also like to thank Concordia University in Montreal and Natural Sciences and Engineering Research Council of Canada (NSERC) for financial support during my research.

Special thanks to my parents: Sitaram and Lakho Devi, my wife: Mamata, and my son: Lance for helping me during my difficult times just saying a simple sentence "you can do it, and just do it".

Table of Contents

| | |
|--|----------|
| Chapter 1: Introduction | 1 |
| 1.1 Overview | 1 |
| 1.2 Limitations of Current Practices for Condition Assessment of Bridges | 2 |
| 1.3 Motivation | 4 |
| 1.4 Scope and Objectives | 5 |
| 1.5 Thesis Organization..... | 7 |
| Chapter 2: Literature Review..... | 9 |
| 2.1 Introduction | 9 |
| 2.2 Remote Sensing..... | 11 |
| 2.2.1 Advanced Technologies | 11 |
| 2.2.2 Suitable Remote Sensing for Surface Defects Analysis..... | 14 |
| 2.3 Current Practices in Automated Bridge Condition Assessment..... | 21 |
| 2.3.1 Damage Evaluation | 22 |
| 2.3.2 Close Range Photogrammetry..... | 23 |
| 2.3.3 Digital images application for civil infrastructure | 24 |
| 2.3.4 Neural Networks Application for Civil Structures..... | 29 |
| 2.3.5 Automated crack detection using digital images..... | 31 |
| 2.3.6 3D Defects Modeling to Assist Visual Inspection | 33 |
| 2.4 Automated Bridge Management Systems | 34 |
| 2.4.1 Bridge Management Systems..... | 34 |
| 2.4.2 Element Condition rating | 41 |

| | |
|--|-----------|
| 2.4.3 Bridge Performance Indicators..... | 45 |
| 2.5 Digital Image Processing..... | 48 |
| 2.6 Measuring Shapes | 57 |
| 2.7 Summary | 60 |
| Chapter 3: Proposed Methodology..... | 61 |
| 3.1 Introduction | 61 |
| 3.2 Proposed Methodology | 61 |
| 3.3 Field and Lab Data Collection | 64 |
| 3.4 Digital image Processing..... | 69 |
| 3.4.1 Pre-processing | 69 |
| 3.4.2 Segmentation | 72 |
| 3.4.3 Morphology..... | 73 |
| 3.5 Data Processing and Condition Assessment | 74 |
| 3.5.1 Neural networks | 74 |
| 3.5.2 Spectral and Fractal Analysis..... | 76 |
| 3.6 Limitations | 79 |
| Chapter 4: Concrete Crack Analysis using Digital Images | 82 |
| 4.1 General | 82 |
| 4.2 Crack evaluation in Concrete Structures..... | 85 |
| 4.3 Proposed Method for Analysis of Cracks | 86 |
| 4.3.1 Imaging Criteria for Data Acquisition | 87 |
| 4.3.2 Image Stitching | 92 |
| 4.3.3 Discrete Crack Detection and Analysis..... | 93 |

| | |
|--|------------|
| 4.3.4 Skeletonization of cracks | 94 |
| 4.3.5 Crack Length and width | 95 |
| 4.3.6 Data Fitting for Crack Depth vs Crack Width..... | 103 |
| 4.4 3D Visualization and Crack Density..... | 109 |
| 4.5 Discussion | 112 |
| 4.6 Summary | 114 |
| Chapter 5: Image-based Automated Element Condition Rating | 115 |
| 5.1 Introduction | 115 |
| 5.2 Proposed Framework..... | 116 |
| 5.2.1 Feature Extraction | 119 |
| 5.2.2 Artificial Neural networks (ANN) | 123 |
| 5.3 Data Analysis and results | 125 |
| 5.3.1 Check for Normal Distribution | 126 |
| 5.3.2 BPNN Models | 127 |
| 5.3.3 Training and validating of the BPNN | 129 |
| 5.3.4 Comparison with other classifiers | 134 |
| 5.3.5 Element Condition Index | 137 |
| 5.4 Summary | 142 |
| Chapter 6: A Study of Defect Propagation..... | 144 |
| 6.1 General | 144 |
| 6.2 Periodic Detection of Defects | 145 |
| 6.3 Fractal Damage Characteristics..... | 145 |
| 6.4 Methodology | 147 |

| | |
|---|------------|
| 6.4.1 The Fractal Analysis of digital images..... | 148 |
| 6.4.2 Computation of Fractal Dimension..... | 149 |
| 6.5 Spectral Analysis..... | 155 |
| 6.6 Analysis and Results..... | 158 |
| 6.6.1 Analysis for isolated cracks..... | 159 |
| 6.6.2 Analysis for crack patterns..... | 163 |
| 6.6.3 Comparison with manually segmented images..... | 170 |
| 6.6.4 Median Filter for Temporal Change Detection..... | 173 |
| 6.7 Summary..... | 175 |
| Chapter 7: Conclusions and Future Work..... | 177 |
| 7.1 Conclusions..... | 177 |
| 7.2 Contributions..... | 180 |
| 7.3 Limitations of the Current Research and Scope for Future Studies..... | 182 |
| References..... | 187 |
| Appendix A..... | 208 |
| Appendix B..... | 209 |
| Appendix C..... | 213 |
| Appendix D..... | 216 |

List of Figures

Chapter 2

| | |
|--|----|
| Figure 2.1: Electro-magnetic Spectrum relation with Energy and Wavelengths..... | 12 |
| Figure 2.2: Spatial Resolution Accuracy and Object Size (Luhmann et al. 2006) | 14 |
| Figure 2.4: The Important Bridge Defects (Norwegian graphic symbols) | 17 |
| Figure 2.5: (a) Spall area < 10 square inches (left); and > 100 square inches (right)..... | 18 |
| Figure 2.6: Successful technologies for Bridge Deck Analysis (Ahlborn et al., 2010) | 21 |
| Figure 2-7: Feature attributes of a defect (Moselhi and Shehab-Eldeen 2000) | 30 |
| Figure 2-8: Photo Visualization in the OBMS (Ontario-BMS, 2012) | 38 |
| Figure 2.9: A Well Composed Digital Images (Navy Bridge, 2008) | 39 |
| Figure 2.10: A Well Composed Digital Image showing the Underside of a Bridge | 40 |
| Figure 2.11: A Poorly Composed Digital Image, No scale for reference, location | 41 |
| Figure 2.12: Current Condition Rating Scale for Reinforced Concrete Decks..... | 42 |
| Figure 2.13: (a) Condition States 2, (b) Condition States 3, and (c) Condition States 4.. | 44 |
| Figure 2.14: (a) Condition States 2, (b) Condition States 3, and (c) Condition States 4.. | 44 |
| Figure 2.15: Bridge Performance Framework | 45 |
| Figure 2.17: (a) A Mask for Point Detection | 50 |
| Figure 2.18: (a) A Mask for Line Detection a) Horizontal, b) + 45 Degrees | 51 |
| Figure 2.20: Sobel Edge Operators (Horizontal & Vertical) | 52 |
| Figure 2.21: Laplacian of Gaussian (LoG) Mask | 53 |
| Figure 2.22: Hough Transform a line AB to A Point “P” | 55 |
| Figure 2.24: Shape Descriptors (F. B. Neal & J. C. Russ, Measuring Shape)..... | 59 |

Chapter 3

| | |
|---|----|
| Figure 3.1: Research Methodology..... | 62 |
| Figure 3.2 : The structure of the proposed Framework | 63 |
| Figure 3.3: The location of Bridge Site for Field Demonstration..... | 65 |
| Figure 3.4: The Elevation of a Bridge Overpass..... | 66 |
| Figure 3.5: Images form Lab Observations | 67 |
| Figure 3.6: Cameras used in for Image Acquisition | 68 |
| Figure 3.7: Artificial Target in the image Frame | 69 |
| Figure 3.8: Image pre-processing techniques | 70 |
| Figure 3.9: Effect of perspective projection model (Solomon & Breckon, 2011)..... | 71 |
| Figure 3.10: Corrected Image form Perspective Error..... | 71 |
| Figure 3.11: Image Segmentation Algorithms (Gonzalez et al., 2009). | 72 |
| Figure 3.12: Combining Erosion and Dilation Processes | 74 |
| Figure 3.13: Neural Network Model for Condition Assessment | 76 |
| Figure 3. 14: Spectral Analysis of Digital Images (Adhikari et al. 2013a). | 78 |
| Figure 3. 15: Fractal Analysis of Digital Images (Adhikari et al. 2013d). | 78 |

Chapter 4

| | |
|--|----|
| Figure 4.1: Proposed Method for Analysis of Cracks..... | 87 |
| Figure 4.3: Projective Transform Work Flow..... | 91 |
| Figure 4.4: Image after Projective Transformation (corrected Image)..... | 91 |
| Figure 4.5: Crack Detection Algorithm | 94 |
| Figure 4.6: Original crack image, (a) Crack Detection..... | 96 |

| | |
|---|-----|
| Figure 4.7: Experimental setup for beam loading under fatigue loads | 97 |
| Figure 4.8: Use of Crack Scale for Width Measurement..... | 99 |
| Figure 4.9: Plot of Cumulative Crack Depth and width | 102 |
| Figure 4.10: Neural network Training Flow Chart..... | 104 |
| Figure 4.11: Data Fitting by Neural Networks | 105 |
| Figure 4.12: Error in Training, Validation, and Test Sets | 105 |
| Figure 4.13: Performance Evaluation of Trained Networks..... | 107 |
| Figure 4.14: Comparison with Boosted Decision Tree..... | 107 |
| Figure 4.15(c): 3D visualization, Front Face Crack Density = 0.0066 mm/mm ²)..... | 111 |
| Chapter 5 | |
| Figure 5.1: The Proposed Methodology | 117 |
| Figure 5.3: Artificial Target..... | 119 |
| Figure 5. 4: Attributes Feature Extraction | 120 |
| Figure 5.5 (a): Scaling Defects region of Interest..... | 121 |
| Figure 5. 6: RGB profile with line width of 1 Unit | 122 |
| Figure5. 7: RGB profile with line width of 30 Units..... | 122 |
| Figure 5.8: Scaling Depth Estimation from RGB Profile..... | 123 |
| Figure 5.9: Forward and backward pass for Back Propagation Algorithm | 125 |
| Figure 5.10: Check for Normal Distribution of input parameters | 126 |
| Figure 5.11: BPNN Models | 128 |
| Figure 5.12: Neural Network Modeling Process | 130 |
| Figure 5.13: Prediction of Actual Depth Vs Model Output..... | 133 |
| Figure 5.14: The Actual Condition State Rating Vs Model Output | 133 |

| | |
|--|-----|
| Figure 5.15: Out of Bag algorithms (Feature Importance factors) | 136 |
| Figure 5.16: Fly over pass at the intersection of street Selby and Greene | 137 |
| Figure 5.17: (a) Detection of the spalled area, (b) defects identified as an object..... | 139 |
| Chapter 6 | |
| Figure 6.1: Proposed Change Detection Algorithm..... | 148 |
| Figure 6.2: Box Counting Work Flow Diagram | 153 |
| Figure 6.4: Spectral Change Detection | 156 |
| Figure 6.5: Fourier Transform of Digital Images at Time T1..... | 156 |
| Figure 6.6: (a) Fourier Transform, Radial, and Angular Plot of Digital Images | 157 |
| Figure 6.8: Cracked Images at Different Loads..... | 160 |
| Figure 6-9: Estimation of Fractal Dimension | 161 |
| Figure 6.11: (a) Fractal images generated by Fractal Tree algorithms | 165 |
| Figure 6.12: Estimation of Fractal Dimension using Box Count Algorithms | 165 |
| Figure 6.13: Change Detection by Fractal Analysis of Concrete Surfaces..... | 166 |
| Figure 6.14: Experimented at different resolutions (Resolution 3.591 pixels/mm) | 167 |
| Figure 6.15: Experiments results of Fractal Images for Fractal Dimension | 168 |
| Figure 6.16: Change Detection by Crack Density | 168 |

List of Tables

| | |
|--|-----|
| Table 2.1: Satellites Spatial and Temporal Resolution (Roy, 2008)..... | 13 |
| Table 2-2: Defects Types in Reinforced Concrete Structures (FHWA, 2006)..... | 16 |
| Table 2.3: Rating based Theoretical Sensitivity for Measurement Technologies | 20 |
| Table 2.5: Current Condition Rating Scale for Reinforced Concrete Decks | 43 |
| Table 2.6: Bridge Condition Index (Ontario Bridges, 2013)..... | 48 |
| Table 4-1: Evaluation of Crack Width and Depth | 102 |
| Table 4.2: ACI 224R-01, 2008 Permissible crack width..... | 103 |
| Table 4.3: OSIM (2008), Crack Classification for Reinforced Concrete Structures | 103 |
| Table 5.2: Neural Networks design criteria | 130 |
| Table 5.4: Contribution factors for Model (a) and Contribution factors for Model (b).. | 131 |
| Table 5.5: Comparison of results from different classifiers..... | 136 |
| Table 5.6: Condition Assessment of a Deck Slab..... | 140 |
| Table 5.7: Evaluation of Bridge Condition Index..... | 141 |
| Table 6.1: Spectral and Fractal Analysis of digital images | 164 |
| Table 6.2: Change Detection based on Spectral Analysis and Fractal Analysis | 169 |
| Table 6.3: Change Analysis based on image registration | 172 |
| Table 6.5: Extraction of Descriptors from Spectral Analysis | 175 |

LIST OF ABBREVIATIONS

2D - Two Dimensional

3D - Three Dimensional

3DOBS - Three Dimensional Optical-evaluation Bridge System

AASHTO - American Association of State Highway and Transportation Officials

ACI - American Concrete Institute

ASCE - American Society of Civil Engineers

BIRM - Bridge Inspector's Reference Manual

BVRCS - Bridge Viewer Remote Camera System

DSS - Decision Support System

FEA - Finite Element Analysis

FFT - Fast Fourier Transform

FHWA - Federal Highway Administration

FOV - Field of View

GIS - Geographic Information System

GPR - Ground Penetrating Radio Detection and Ranging

GPS - Global Positioning System

IR - Infrared

LASER - Light Amplification by Stimulated Emission of Radiation

LiDAR - Light Detection and Ranging

LVDT - Linear Variable Differential Transformer

MTO - Ontario Ministry of Transportation

NBI - National Bridge Inventory

NCHRP - National Cooperative Highway Research Program

NDE - Non-destructive Evaluation

NDT - Non-destructive Testing

SAR - Synthetic Aperture Radar

SHM - Structural Health Monitoring

Thermal IR - Thermal Infrared Imagery

TIF - Tagged Image File

NTSB – National Transportation Safety Board

Chapter 1: Introduction

1.1 Overview

2013 report card published by American Society of Civil Engineers for America's Infrastructures reveals that the average age of bridges in the USA (i.e. 607,380) is 42 years and about 11% of the bridges are rated as structurally deficient (ASCE 2013). Likewise, in Canada, more than 40% of the bridges currently in use were built over 50 years ago, and they are in need of immediate upgrade (Bisby and Briglio 2004). To maintain the condition of such infrastructure, there exist different inspection programs for monitoring the conditions of a structure during its life span. However, the importance of bridge inspection was not fully understood until the collapse of I-35 W Mississippi River Bridge which was built in 1964. According to the investigation report of the National Transportation Safety Board (NTSB, 2008), the Mississippi River Bridge on I-35 was inspected a year before the catastrophic failure of the deck truss at 6.05 p.m. on August 2007. As a result of the collapse, 1000 ft of the 1,907 ft long bridge fell to the water, 13 people lost their lives, 145 people injured, and 111 vehicles were involved in the accident. In further investigation, the inspection report showed that the bridge was rated 4 out of 9 resulting in the continuation of the bridge operation without any load restriction. The tragic accident of the Mississippi River Bridge revealed that the condition of such deficient bridges could have been worse than what bridge inspectors had reported in inspection report. Such accidents drew serious attention towards proper inspection guidance's and technologies for accurately assessing the condition state of bridges for effective Bridge Management System (BMS) (National Transportation Safety Board, 2008).

In order to improve the effectiveness of a BMS, data collection and interpretation strategies need to be improved. In general, routine bridge inspection is carried out every two years to collect information on bridge conditions in the form of text, images, and drawings based on inspection manual guidelines (Navy Bridge Inspection Program, 2008). Routine inspections are generally carried out through visual inspection which is an arm's length inspection of all portions of structures using some fundamental measuring methods and tools. However, the reliability of visual inspection regarding consistency and objectivity of inspected data has been questioned in literature (Moore et al. 2001).

1.2 Limitations of Current Practices for Condition Assessment of Bridges

Although several satellites such as (LANDSAT TM, SPOT4, IRS, and RADARSAT) are capable of identifying objects lying on the Earth surfaces, the defect detection and quantification of civil infrastructure are not possible due to the limitations of spatial resolution, temporal resolution, radiometric resolution, swath width, and spectral bands (Roy, 2008). The commonly used non-destructive techniques for condition evaluation of concrete decks are visual inspection, liquid penetrant dye, chain drag, Half-cell potential (HP), acoustic emission, ultrasonic pulse velocity, ground penetrating radar (GPR), impact echo (IE), and IR thermography (Yehia et al. 2007). However, these technologies are unable to provide the desirable accuracy in terms of extent and severity of defects required for effective BMS. To prove this point, a systematic study for the condition assessment of concrete bridge decks through experimental and field testing was conducted using several

remote sensing technologies listed above (Ahlborn et al. 2010). The study showed that the Bridge Viewer Remote Camera System (BVRCS) technique based on the close range 3D photogrammetry technique, and GigaPan Techniques based on Street View-style photography are the best technologies for defect measurement in concrete decks (Ahlborn et al., 2010).

Previously, Abudayyeh et al. (2004) proposed a framework for automated bridge imaging system based on digital image processing and integrated with Bridge Management Systems (BMSs) PONTIS. However, the assignment of condition rating for bridge elements was done manually by displaying the collected images on computer screens. The current version of PONTIS 5.1.2 allows multi picture uploading just by selecting all images stored in a folder (AASHTOWare Bridge, 2012). The approach provides great advantages over old version where pictures were uploaded one at a time. However, these images are not used for defect quantification purposes. They are just kept for references or visual comparisons.

The New Zealand Office of the Auditor General (2010) addressed the need for improved data collection in order to adopt the advanced bridge asset management system. Since the current practices of data collection is based on visual inspections, the approaches are not providing consistent or reliable information, and often they are not able to detect critical problems in bridge components (Bush et al. 2012). Therefore, there is a need for integration of non-destructive evaluation (NDT) techniques with the data collection needed for bridge management system. The validation of NDT program for defects assessments requires

developing a laboratory based specimens with embedded defects obtained from decommissioned bridges. Such approach will enhance the reliability of NDT program for further applications.

1.3 Motivation

Civil infrastructure, especially bridges, plays an important role for economic development of a country. The bridges not performing as per current code requirements can threaten human lives. Thus, regular maintenance and proper rehabilitation actions are necessary in order to maintain the functionality of bridges in preventing sudden failures. In spite of regular inspection of De La Concorde overpass in Quebec, on September 20 (2006), the bridge collapsed leaving five people killed and six people wounded (Vaysburd & Benoit, 2007). The investigation done by Vaysburd and Benoit (2007) showed that the inspection reports of de la Concorde were not consistent. There was a misinterpretation of abutment definition of de la Concorde Bridge. Until 1999, the bridge was defined as single span bridge, but from 1999, the bridge was started to be called a three span bridge taking into consideration of the cantilevers on both sides. In another report, it was admitted that bridge defects were rarely sketched; the location and extent of distresses were almost never reported, and that prevented the accurate evaluation of the bridge condition assessment over time (Commission of Inquiry 2007). The failure of the bridge underscored the importance of tracking of critical bridge element during bridge inspection.

The current practices of bridge inspections, which are based on visual inspections, are not reliable in terms of data consistency, and information reliability; and they are often unable to detect critical problems in structural components (Bush et al. 2012). The analysis of a critical element requires the tracking of progression of a particular defect over time so that necessary actions can be performed before any emergency situation. The advancement of information technologies and their application in civil engineering have made possible to acquire such information digitally in order to track the conditions of bridge elements, periodically (Brilakis et al. 2006).

Additionally, there exists several remote sensing technologies for accessing bridge defects; however, they do not provide reliable information such as the extent and severity of defects required for the effective application of BMS. This research presents a methodology based on digital image processing for condition assessment of the critical elements in a bridge, suitable for the application of BMS, as well as, a procedure for tracking of progression of defects in critical bridge elements.

1.4 Scope and Objectives

The condition assessment of bridge structural components encompasses diagnosis and monitoring of external and internal defects. This thesis considers only external defects with a focus on improving current practices for concrete bridge inspection, which is based on digital image analysis. The aim of this research is to develop tools and techniques in order

to enhance the reliability of visual inspection for effective performance of BMS using digital image processing.

In order to achieve the above main objective, the entire activities relating to condition assessment of concrete bridges have been categorized into two parts: a) Defect Quantification Module, and b) Change Detection Module. For further development of these modules, this thesis considers three major categories of surface defects in reinforced concrete elements, which are: a) Spalling, b) Scaling, and c) Cracking. These defects including the crack map are to be captured by commercially available digital cameras, and processed for condition assessment of reinforced concrete beams/decks.

In order to fulfill the main objective, the following sub-objectives are identified.

- 1) Study the current practices, related literature, and limitations of remote sensing technologies for condition assessment of concrete bridges in order to support BMS.
- 2) Develop a methodology for condition assessment of concrete beams that accounts for not only individual cracks, but also crack patterns.
- 3) Design a prototype software application for automated prediction of element condition rating based on identified concrete bridge scaling defects.
- 4) Develop an application for change detection in order to track progression of critical defects for improved condition assessment of bridge structures.

1.5 Thesis Organization

Chapter two presents a literature review on the current practices of condition assessment of bridge structures. The chapter starts with introduction followed by the application of remote sensing technology for civil infrastructure. Previously, the remote sensing application was limited for geometry measurement; however, due to current development of digital cameras, now it is possible to quantify defects in bridge structures in addition to capturing the geometries of bridge components. One of the sections of this chapter focus on digital image processing such as automated detection of lines, points, image pre-processing, and image segmentation. Also, the chapter discusses the importance of 3D visualization of bridge defects through the digital images which can mimic the on-site visualization of bridges.

Chapter three presents the proposed methodology describing the main aspect of this research. In broad sense, the methodology consists of three main components: a) digital image processing, b) data processing, c) condition assessment modules. The condition assessment module is again sub-divided into three sub-modules which form the three next chapters as described here.

Chapter four, five and six develop procedures for crack quantification model, condition rating model, and change detection model for automated process of condition assessment of concrete bridges using digital images. For example, chapter four develops step by step process for crack detection and its length estimation based on crack skeleton itself. The

approach shows significant improvement over the previous approach of crack length estimation based on bounding box obtained by segmenting cracks. Also, the chapter presents a method to estimate crack density of a beam element, which is defined as total length of cracks over the total surface area, by developing 3D visualization models.

In chapter seven, the results of the present research are summarized, the main contributions are listed, and the recommendations for further research are presented.

Chapter 2: Literature Review

2.1 Introduction

The bridge infrastructure plays an important role for a country's development. The social, economic, and political development of a country is largely dependent on the effective operation and management of the civil infrastructure. Bridges are one of the major components of highway infrastructure connecting people from different places economically and emotionally. However, in current scenarios, the condition of bridges in North America is rapidly degrading and it poses a major challenge in managing the effective distribution of financial packages for maintenance and rehabilitation of infrastructure (Hammad et al. 2007).

Since 40 years, in spite of technological development in North America, there has been insignificant improvement in routine bridge inspection. In general, routine bridge inspection is carried out in every two years through visual inspection which has been identified with several limitations. To overcome these limitations, there is an urgent need for developing methodologies to enhance the reliability of visual inspection without adding financial burdens to users for the effective management of civil infrastructure (Hammad et al. 2007). The American Society of Civil Engineers (ASCE) started to publish a Report Card in the beginning of 1988 to grade the nation's infrastructure conditions. According to the latest report in 2012, about 11% of nation's bridges (i.e. total bridges in USA 607,380) were classified as structurally deficient due to increased traffic, aging of construction

materials, and several environmental effects (ASCE Report 2013). Likewise, in Canada, more than 40% of bridges are older than 50 years (Bisby and Briglio 2004). Such bridges require immediate actions for condition evaluation to ascertain that they still meet the service requirements, and are safe for operations. In the past, several bridge management systems (BMSs) were developed for managing bridge structures such the Pontis bridge management system (PONTIS) developed by FHWA in 1989 (AASHTO, 2005) and later, the BRIDGIT bridge management system developed by the National Cooperative Highway Research Program (NCHRP) (Hawk, 1999). The input data source required for such BMSs are generally obtained through visual inspections which have been identified with several limitations such as they being time consuming, influenced by inspector's experiences, and unreliability of element condition ratings (Gutkowski and Arenella, 1998; FHWA, 1995). The FHWA report in 2001 indicated that the condition rating assigned through visual inspection can vary significantly which raises questions on the reliability of visual inspection (Moore et al., 2001). The current BMSs require information on the defects in terms of their extent and severity in order to assign condition rating for the bridge elements. At this point, an accurate method of defect detection and quantification is essential for a reliable output from any automated trading systems such as PONTIS. Therefore, automated quantification of bridge defects using computer vision approaches needs to be explored further. Currently, a number of remote sensing techniques are available to evaluate the exterior or interior defects in bridge components. However, the major challenges are the cost and time. One of the promising approaches to enhance the reliability of visual inspection is through the use of digital image processing. Based on the processing of digital images, (Abudayyeh et al., 2004) developed an imaging data model for automated

condition assessment of concrete bridges. The model was integrated with an automated Bridge Management System (BMS), which was capable of generating automated inspection reports with the application of computers. However, in their approach, the assignment of condition rating for bridge elements was done manually by visualising images on computer screens by inspection experts. Thus, the literature review reveals that there is a need for the development of automated methodologies for predication of condition rating for bridge components. Such methodologies can be integrated with an automated bridge management system in order to enhance the current practices of visual inspections.

The next section presents the issues in current practices of routine bridge inspection with a focus on evaluating bridge condition rating and condition index associated with bridge components with multiple defects. Additionally, the chapter discusses the automation aspect of visual inspection through the application of digital image processing, and also the importance of shape descriptors for numerical representation of bridge defects. The chapter will also highlight the importance of 3D visualization of bridge defects through digital image processing in order to simulate on-site visual inspection through the use of modern technologies to assist in routine bridge inspection.

2.2 Remote Sensing

2.2.1 Advanced Technologies

The application of remote sensing in civil engineering can be defined as deriving information about the characteristics of civil infrastructure without being in contact with

them (Aronoff, 2005). The principle relies on reflectance signature of different surface materials over various portions of electromagnetic spectrum as shown in Figure 2.1 (NASA, 2013). Figure 2.1 clearly demonstrates that radio waves have larger wavelength with lower energy content, whereas gamma waves have shorter wavelength with higher energy content. Although, remote sensing can be carried out at any part of the light spectrum, the common form of light bands used in the management of civil infrastructure include visible and infrared light bands. The digital photography is limited to visible light bands occupying a small portion of the spectrum varying from 400 nanometers (nm) to 700 nm as shown in Figure 2.1.

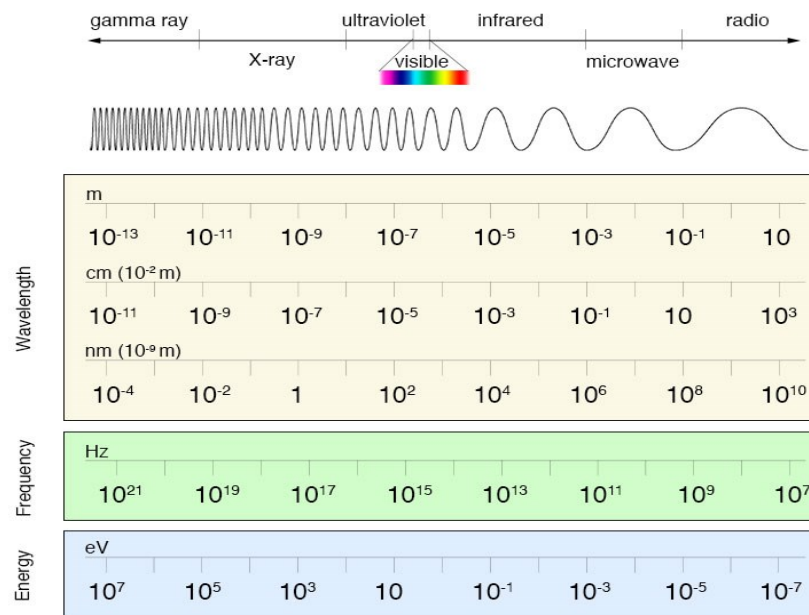


Figure 2.1: Electro-magnetic Spectrum relation with Energy and Wavelengths

Although several satellites such as LANDSAT TM, SPOT4, IRS, and RADARSAT are capable of identifying objects lying on the Earth surface, the defect detection and quantification of a civil infrastructure are not possible due to the limitations of spatial

resolution, temporal resolution, radiometric resolution, swath width, and spectral bands (Roy, 2008). Table 2.1 displays the capabilities of four types of international satellites currently working the sky for gathering spatial and temporal information about the earth surfaces. The RADARSAT-1, a Canadian space satellite launched in November 4, 1995, is still active; however, the spatial resolution of digital images is just above 3 meters which are not sufficient for quantification of defects associated with civil infrastructure. The temporal resolution of the above mentioned four satellites varies from 16 days to 24 days which is sufficient enough to compare change detection for further recommendations after heavy flood or natural disasters.

Table 2.1: Satellites Spatial and Temporal Resolution (Roy, 2008)

| System | Altitude (KM) | Bands | Swath (KM) | Spatial Resolution (m) | Temporal Resolution (days) | Scales |
|----------|---------------|-------|------------|------------------------|----------------------------|-----------|
| LANDSAT | 705 | 7 | 185 | 30 | 16 | 1:50,000 |
| SPOT4 | 803 | 4 | 60 | 20 | 26 | 1:50,000 |
| IRS | 900 | 4 | 147 | 36 | 22 | 1:125,000 |
| RADARSAT | 798 | 1 | < 500 | >3 | 24 | 1:50,000 |

Apart from the satellite remote sensing, Aerial Photogrammetry which is also called passive sensors is very popular in civil engineering. The commonly used active sensors for the geometry measurement of civil infrastructural components are LIDAR (Light Detection and Ranging) and IFSAR (Interferometric Synthetic Aperture Radar). So, it is important to

select right sensors for a particular problem of interest because sensors selection is application dependent.

Figure 2.2 demonstrates the selection of different remote sensing technologies based on the required resolution and object sizes (Luhmann et al. 2006). Luhmann and others summarized that smaller objects required higher accuracy. The engineering photogrammetry yields accuracy in mm range for objects ranging from few meters to 100 meters.

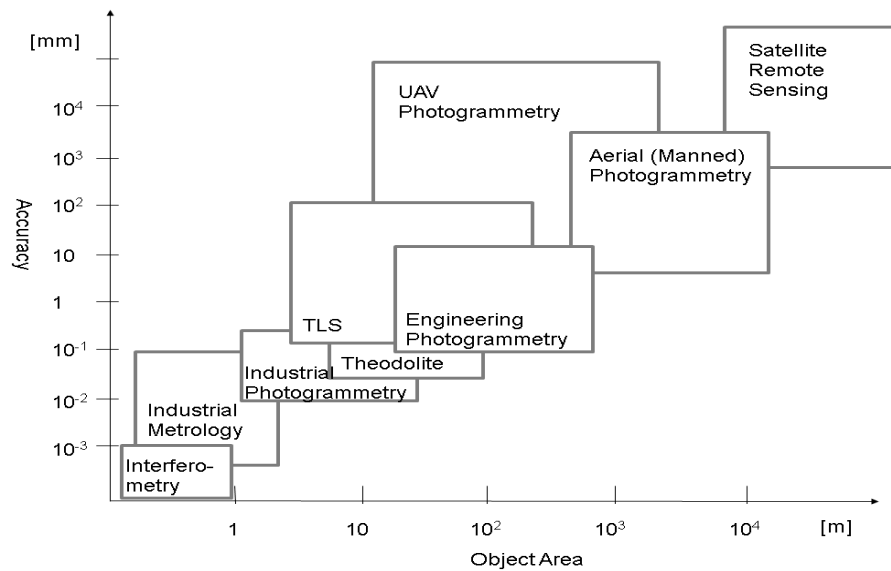


Figure 2.2: Spatial Resolution Accuracy and Object Size (Luhmann et al. 2006)

2.2.2 Suitable Remote Sensing for Surface Defects Analysis

Although bridges are composed of variety of materials such as concrete, timber, and steel, the current thesis focuses on reinforced concrete Bridges. Most of bridge structures can be classified into three major components as shown in Figure 2.3.

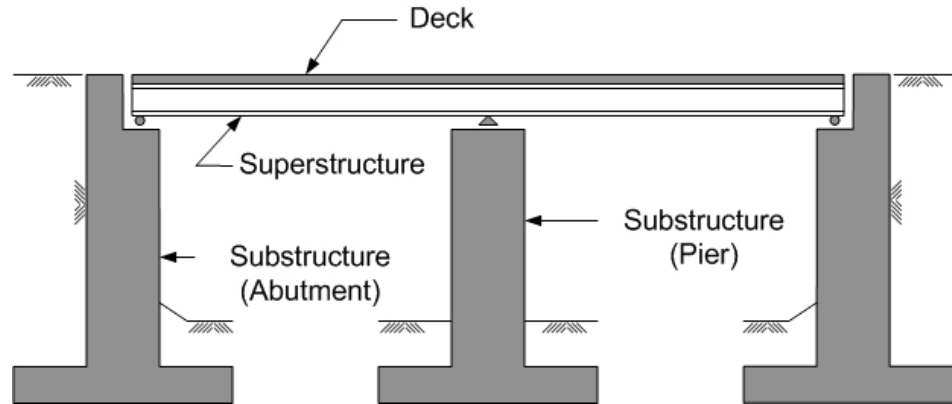


Figure 2.3: Major Bridge Components (BRIM -1, 2012)

Out of the three major components of bridges (Decks, Piers, and Abutments), bridge decks are the most vulnerable part of any bridges. Because of direct contact with traffics, they are prone to wear and tear in comparison to structural bridge components (Ryall, 2003). Table 2.2 lists seventeen defects required to be studied for complete condition assessments of reinforced concrete structures; however, all the defects may not be present in a particular bridge component in question (FHWA, 2006). In general, the details of information necessary for condition assessment of bridge components are a) types of damages, b) location of damages, c) damage intensity, and d) damage extent (Bien, 1999).

Table 2-2: Types of defects in Reinforced Concrete Structures (FHWA, 2006)

| Material | Defect |
|----------|--|
| Type | Type |
| Concrete | Cracking, Spalling, Scaling, delaminations, chloride contamination, efflorescence, formation, honeycombs, pop-outs, wear, collision damage, abrasion, overload damage, reinforcing steel corrosion, prestressed concrete deterioration |

The Norwegian graphic symbols list the important damage types necessary for condition assessment of bridge structures in Figure 2.4 (NCHRP SYNTESIS 375). The figure explores five major types of defects in concrete bridge structures. These defects are further classified into sub-classes according to their severity and impact on structural integrity of bridges.





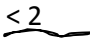
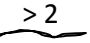
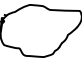

| | |
|---|------------------------------------|
|  | Casting Joint |
|  | Delaminations, Spalling |
|  | Porous or Bad Quality Concrete |
|  | Cracks |
|  | Cracks > 0.2 mm, and < 2 mm |
|  | Cracks > 2 mm |
|  | Cracking |
|  | Visibly Corroding Reinforcement |

Figure 2.4: The Important Bridge Defects (Norwegian graphic symbols)

The thesis considers only external defects which can be captured with digital images. For condition assessment of reinforced concrete beams/decks, the three types of defects considered in this thesis are: a) Spalling, b) Scaling, and c) Cracking or Crack Map. The typical Spalling, Scaling, and Cracking defects are shown in Figure 2.5.



Figure 2.5: (a) Spall area < 10 square inches (left); and > 100 square inches (right) - (Project Scoping Manual, 2013)



Figure 2.5: (b) Crack Map on bridge deck surface (FHWA 2006)



Figure 2.5: (c) Concrete deck surface scaling (FHWA 2006)

For detection and quantification of bridge defects listed in Figure 2.4 needs a number of remote sensing technologies to be integrated for complete condition assessment of infrastructure. The commonly used non-destructive techniques for condition evaluation of

concrete decks are visual inspection, liquid penetrant dye, chain drag, Half-cell potential (HP), acoustic emission, ultrasonic pulse velocity, ground penetrating radar (GPR), impact echo (IE), and IR thermography (Yehia et al. 2007). For example, GPR, IE, and IR thermography were found promising techniques for detection of internal defects in concrete bridge decks (Yehia et al. 2007), while others could be suitable for surface defects.

How these technologies can be helpful in enhancing the task of visual inspections are of great interest to researchers in managing civil infrastructure. A systematic study for the condition assessment of concrete bridge decks through experimental and field testing was conducted using Three Dimensional Optical Bridge Evaluation Techniques (3DOBS), Bridge Viewer Remote Camera System (BVRCS), GigaPan, LIDAR, Thermal IR, Digital Image Correlation (DIC), Ground Penetrating radar (GPR), Remote Acoustics, and high resolution Street View-style digital photography (Ahlborn et al. 2010). The study showed that 3DOB or BVCRS techniques based on the close range 3D photogrammetry technique and GigaPan techniques based on Street View-style photography are the best technologies for defect measurement for bridge inspections as illustrated in Table 2.3 (Ahlborn et al., 2010). An element receives the best score of 16 based on eight evaluation criteria from A to H which is rated to 0, 1, and 2 depending upon the condition of elements. The detailed information about rating of different techniques can be found in Appendix B.

The most successful technologies for bridge deck evaluation based on the field, as well as laboratory test verification have been listed in Figure 2.6 (Ahlborn et al., 2010). The rest of the sections discusses on the application of digital image processing for condition assessment of concrete bridge structures.

Table 2-3: Rating based Theoretical Sensitivity for Measurement Technologies

(Ahlborn et al., 2010)

| Location | Challenges | Indicator | GPR | Spectra | 3D Photography | Satellite Imagery | Optical | Interferometric | LiDAR | Thermal IR | Acoustics | DIC | Radar | InSAR | StreetView | Images |
|---------------|-----------------|--------------------------|-----|---------|----------------|-------------------|---------|-----------------|-------|------------|-----------|-----|-------|-------|------------|--------|
| Deck Surfaces | Expansion Joint | Cracks Within 2 ft | 0 | 8 | 14 | 0 | 12 | 12 | 11 | 0 | 0 | 9 | 0 | 13 | | |
| | | Spalls within 2ft | 0 | 8 | 14 | 12 | 12 | 12 | 11 | 0 | 0 | 9 | 0 | 13 | | |
| | Map | Surface | 0 | 8 | 14 | 12 | 12 | 12 | 11 | 8 | 0 | 9 | 0 | 13 | | |
| | Cracking | Cracks | 0 | 8 | 14 | 12 | 12 | 12 | 11 | 8 | 0 | 9 | 0 | 13 | | |
| | Scaling | Depression in Surface | 0 | 8 | 14 | 12 | 12 | 12 | 11 | 0 | 0 | 9 | 0 | 13 | | |
| | Spalling | Depression with Fracture | 0 | 8 | 14 | 12 | 12 | 12 | 11 | 0 | 0 | 9 | 0 | 13 | | |




| 3D optical bridge Evaluation system (3DOBS) | Bridge Viewer Remote Camera System (BVRCS) | GigaPan |
|---|---|---|
|  |  |  |

Figure 2.6: Successful technologies for Bridge Deck Analysis (Ahlborn et al., 2010)

2.3 Current Practices in Automated Bridge Condition Assessment

The Navy Bridge Inspection Program Manual (2008) for bridge inspection lists seven types of bridge inspections required to document a bridge conditions over its useful life. They are 1) Initial Inspection, 2) Routine Inspection, 3) In-Depth Inspection, 4) Damage Inspection, 5) Fracture Critical Inspection, 6) Underwater Inspection, and 7) Interim Inspection. However, the discussion here is only focused on routine bridge inspection which has been defined as an arm’s length visual inspection of all parts of bridge structures using simple instruments supported by comments and photographs (Navy Bridge Inspection Program Manual, 2008). During routine inspections, it is necessary to assign the condition rating of all elements in accordance with FHWA guidelines (Recording, 1995). Although such method of assigning bridge condition rating is very popular, the

reliability of visual inspection has been questioned in literature (Moore et al., 2001). The reliable inspection information regarding to bridge elements are important for advance bridge management system.

2.3.1 Damage Evaluation

A damage inspection can be defined as an unplanned inspection i.e. not following any schedule to assess structural damages resulting from environmental factors or human actions (Ohio DOT, 2010). The purpose of this type of inspection is to determine the nature, severity, and extent of structural damages after any kinds of extreme events, traffic collisions/accidents to evaluate the safety requirement of structural members. Liu (2010) studied 69 collapsed bridges in the USA from 1967 to 2008. The result showed that more than 50% bridges were collapsed due to collisions, and natural disasters. These events trigger or initiate defect at an element level and progresses in due time during the service life of infrastructure. When these events will happen is unknown in advance, and therefore, it is difficult to establish a common inspection interval which can take care of impact on structural components resulted through such events. One way to tackle this problem is to revise the inspection frequency based on event-based management strategies. However, since bridge monitoring and inspection is expensive program, there is a need for developing automated tools using current technologies to assist routine bridge inspection. In the previous section, it has been discussed that the best way for concrete damage detection and quantification by using remote sensing technologies is the use of digital images (Ahlborn et al., 2010). Several researchers have worked on digital images for condition assessment of civil infrastructure in recent years as explained next.

Abudayyeh et al. (2004) proposed a framework for automated bridge imaging system based on digital image processing and integrated with Bridge Management Systems (BMSs) PONTIS. Their models were capable of storing different surface defects in a structured way and generated automated inspection reports. However, the assignment of condition rating for bridge elements was done manually by displaying images on computer screens. To automate this process, a model for automated prediction of condition rating is required which can assign a unique number based on the severity and extent of defects. The approach requires training of expert functions for prediction of condition rating as an output based on selected input parameters.

2.3.2 Close Range Photogrammetry

Photogrammetry can be defined as measuring of geometry of physical objects from two-dimensional photographs. Depending upon how the digital images are acquired, the photogrammetry can be defined in two types: a) Aerial Photogrammetry and b) Terrestrial Photogrammetry (Gruen, 2000). Furthermore, the terrestrial photogrammetry is also called close-range photogrammetry when the object size and camera-to-object distance are both less than 100 meters (Jiang et al., 2008). Since the close-range photogrammetry has the ability to acquire detailed images of physical objects, it has been many applications in engineering (Fryer, 2000). In the development of automated bridge inspection tools, researchers have worked on ground-based remote sensing techniques for infrastructure monitoring using close range photogrammetry (Jiang et al., 2008). They presented a detailed literature review on the potential application of close-range photogrammetry in

bridge engineering. Their work briefly summarizes the basic development of ground-based remote sensing related to bridge deformation and geometry measurement, as well as structural health monitoring and documentation of historical infrastructure. Table 2-4 summarized work done from 1985 to 2003 based on the use of different types of cameras, target and control points application, and softwares covering the automated aspects of bridge inspection. Due to the rapid development in information technology in processing of digital images, the analysis of bridge defects such as cracks, spalling, and scaling is possible with reasonable accuracy which can be used to enhance the reliability of visual inspection. The next section will demonstrate the necessary steps required to analyze digital images to extract useful information.

2.3.3 Digital images application for civil infrastructure

As discussed in the previous section, Abudayyeh et al. (2004) proposed a framework for automated bridge imaging system based on digital image processing and integrated with Bridge Management Systems (BMSs) PONTIS. This was the first attempt to work with bridge defects by visualizing digital images on the computer screen.

The proposed methodology documented bridge defects digitally and automated reports were produced, however, the condition rating was assigned manually. The current thesis fulfills the gap by developing automated prediction of condition state rating based on digital image analysis. A considerable volume of literature has been published in the domain of construction industries using digital images to augment the effective infrastructure management systems.

Table 2-4: Application for Bridge Deformation and Geometry Measurements (Jiang 2008)

| Researcher | Test object | Type of measurement | Target and type of photography | Camera used | Network control | Software used |
|---|---|-----------------------------------|---|---|--------------------------------------|---------------------------------|
| Bales (1985) | Reinforced concrete deck | Crack length and width | Diffuse targets, non-flash photography | Zeiss MK 10/1318, metric film camera (100 mm lens) | Control point survey | Stereoscopic comparator |
| Bales and Hilton (1985) | Steel I – Beam Steel girder bridge | Vertical deflection | | | | |
| Kim (1989) | Highway Bridge | Long-term deformation | Diffuse targets, non-flash photography | Metric film camera (150 mm lens) | Control point survey | Self-developed |
| Abdel-Sayed et al. (1990) | Soil-steel Bridge | Geometry, deformation | Retro-reflective targets, flash photography | Leica film camera (24 mm lens) | Scale bars | Elcovision 10 |
| Cooper and Robson (1990) | Steel bridge | Deformation | Retro-reflective targets, flash photography | Zeiss MK 10/1318 metric film camera (100 mm lens) | Control points | Inter map analytical comparator |
| Forno et al. (1991) | Arch bridge | Deformation | Retro-reflective targets, flash photography | Zeiss MK-10 N metric camera (2.1 m lens) | Control points | Microscope |
| Albert et al. (2002) | Reinforced concrete beam Concrete arch bridge | Vertical deflection | Diffuse targets, non-flash photography | Kodak DCS660 digital camera, machine vision camera (24 mm lens) | Distance measurement between targets | Ellipse operator |
| Leitch (2002) Jauregui et al. (2003) | Steel beam P/C girder Bridge | Vertical deflection Deflection | Diffuse targets, non-flash photography | Kodak DCS660 digital camera (28 mm lens) | Control point survey | FotoG |
| Norris (2003) Johnson (2001) | Suspension Bridge | Geometry | Retro-reflective targets, flash photography | Imetric and Kodak DCS660 digital cameras | Control point survey | Imetric |

Digital photograph of construction sites provides the evidence of as-built project and the digital information can be used for effective infrastructure management which can assist a large number of construction inspection and management applications such as construction productivity and progress monitoring (Brilakis et al. 2006, Brilakis & Soibelman, 2008).

The above work was the first step in recognizing construction objects from images obtained from actual construction sites. They developed an automated recognition of construction materials (steel, concrete, or wood) using similarity-based criteria obtained from color or texture properties of material surfaces. They also added a content-based attribute (shape recognition) to recognize beam, columns, and wall related to construction activities.

These works are further studied by Zhu et al. (2010) and they proposed a novel method for detecting large-scale concrete columns for the purpose of developing an automated bridge condition assessment system. Since columns are large structural members, several images were taken and image stitching algorithm developed by Brown and Lowe (2007) was used to combine individual images into a single image. A neural-network based material classification method was reported in FANN (2009). Although above researchers worked for enhancing the effective bridge management systems, there were little attentions paid towards developing concrete defect models which could be an input to any BMS for concrete bridges. However, there has been a significant improvement in developing models for crack quantification.

Advantage and limitations of Google Street View Imaging

The Google Street view provides a continuous 360 degrees viewing environment for civil infrastructure. The technology is suitable for assessing the condition of an infrastructure by the inspectors from the offices without travelling to the site. Recently, Hinzen (2013) demonstrated the feasibility of damage detection and quantification based on Google Street View images. However, since the technology is based on vehicle-mounted instrumentation, this approach may not be suitable for condition assessment for elements at the underside of a bridge.

Since the imaging model is based on remote sensing technology, there is less disruption of traffic. By developing a technology which can be fixed with traffic moving at the same highway speed will maximize the benefit of such techniques. Although digital image-based analysis of condition assessment of infrastructure provides low capital cost, rapid deployment, and useful metrics (can compare condition over time, % area, volume, crack density, and roughness index), the slow speed of data collection (usually less than 5 mile per hour), traffic disruption, requires high resolution images, field of view, and data processing time are the challenges that need to be improved further (Ahlborn et al. 2010).

It is unlikely that fine cracks can be detected with the available resolution in the Google Street View; however, the detection accuracy of cracks can be increased using high resolution digital cameras. Currently, there are not enough guidelines available on the required resolution for detecting fine cracks. However, the resolution available in the Google Street view images is useful for condition evaluation of bridge deck surfaces

including spalling and scaling of bridge deck surfaces, mapping of cracks, joint damage, and delaminations expressed as surface damages (Ahlborn et al. 2010).

In order to improve the reliability of visual inspection, the developed methodology based on digital images needs to be integrated with existing bridge management system which is another challenge to be considered in developing an effective imaging model. In terms of cost, LiDAR scanners are very expensive for data acquisition and processing because they require digital cameras, scanners, positioning systems, computers, and related software tools. Similarly, the data collection by a digital camera is much cheaper than a GPR system (Ahlborn et al. 2010). Since each of the image-based technologies has its own advantages and disadvantages, a proper combination of such technologies is required to provide appropriate results.

Often, the dimension of a surface defect captured by a digital image is measured in pixels. However, the defect measurement needs to be expressed in engineering units such as, feet or millimeters. Also the defect size is relative to the dimension of the image frame, and the actual size of the frame or the defect in physical/engineering units depends on many factors including image resolution, distance at which the image is taken etc. Several authors have used either artificial or natural scales of benchmark in the image frame for obtaining the actual dimension of a defect from a digital image (Adhikari et al. 2014, and Ahlborn et al. 2010). While working with digital images, the criteria need to be considered are: a) color images, b) the distance between camera and object which is called field of view shall be such that the minimum resolution on an image is 1 pixel per mm, c) lighting should be

uniform to maintain images are consistent, and images shall be overlapped to ensure full coverage (McRobbie et al. 2008). Apart from the general conditions, they suggested that for defect evaluation, an image shall be acquired orthogonal to the plane on which a defect lie in order to improve accuracy of defect quantification by avoiding parallax and projection errors (McRobbie et al. 2008).

2.3.4 Neural Networks Application for Civil Structures

Neural Networks mimic the thought process of human brain by assigning weights to individual inputs attributes and output is mapped through a simple transfer functions (Liu, 2001). In the existing literature, neural networks (NN) have been reported to be used for several purposes for developing data fitting regression models as well as to solve classification problems where direct relations among input parameters do not exist (Moselhi and Shehab-Eldeen 2000, Bień and Rewiński, 1999). Neural Networks can be used as an intelligent system to assist bridge management systems for efficient operations as well as the maintenance schedule of structures. The systematic application of NN was listed in four categories for efficient bridge management systems (Bień, 2000). They are: 1) technical condition assessment processes, 2) maintenance technology selection processes, 3) real time data management systems, and 4) monitoring of structural parameters. However, the information required for training of NN was based on the result of visual inspection (Bień, 2000).

Over the past few decades, the application of NN was also very popular in automation of civil infrastructure management based on digital image processing. Neural networks were

used for automatic classification of defects in sewer pipe lines where digital images of sewer defects were used for extraction of geometric parameters required for training of neural networks (Moselhi and Shehab-Eldeen 2000). The accuracy of their prediction and classification of sewer defects was reported to be 98.2%. The geometric attributes used by them were area, perimeter, and major as well as minor axis lengths of defects as displayed in Figure 2.7.

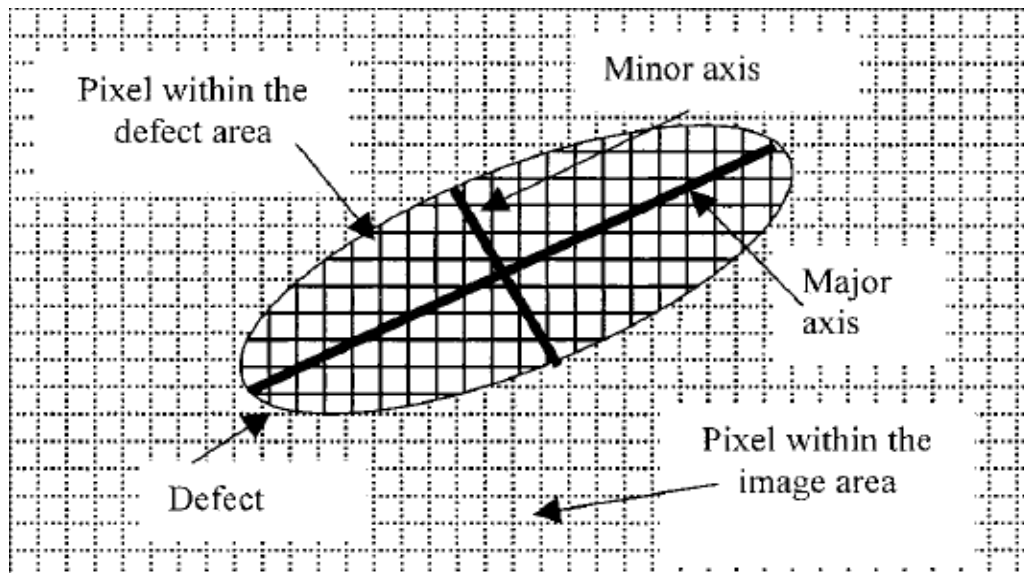


Figure 2-7: Feature attributes of a defect (Moselhi and Shehab-Eldeen 2000)

Similarly, Khan et al. (2010) also used neural networks to analyze structural behavior of sewer pipes in terms of the variation of condition ratings, and the success rate of the developed model for the prediction of condition rating was reported to be 92.3%. However, the geometric attributes obtained for training of NN were obtained from visual inspection. Also, decision processes regarding to future conditions of an infrastructure depend on many

variables. Such uncertainties in the classification of defects in sewer pipes were discussed using neural-fuzzy networks (Sinha et al. 2003). One of the most relevant applications of neural networks was developed for predicting the fatigue life and failure of reinforcing bars in concrete elements. A recent paper written by Abdalla and Hawileh (2013) tested 15 specimens to measure fatigue failure of reinforcing bars and then neural networks were trained to predict failure patterns for the chosen samples.

2.3.5 Automated crack detection using digital images

In recent years, several automated crack detection algorithms have been proposed in the literature which can assist in condition assessment of reinforced concrete bridges. Abdel-Qader et al. (2003) compared the performance of crack edge detection against Fast Haar Transform (FHT), Fast Fourier Transform, Sobel, and Canny algorithms. It was concluded that FHT produced the best result over the other algorithms in detecting crack edge. Likewise, a Principal Component Analysis (PCA) was applied successfully for pattern recognition to determine whether a concrete surface was cracked or not, based on the Euclidean Distance as similarity criterion (Abdel-Qader et al. (2006). The crack analysis is necessary for automatic repair and maintenance of concrete surfaces. Haas et al. (1992) developed an automated field prototype crack sealing system which required fully automated crack detection, surface mapping, and control systems. In the digital imaging process, crack pixels need to be separated from their background. For segmentation of a crack from its background, a threshold is used for extracting the crack boundary pixels. The threshold can be estimated from mean and standard deviation of gray-level images (Cheng et al., 2003). However, this method does not ensure proper crack connectivity. To

solve this problem, the percolation-based image processing method was suggested to correctly detect cracks on concrete surfaces (Yamaguchi and Hashimoto, 2009). The result of this approach indicated that the percolation-based method is efficient even for larger-size concrete surfaces. In a later development, mathematical morphology was adopted in an image segmentation method where images were partitioned based on either similarity or discontinuity. Iyer and Sinha (Iyer and Sinha, 2006) adopted morphological filters with linear structuring elements for defect identification in sewer pipelines. Several types of concrete defects such as cracks, holes, joints, and collapsed surfaces were identified based on image processing and morphological segmentation approach which is necessary for automated classification of defects in sewer pipelines (Sinha, Fieguth, 2006). However, this approach was not suitable to discriminate all kinds of defects in sewer pipelines. Therefore, certain objects like joints and lateral displacements were classified by using the shape or texture features such as, roundness and compactness (Sinha, Fieguth, 2006).

The purpose of image processing is to extract the areas of interest from a given image frame. For example, the extraction of length and width of a crack is necessary for crack analysis of concrete members. So, proper definition of crack length and width needs to be stated explicitly. For practical purpose, average crack width is required to prepare a bid for repair and maintenance purposes. This could be possible by dividing a long crack into small crack segments and retrieving average length and width for each segment. In recent study, crack segmentation was achieved by searching of crack connectivity and matching the pixel orientations (Zhu et al., 2011). This approach needs input of at least one crack skeleton pixel to start searching of crack connectivity. Moreover, the length of a crack is

estimated from object-oriented bounding box which ignores the tortuosity of cracks (Zhu et al., 2011). The current thesis aims to fill the gaps by developing an automated crack quantification model using digital image processing.

2.3.6 3D Defects Modeling to Assist Visual Inspection

Many software systems have been developed for the design of structural components, however, little attention has been given to modeling defects in concrete elements based on defect parameters such as extent, severity and intensity of defects. The simplest way to obtain the geometry of defects is to collect the data of defect size, shape etc. by an inspector. But, such an approach is time consuming, costly, and prone to subjectivity. Therefore, modeling of defects from images for condition assessment of structural components provides an attractive alternative which can serve to augment the information obtained from visual inspection.

In order to overcome the limitations of visual inspection, several attempts have been proposed to automate the current bridge inspection process. One such attempt is to automatically retrieve the three dimensional (3D) as-built/as-is bridge information using remote sensing techniques. Although the 3D as-built/as-is bridge information is useful, the retrieval of such information is a challenging task (Remondino and El-Hakim, 2006). McRobbie et al. (2010) investigated several off-the-shelf 3D software tools, such as, MeshLab, Rhino, TrueSpace, and Phtosynth, and found that existing tools could not fully support the automatic retrieval of 3D as-built/as-is bridge information. A lot of manual editing and correction work are still required, which makes the overall information retrieval

process labor-intensive and time-consuming (Zhu, 2012). A photographic technique was demonstrated for 3D visualization of bridge components in quantitative assessment of bridge defects (Maksymowicz, 2011). However, the authors added an additional tool called “Damage Assessment Graphic Analysis — DAGA” for modeling defects from photographs. The above system was equipped with an advanced graphical editor enabled with fast creation of 3D models of bridge components and presentation of the results graphically. A quick 3D visualization model based on digital images and available software tools is required to assist the condition assessment process for concrete bridges.

However, one of the challenges still exists is how to reflect the current level of deterioration in the structure on a 3D model so that they could be reviewed on computer simulating the on-site visual inspection process. The thesis attempts to address this issue with the application of current available commercial software tools.

2.4 Automated Bridge Management Systems

2.4.1 Bridge Management Systems

A Bridge Management system (BMS) can be defined as an automated system for tracking the condition of bridges in a highway network which helps in prioritizing the task of maintenance and rehabilitation for better performance of infrastructure (Tonias and Zhao, 2007). A BMS is composed of several components consisting of bridge inventories, inspection reports, bridge deficiencies, financial evaluation, and management components (AASHTO, 2005). In USA, the importance of bridge safety through routine inspection and

maintenance regulation had not been realized until the collapse of Silver Bridge at Point Pleasant, West Virginia where 46 people were killed in 1967 (Lichtenstein, 1993). In 1971, the minimum standard required for bridge inspection was set up by the National Bridge Inspection Standards (NBIS) consisting of Bridge Inspector's Training Manual by the Federal Highway Administration (FHWA), Manual for Maintenance Inspection of Bridges by the American Association of State Highway Officials (AASHTO), as well as the FHWA's Recording and Coding Guide for the Structure Inventory and Appraisal of the Nation's Bridges (Liu, 2010). The development of BMS goes back to 1991, when the Intermodal Surface Transportation Efficiency Act (ISTEA) of USA mandated the requirement for the use of Bridge Management Systems by each state Department of Transportation (DOT). Soon, a rigorous BMS software package, Pontis, was developed and implemented in several states for effective bridge asset management (Gutkowski & Arenella, 1998). Today, more than 44 states are licensed with Pontis BMS. However, the level of implementation of a BMS varies from state to state (AASHTO, 2009). The literature revealed that the application of a BMS is different from not only from one country to another, but also from one state to another state. Several BMSs are listed here adopted in different countries, for examples, BRIME BMS is used in Europe (Woodward et al. 2001), Finland uses Finnish-BMS (Soderqvist 2004), Denmark uses DANBRO (Bjerrum and Jensen 2006), Taiwan uses T-BMS (Liao et al. 2008), and Argentinean-BMS is used by Argentina (Ruiz et al. 2008).

In spite of the fact that a majority of the states have used BMSs for managing infrastructure, less than 50% of the states consider BMSs recommendations for selecting bridge projects

because of skepticism of the simulation modeling, and resource limitations (Bektas, 2011). For effective application of BMS, a robust data management system is required. Inspection data required for BMS, in general, is collected through visual inspection. The first inspection, also called initial inspection, is necessary immediately after bridges are opened for traffic so that a baseline inspection target can be defined to compare the condition of bridge components over the service life of structures (Moore et al., 2000). As discussed in the previous section, visual inspection suffers from several limitations, and the application of advance information technology can enhance the reliability of BMS output. The current thesis adopts digital image processing application in enhancing the task of assigning condition rating for bridge elements. The next paragraph discusses the BMSs adopted by Canadian provinces.

Canadian provinces have developed different BMSs to suite their individual needs; for example, Alberta uses Transportation Infrastructure Management System (TIMS), Ontario uses Ontario-BMS, and Quebec has Quebec-BMS (Hammad et al., 2007). The Ministry of Transportation of Ontario (MTO) developed the Ontario Bridge Management System (OBMS) to store inventory and inspection data which can be processed for decision making purpose to identify the need of immediate repair, maintenance, and rehabilitation for bridges. The newly developed BMS in Ontario works at the network-level, as well as, at the project-level (Thompson and Ellis, 2000). The OBMS, which was first implemented in 1999, consists of five structural data records: Inventory, Elements, Inspections, Work History and Documents (Ontario-BMS, 2012). The regular inspection module of OBMS consists of Biennial Detail Tab and Recommendation Tab. The Biennial Details record the

element condition data, comments, and performance deficiencies for each element. Similarly, the recommendation Tab allows the inspector to recommend the immediate actions to be taken if required for further investigation or maintenance activities. Here, the Biennial Details and Recommendations are entirely based on the inspector's personal experience.

To support the inspector's views and recommendations, the OBMS allows the inspector to store three types of documents: Photos, Drawings, and Reports. Photos and drawings are related to element inspection, whereas, the drawings are concerned with construction and rehabilitation related problems. Due to the limitation of storage problem, the OBMS resizes the original photograph to a resolution of 1024 x 768 to the database. Figure 2.8 illustrates the screenshot of crack photo displayed on monitor in the documents module of the OBMS software (Ontario-BMS, 2012).

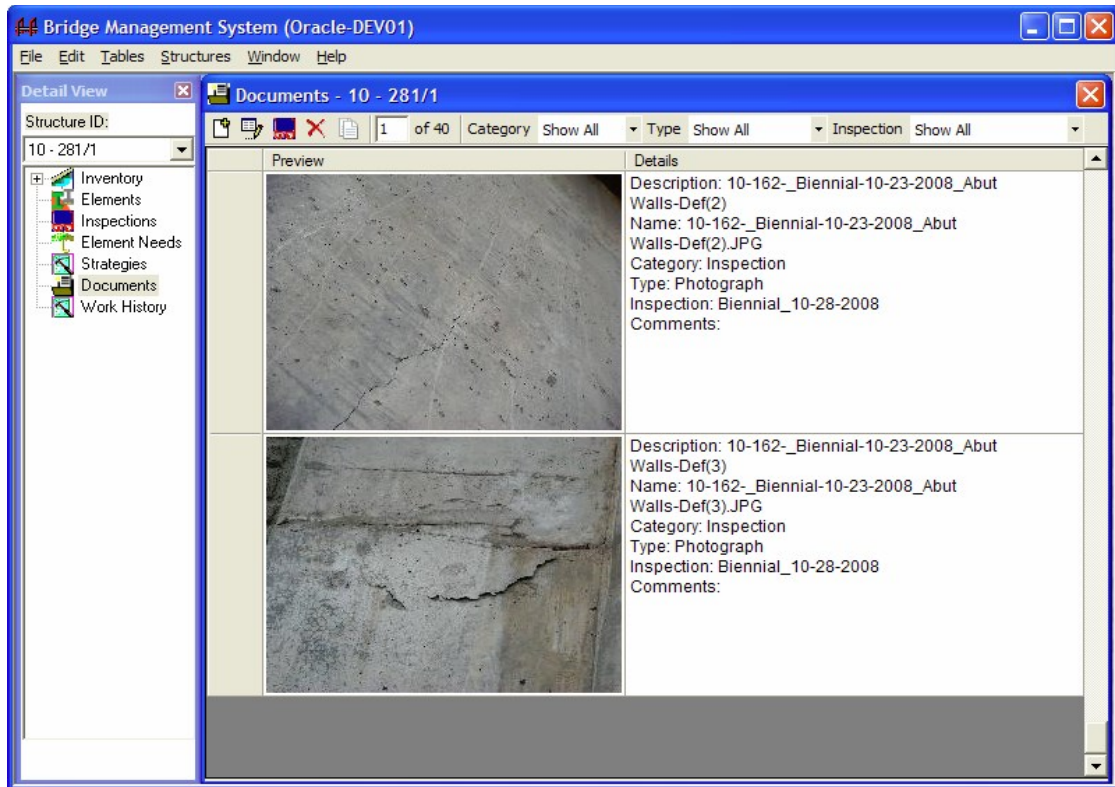


Figure 2-8: Photo Visualization in the OBMS (Ontario-BMS, 2012)

The software also allows users to upload a key photograph showing the current condition of structures. The key photo shall be taken such a way that the whole structure in question should be visible from a single location, usually taking photograph from a corner of a structure. However, these photos are used only for reference purposes or visual based decisions are made by visualizing the images on computer screen. The current thesis focuses on the use of digital images for quantification purpose using digital image processing.

The Navy Bridge Inspection Manual outlines requirement of images for condition evolution of structural components based on photographs (Navy Bridge, 2008). According to the manual, the photos shall be taken digitally with a 3 mega pixels camera in order to produce clear images of 3 inch by 6 inch. Likewise, a digital image with a minimum resolution of 240 dpi in JPEG format needs to be taken for a typical and significant structural condition evolution. The key aspect in acquiring digital image is to place a scale or inspection tool (e.g. hammer, tape, or pencil) in order to provide a frame of reference for the subject of photograph. A sample of well composed photograph is shown in Figure 2.9 (Navy Bridge, 2008).



Figure 2.9: A Well Composed Digital Images (Navy Bridge, 2008)

Further, the manual suggests acquiring a minimum number of photographs considering the following areas: a) an elevation view from each side of a bridge, b) a typical view of any deficiencies, c) a photograph of each approach road, d) a view looking upstream and a view looking downstream, e) minimum of two typical views per span and one per superstructure (Navy Bridge, 2008). In addition to the above mentioned photographs, all major defects found on the surface of structural elements shall be photographed and documented. Figure 2.10 illustrates a well composed photograph of underside of a bridge deck, and Figure 2.11 shows a poorly composed photograph.



Figure 2.10: A Well Composed Digital Image showing the Underside of a Bridge Deck
(Navy Bridge, 2008)



Figure 2.11: A Poorly Composed Digital Image, No scale for reference, location or orientation (Navy Bridge, 2008)

2.4.2 Element Condition rating

In BMS, bridges are recognized as assembly of structural elements. In Pontis, AASHTO Commonly Recognized (CoRe) elements are used to represent the structural components of bridges. The bridge inspectors collect element level information such as the extent and severity of different defects through visual inspections. In general, the outcome of routine bridge inspection is reported in the form of element condition rating (Hearn & Shim, 1998). According to the Recording and Coding Guide for the Structure Inventory and Appraisal of the Nation's Bridges, the element condition rating is expressed on a scale of nine (9;

excellent condition) to zero (0; failed condition) (FHWA, 1995). However, the current BMS software like PONTIS uses four-state and five-state condition rating scales depending upon the types of materials used for construction of bridge structures especially developed for the commonly recognized (CoRe) elements (Hearn & Shim, 1998). The application of different condition rating scales for a reinforced concrete bridge structures is displayed in Figure 2.12. The bridge performance is measured by finding utilizing weighted sum of the element condition ratings.

| | | | | | | | | | |
|------------------------|------|-------|--------|--------|------|---|---|---|---|
| NBI Rating | 9 | 8 | 7 | 6 | 5 | 4 | 3 | 2 | 1 |
| Pontis Condition State | 1 | 2 | 3 | 4 | 5 | | | | |
| Spalls | 0 % | < 2 % | < 10 % | < 25 % | >25% | | | | |
| Visible State | Good | Fair | Poor | Bad | | | | | |

Figure 2.12: Current Condition Rating Scale for Reinforced Concrete Decks

The above Figure shows the quantitative information required for assigning each condition states in Pontis for condition assessment of bridge decks. During a bridge deck inspection, the top and bottom of bridge decks are evaluated against cracking, spalling, scaling, and delaminations to assign condition rating for top and bottom surfaces, respectively. The deficiencies on the top surface of a bridge deck is defined as “the percent of deck surface area that is spalled, delaminates, or patched with temporary patch material” and the defect on the bottom surface not concealed by the stay-in-place forms is defined as “the percent

of deck underside area that is spalled, delaminated, or map cracked” (Aktan et al., 2013). The element condition rating is highly dependent of all types of defects that exist in a particular element. However, in the current practice of assigning element condition rating, the relative importance of all defects in a bridge element is often not considered (Akgul, 2012). In the conventional way, the quantitative analysis of element condition rating is based on visual inspection. Hence, the reliability of such approach of assigning element condition rating information need to be enhanced by using emerging technologies such as, digital image processing. As per Pontis Bridge Inspection manual (2009), the detailed description of the four condition states are shown in Table 2.5.

Table 2.5: Current Condition Rating Scale for Reinforced Concrete Decks

(Pontis Bridge Inspection Manual, 2009)

| Condition (Index) | Description |
|-------------------|--|
| “Good” (1) | The element shows little or no deterioration. |
| “Fair” (2) | Minor cracks and spalls may be present but there is no exposed reinforcing or surface evidence of rebar corrosion. |
| “Poor” (3) | Some delaminations and/or spalls may be present and some reinforcing may be exposed. |
| “Serious” (4) | Advanced deterioration. |

Based on the above criteria, the condition rating of concrete columns and concrete abutments have been assigned as condition ratings of 2, 3, and 4 as shown in Figure 2.13 (a), (b), and (c) , as well as, Figure 2.14 (a), (b), and (c) respectively.

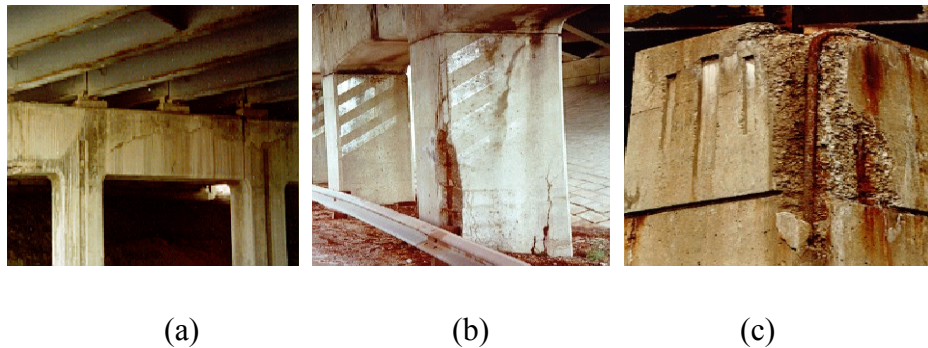


Figure 2.13: (a) Condition States 2, (b) Condition States 3, and (c) Condition States 4 of bridge columns (Pontis Bridge Inspection Manual, 2009)

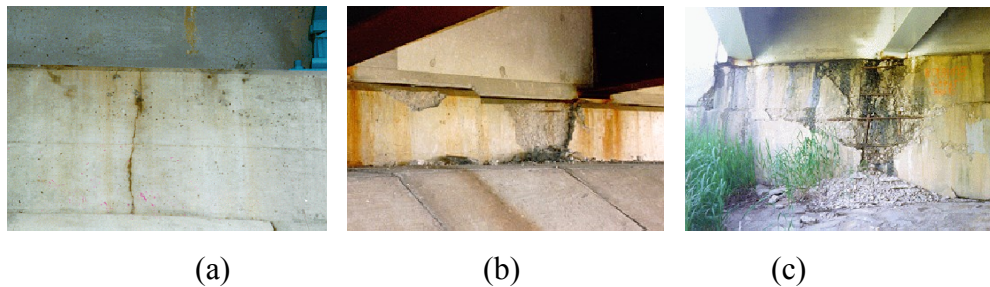


Figure 2.14: (a) Condition States 2, (b) Condition States 3, and (c) Condition States 4 of bridge Abutments (Pontis Bridge Inspection Manual, 2009)

The Bridge Inspector's Reference Manual suggests collecting the photographs of the defects highlighting the degrees of deterioration reflected on bridge components during the data collection required for BMS through visual inspection techniques (FHWA, 2006). However, such images are not usually utilized for analysis of the defects. The thesis

proposes the application of digital images in evaluating element condition rating which can assist in improving the reliability of visual inspection.

2.4.3 Bridge Performance Indicators

Several types of bridge performance data are measured against defined assessment criteria such as condition assessment, seismic assessment, loading assessment, and scour assessment for a particular bridge element. Ghasemi et al. (2009) expressed the idea of ideal bridge should have the following characteristics: a) minimal hazard to users and minimal traffic obstruction, b) minimal negative impact on the local and global environment, c) pleasing appearance, and d) minimum whole-of-life cost. A summarized version of bridge performance issues is expressed in Figure 2.15.

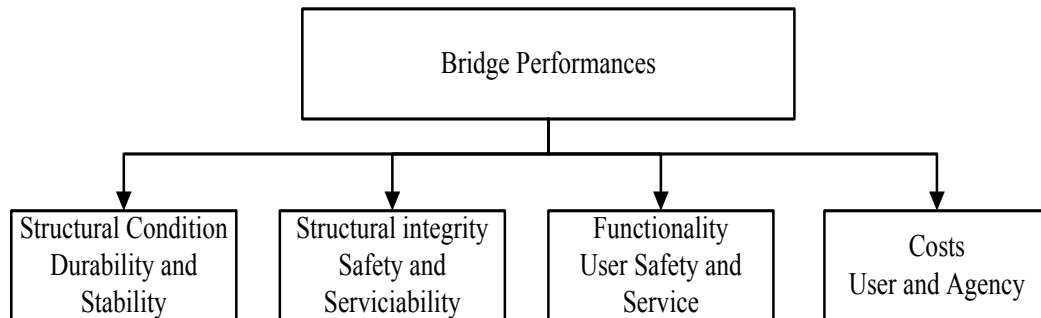


Figure 2.15: Bridge Performance Framework

After determining the individual performance of bridge components by assigning their condition rating based on the extent and severity of defects, the individual element rating

is again combined together to evaluate an integrated bridge performance by assigning a number from 0 to 100. The PONTIS software uses performance indicator as Bridge Health Index (HI), whereas the Ontario and Australian BMS use Bridge Condition Index (BCI) (Thompson & Shepard, 1994; OSIM 2000; Austroads, 2002).

Mathematically, HI can be defined as the ratio of the current element value to the initial element value summed for all elements of a bridge as expressed by equation 2.1 (Roberts & Shepard, 2000).

$$\text{Health Index} = \left\{ \frac{\sum \text{CEV}}{\sum \text{TEV}} \right\} \times 100 \quad 2.1$$

where: Total Element Value (TEV) = Total element quantity * Failure cost of element (FC), Current Element Value (CEV) = $\sum (\text{Condition State}_i * \text{WF}_i) * \text{FC}$, and the condition state weight factor (WF_i) can be expressed as:

$$\text{WF}_i = [1 - (\text{Condition State} \# - 1) * (1 / \text{Total State Count} - 1)] \quad 2.2$$

When maintenance and rehabilitation actions are performed, the HI is likely to be increased for that element since corresponding asset value of the element will be increased. Figure 2.16 below represents the ranking of defects corresponding to the health index (Roberts & Shepard, 2000).

| | | | | |
|---|---|---|--|---|
|  |  |  |  |  |
| Health 100 | Health 90-99.5 | Health 80-89.5 | Health 70-79.5 | Health below 70 |

Figure 2.16: Bridge Health Index

The bridge Health Index (HI) is an important measure in accessing the condition of overall rating of bridges. If any one of the bridge components fails, then the component needs to be treated separately as a critical defect in bridge which requires immediate action without any delay. HI can be used for managing budget in a long term planning of assets.

The Bridge Condition Index used by Ontario BMS combines inspection information into a single value. The ministry of transportation of Ontario uses the bridge condition index for repair and maintenance planning purpose, and not for bridge safety purpose. If there is a question of safety of a bridge, immediate actions are required to maintain the bridge. The Bridge Condition Index (BCI) is evaluated in similar way as Bridge Health Index, but the BCI utilizes the replacement value of an element instead of an element failure cost shown in Equation 2.3 (Hammad et al. 2007).

$$BCI = (\text{Current Replacement Value} / \text{Total Replacement Value} * 100) \quad 2.3$$

Table 2.6 below highlights the performance indicator of bridges based on Bridge Condition Index obtained from element replacement value (Ontario Bridges, 2013).

Table 2.6: Bridge Condition Index (Ontario Bridges, 2013)

| Ontario BCI | Performance |
|-------------|-------------|
| 70 - 100 | Good |
| 60 - 70 | Fair |
| < 60 | poor |

CSS Bridge Group in UK developed Bridge Condition Score which had the scale as the Element Condition Score ranging from 1 (Best) to 5 (Worst). However, the scale was considered to be difficult to understand and confusing for those outside the engineering community. Hence, a Bridge Condition Index (BCI) was introduced with a scale ranging from 100 (Best) to 0 (Worst) (Bridge Condition Indicators, 2002).

$$BCS = \frac{\sum (BCI * EIF)}{\sum EIF} \quad 2.4$$

where: BCI = Bridge Condition Index derived from the following relation.

$$BCI = ECS - ECF$$

where: EIF = Element Importance Factor, and ECF = Element Condition Factor. Although, the above equations hold good for evaluating Bridge Condition Score, the critical elements need to be treated separately in order to prevent sudden failure of bridge components.

2.5 Digital Image Processing

Digital images have been proved to be very effective for condition assessment of concrete structures because magnified digital images are possible to acquire through the recent advancement in camera technology. However, the acquired digital images need to be

processed in order to derive meaningful or useful information required for a particular application. A number of useful techniques for image processing are: pre-processing, segmentation, edge detection, dilation, and image representation (Gonzalez et al., 2009). Some of the important image processing steps are described in the next sections.

Point and Line Detection

Image analysis is a fully developed area of computer science; however, the application in civil engineering has been growing fast since past decades. The application of image in civil engineering provides quantitative information on objects contained in an image frame, which enabling engineer's confidence in the decision making processes. Since the process can be automated using computer vision application, several complex engineering problems have been solved in the past (Moselhi and Shehab-Eldeen 1999a, 1999b, 2000, Shehab-Eldeen 2001, Weil 1998, Ritchie et al. 1991, Chen and Abraham 2001, and Chen and Chang 2000). Image segmentation is the most important task in machine vision approaches. It can be handled by sub-dividing a given image into its different constituent objects so that high level machine vision analysis can be performed to extract desired information. The segmentation approach requires identifying points, lines, and edges (Gonzalez et al., 2009). These attributes can be obtained by mask processing techniques as illustrated in Figure 2.17.

| | | |
|----|----|----|
| -1 | -1 | -1 |
| -1 | 8 | -1 |
| -1 | -1 | -1 |

Figure 2.17: (a) A Mask for Point Detection

A mask operation can be defined by the Equation 2.5:

$$R = \sum_{i=1}^9 w_i z_i \quad 2.5$$

For point detection, the mask used is shown in Figure 2.17, where the center pixel contains the number 8 and neighbouring pixels contain the number -1. An isolated point is detected if the corresponding value of $|R|$ as shown in Equation 2.5 is greater than T (i.e. $|R| > T$), where T is non-negative threshold value, R is the sum of product of coefficient within the mask region, and then the point is said to be detected.

Similarly, after the detection of points, lines can also be detected. The above mask as shown in Figure 2.18 (a, b, & c) can be used to detect the lines lying on horizontal plane, + 45 degrees, and - 45 degrees.

| | | |
|----|----|----|
| -1 | -1 | -1 |
| 2 | 2 | 2 |
| -1 | -1 | -1 |

(a)

| | | |
|----|----|----|
| -1 | -1 | 2 |
| -1 | 2 | -1 |
| 2 | -1 | -1 |

(b)

| | | |
|----|----|----|
| 2 | -1 | -1 |
| -1 | 2 | -1 |
| -1 | -1 | 2 |

(c)

Figure 2.18: (a) A Mask for Line Detection a) Horizontal, b) + 45 Degrees, c) -45 Degrees,

Edge Detection

In digital images, edges show drastic change in the gray level intensities. To determine the change in the gray level intensities, the first and second derivatives of the intensities need to be determined for a given image profile. Since the second derivative is very sensitive to noise, it is normally used to locate the crossing points which identify the zero intensity points. In order to find the first derivative of an image $f(x, y)$, the gradient vector (∇f) is calculated as shown in Equation (2.6).

$$\nabla f = \begin{pmatrix} G_x \\ G_y \end{pmatrix} = \begin{pmatrix} \frac{\partial f}{\partial x} \\ \frac{\partial f}{\partial y} \end{pmatrix} \quad 2.6$$

and the magnitude of this vector is given by

$$\nabla f = \text{mag}(\nabla f) = \{G_x^2 + G_y^2\}^{1/2}$$

There are a number of operators developed for computing the image gradient for edge detection. The Prewitt Edge Operator (Figure 2.19) finds the image gradient operators i.e. G_x and G_y in order to compute the strength of edge detection; and another operator called Sobel Edge Operator is defined by two masks horizontal and vertical as shown in Figure 2.20 (Gose et al. 1996, Russ 1992; Batchelor and Whelan 1997).

| | | |
|----|----|----|
| -1 | -1 | -1 |
| 0 | 0 | 0 |
| -1 | -1 | -1 |

| | | |
|----|---|----|
| -1 | 0 | -1 |
| -1 | 0 | -1 |
| -1 | 0 | -1 |

Figure 2.19: Prewitt Edge Operators (Horizontal & Vertical)

| | | |
|----|----|----|
| -1 | -2 | -1 |
| 0 | 0 | 0 |
| -1 | 2 | -1 |

| | | |
|----|---|----|
| -1 | 0 | -1 |
| -2 | 0 | 2 |
| -1 | 0 | -1 |

Figure 2.20: Sobel Edge Operators (Horizontal & Vertical)

It has been found that Sobel edge operator performed better than Prewitt edge operator because Sobel operator takes care of noise by averaging the image intensities, whereas

Prewitt does not consider noise components (Gonzalez et al., 2009). Similarly, the second derivative operator can be found by Laplacian Operator which is given by Equation 2.7.

$$\nabla^2(f) = \left\{ \frac{\partial f^2}{\partial x^2} \right\} + \left\{ \frac{\partial f^2}{\partial y^2} \right\} \quad 2.7$$

Since Laplacian Operator is very sensitive to noise, it is not used for edge detection. However, the effect of noise can be reduced by first operating with Gaussian Operator which is called Laplacian of Gaussian (LoG Operator). The LoG mask in two dimensions is shown in Figure 2.21.

| | | | | |
|----|----|----|----|----|
| 0 | 0 | 0 | 0 | 0 |
| 0 | -1 | -2 | -1 | 0 |
| -1 | -2 | 16 | -2 | -1 |
| 0 | -1 | -2 | -1 | 0 |
| 0 | 0 | -1 | 0 | 0 |

Figure 2.21: Laplacian of Gaussian (LoG) Mask

Edge Linking and Threshold

Due to various reasons, the edges of an object operated by Sobel Edge Detector are not continuous. However, the edge linking operations can be done by either local edge linking or global edge linking processes. The local processing is based on a similarity measure defined by the strength and direction of the detected edge (Gonzalez et al., 2009). In practices, the detected edges are not continuous due to non-uniform illumination and the presence of noise. So, the next step requires the disconnected edges to be linked together forming continuous edges. One of the popular methods used for linking the edges is called Hough Transform which is defined as mapping from spatial domain to parametric domain. Figure 2.22 shows the mapping of a straight line AB in spatial domain to a point P in parametric domain, and mapping of a point in spatial domain to a straight line in parametric domain.

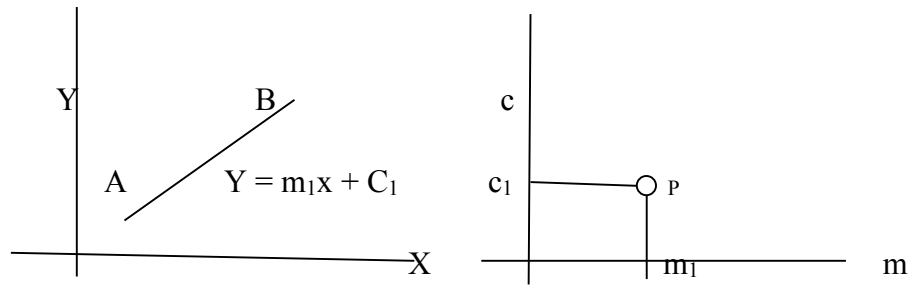


Figure 2.22: Hough Transform a line AB to A Point “P”

To avoid the situation of infinite slopes in spatial domain, a polar coordinate system can be used instead of rectangular a coordinate system. A straight line among any points can be drawn or detected by Hough Transform by selecting the parametric values which corresponds to the intersection points in the parametric domain (Gonzalez et al., 2009).

In digital image processing, thresholding is the simplest way of image segmentation. During thresholding process, all the image pixels greater than threshold value are called “Object”, and all the image pixels less than threshold are called “Background”. Generally, objects pixels are assigned a value of 1, and background pixels are assigned as 0. In case of bi-model histogram, it is very convenient to automate the process of deterring the threshold value by analysing the histogram of images as shown in Figure 2.23.

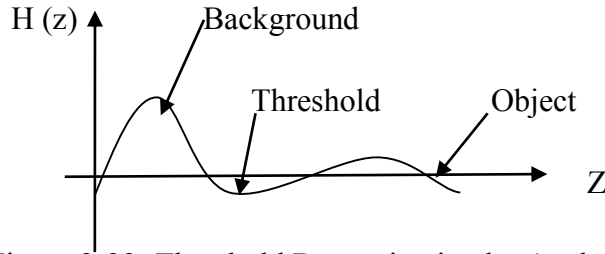


Figure 2-23: Threshold Determination by Analyzing Histogram

Figure 2.23 demonstrates the histogram plot of an image, where the threshold image can be mathematically represented by Equation 2.8. In the case of multimodal histogram, more than one objects need to defined to isolate from image background.

$$g(x,y) = \left\{ \begin{array}{l} \text{Object (1) = if } (x,y) \geq T \\ \text{Background (0) = if } (x,y) < T \end{array} \right\} \quad 2.8$$

As explained above, the threshold is not only dependent on pixel intensities, but also it is dependent on pixel location and local properties in a neighbourhood. Hence, the threshold can be defined as a function of three parameters as shown in Equation 2.9 (Gonzalez et al., 2009).

$$T = T\{ (x,y), f(x,y), p(x,y) \} \quad 2.9$$

where, (x, y) = Pixel Location, $f(x, y)$ = Pixel intensities, and $p(x, y)$ = Pixel local properties in the neighbourhood. Depending upon above three parameters, the threshold could be Global, Local or Adopting threshold value. The three types of thresholds are defined in Equation 2.10.

$$T = \left\{ \begin{array}{l} \text{Global Threshold} = T(x,y) \\ \text{Local Threshold} = T < p(x,y), f(x,y) > \\ \text{Adoptive Threshold} = T < (x,y), f(x,y), p(x,y) > \end{array} \right\} \quad 2.10$$

Global thresholding can be easily automated based on histogram analysis as it is not dependent on pixel location. However, in the real life, the global thresholding may not be applicable for a given image due to non-uniform variation of the pixel intensity. In such a case, the global threshold will fail and an Adaptive/Dynamic threshold operation may need to be applied.

2.6 Measuring Shapes

Dryden and Mardia (1998) defined “shape” as all the geometric information that remains when the location, scale, and rotational effects are filtered out from an object. However, describing the images with a few numbers of parameters or metrics is a challenging task (Neal and Russ, 2012).

Traditionally, man-made objects can be easily classified using the geometric parameters such as, area, length, and perimeter based on the Euclidean geometry. These 2D features are well developed for image interpretation and can be calculated using mathematical modeling (Ghosh and Deguchi, 2008). However, these features are not suitable for natural defects occurring in bridge decks because of irregular size and wide range of variability in texture patterns. Problem also arises when working with a large number of individual images which have been photographed at different locations (Nishimura, 2012). It is not possible to work with individual images in finding their locations and image scales. This

thesis discusses the features which are invariant to translation, rotation, and scale manipulation in describing objects.

The shape of an object is primarily controlled by the material characteristics, processing and history, and environmental effects. The shape of an object changes at different point of time. The shape metric extracted using the image analysis can be useful to determine the behavior of an object and compare the change in a bridge element determined from inspection, which is the major focus area of this work.

Loncaric (1998) explained that finding few metrics for describing shape is an important goal for computer vision approach. However, the selection of the best set of few metrics that will provide adequate uniqueness and show correlation with human intuition is a complex task. Figure 2.24 describes different types of shape descriptors based on either the entire perimeter or the entire area. Some features allow reconstructing the original image completely and others do not. The choice of descriptors depends on a particular application. However, for this work, the methods which produce a few set of shape numbers and are invariant to image manipulations are selected for change detection. In the past, several feature vectors had been chosen for quantification of defects contained in digital images. Some of the feature vectors extracted from digital images for defect representation have been discussed briefly.

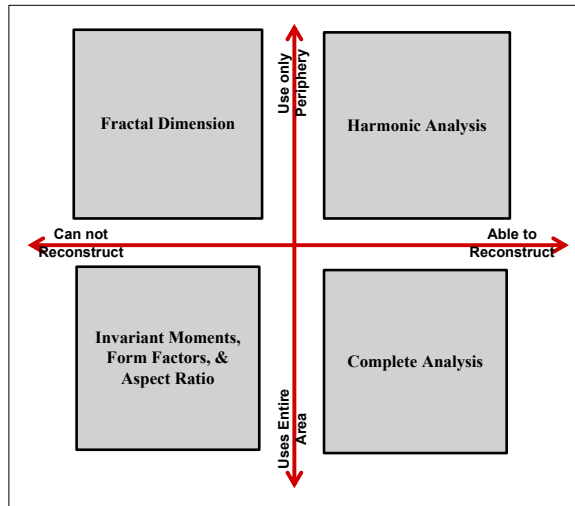


Figure 2.24: Shape Descriptors (F. B. Neal & J. C. Russ, Measuring Shape)

2.7 Summary

The literature review highlighted the current development in condition assessment of concrete structures using remote sensing applications. It was observed that digital based technology is the best for concrete surface defect quantification purpose. Based on the literature review, three problems are identified to conduct this research. The first problem is to determine the depth of crack in a reinforced concrete beam if a crack width is known. In practices, the concrete beams are concealed and it is a challenging task to measure the depth of cracks. For this problem, this research develops crack detection and quantification models based on digital images. The second problem is to develop an automated prediction of condition rating tool for bridge elements based on severity and extent of defects. For this problem, digital images are suggested to use for defect data collection associated with bridge elements. And the last problem is to investigate the propagation of defects with change in time periods. Such tracking of defects will show that when and how the financial budget need to be spent on structures in order to maintain the safe operation. The next chapter deals with the methods how to approach the identified problems.

Chapter 3: Proposed Methodology

3.1 Introduction

The previous chapter on literature review summarized the application and importance of digital image processing to help solving the problems of condition assessment of civil infrastructure (Abudayyeh et al. 2004, and Brilakis et al. 2006). Recent literature clearly demonstrated that the use of high resolution digital cameras provides the best results for defect quantification using non-destructive technology in reinforced concrete bridges (Ahlborn et al., 2010, McRobbie 2008/2009, and McRobbie et al. 2010). However, the application of non-destructive testing technologies for the enhancement of visual inspection in conjugation with the bridge management system needs to be explored further. In current practices of condition assessment of civil infrastructure, digital images and sketches are used to supplement the inspection findings by maintaining photo logs and filling bridge inspection forms similar to one given in Appendix B (BIRM 2012). This thesis aims to integrate the output of digital image processing with bridge management system in order to enhance the reliability of visual inspection by analyzing digital images. The adopted methodology for this research has been explained next.

3.2 Proposed Methodology

The proposed research methodology is shown in Figure 3.1 and the detailed methodology framework which encompasses three modules: digital image processing module, data processing module, and condition assessment module as illustrated in Figure 3.2. The thesis

work started with reading literature on remote sensing application for condition assessment of civil infrastructures. During literature review, it was found that there is a need for improved method of data acquisition and interpretation for enhancing the reliability of visual inspection process for bridge condition assessment. This thesis proposes several modules which have been described in brief here.

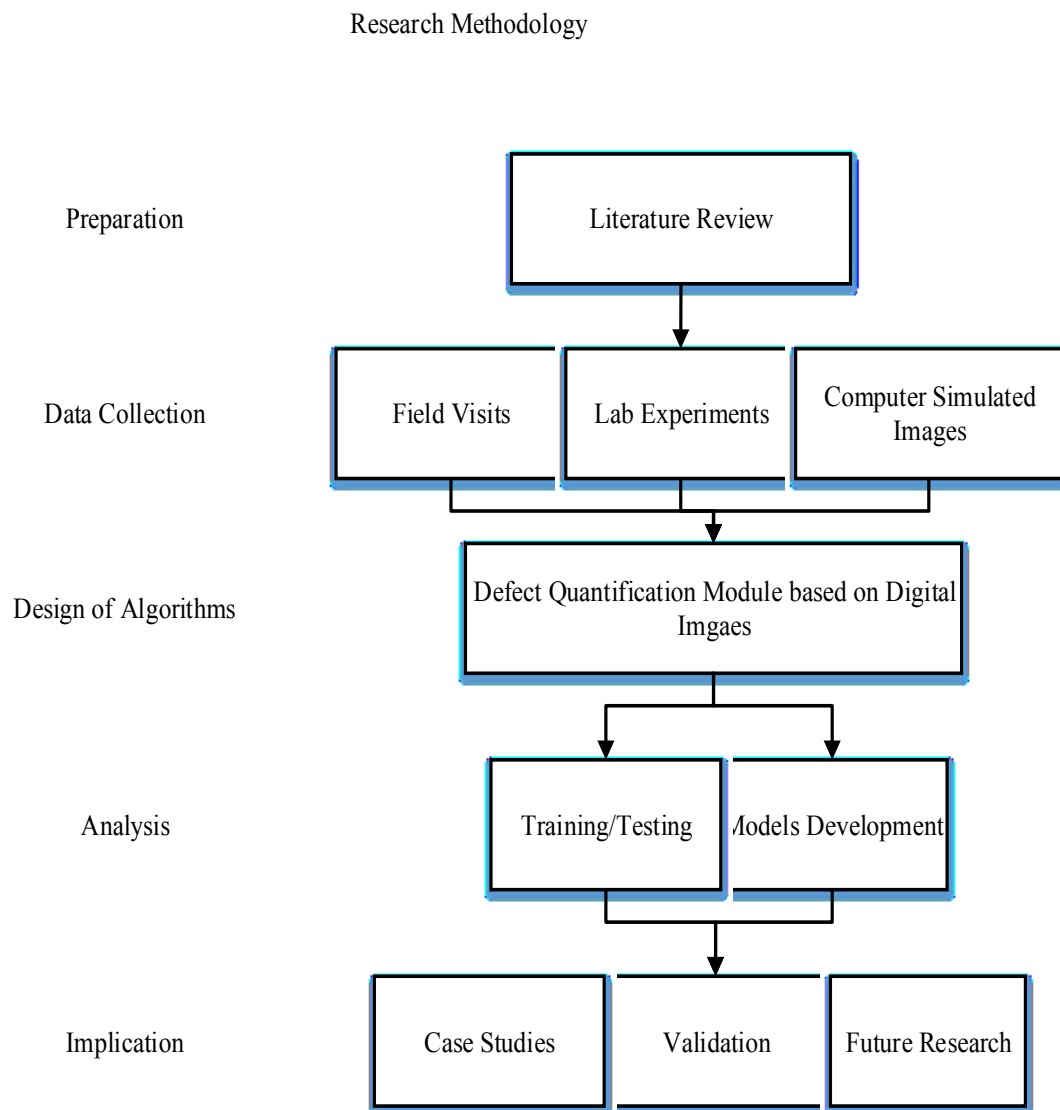


Figure 3.1: Research Methodology

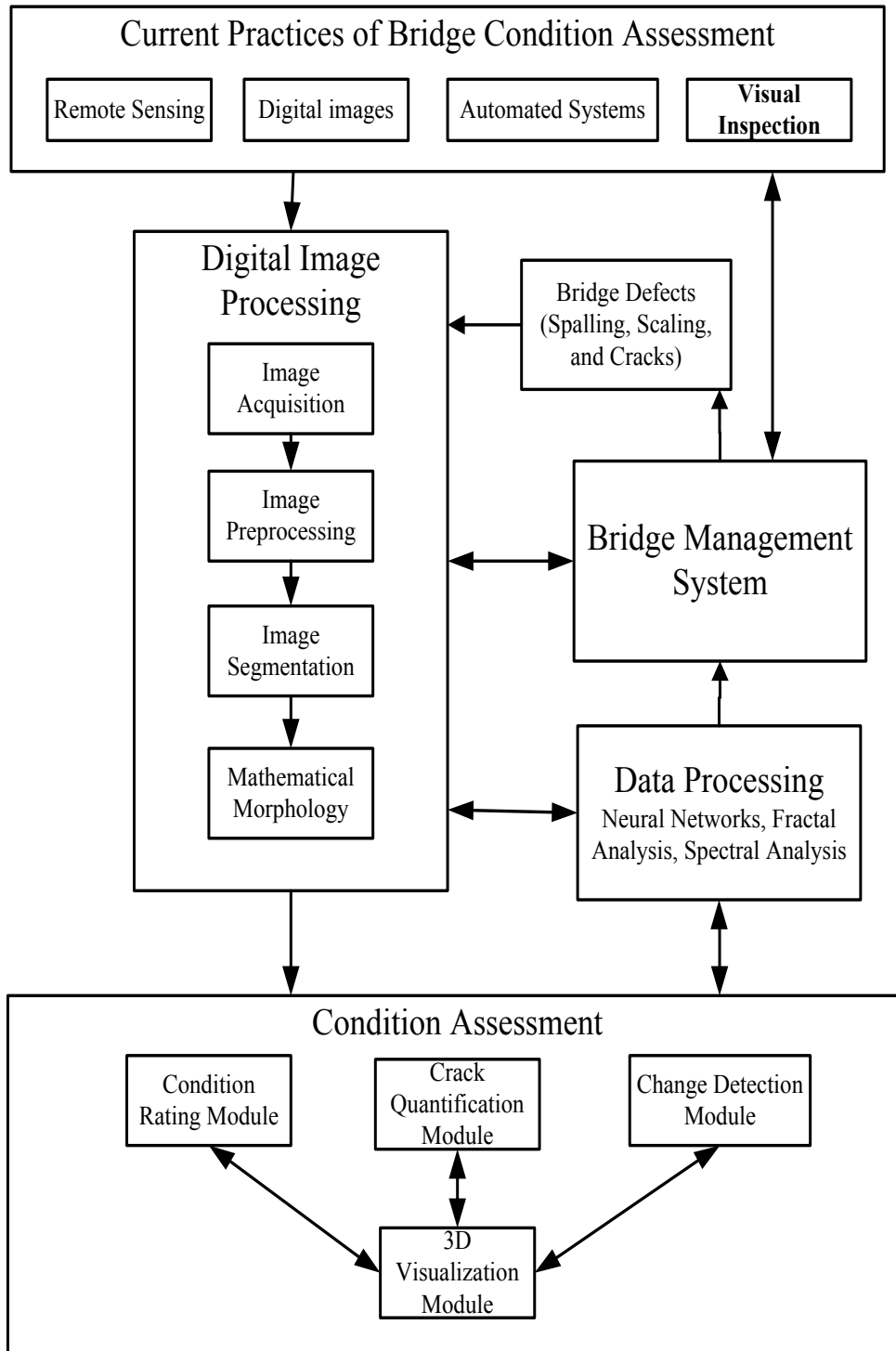


Figure 3.2 : The structure of the proposed Framework

To develop the proposed methodology, the thesis considers three types of major defects associated with reinforced concrete bridge decks and supported beams. The first type of defects considered here is cracking of concrete surfaces which show crack patterns due to material failure or other reasons.

For reinforced concrete beams and decks, crack widths of less than 0.3 mm (0.01 in.) have little consequence in terms of overall corrosion of reinforcing steel (Houston et al. 1972, Ryell and Richardson, 1972). When the width of a crack is more than 0.3 mm, the chance of corrosion increases in reinforcing steel leading to concrete spalling. Any concrete cracks wider than 0.9 mm (0.035") require to be maintained by contractors according to Colorado Department of Transportation in USA (0.035") (Yunping et al. 2003, OSIM 2008). The second type of defects considered in this thesis is spalling which is an issue with the concrete surfaces resulting from the loss of concrete material due to delaminations in the concrete decks. The third type of defects considered is scaling defined as loss of deck surface due to physical or chemical material properties. The magnitude of scaling defect varies from 1/4 inch to 1.5 inch in depth for demonstration of the proposed methodology.

3.3 Field and Lab Data Collection

Generally, bridge locations are inaccessible due to traffic movements, river crossing, train crossing, tunnels, and many more to list. However, to demonstrate a real bridge example, the easy accessible overpass bridge site at the intersection of Selby Street and Greene St.

in Montreal was selected to collect photographs of the bridge as shown in Figure 3.3. Only a small portion of the overpass was modeled to illustrate the application of digital image processing for defect quantification. Based on visual inspection in the selected portion of the overpass, the condition rating was assessed to be 2 based on observation that the area of spalling is less than 2 percent for the entire deck soffit. The elevation of the overpass has been shown in Figure 3.4.

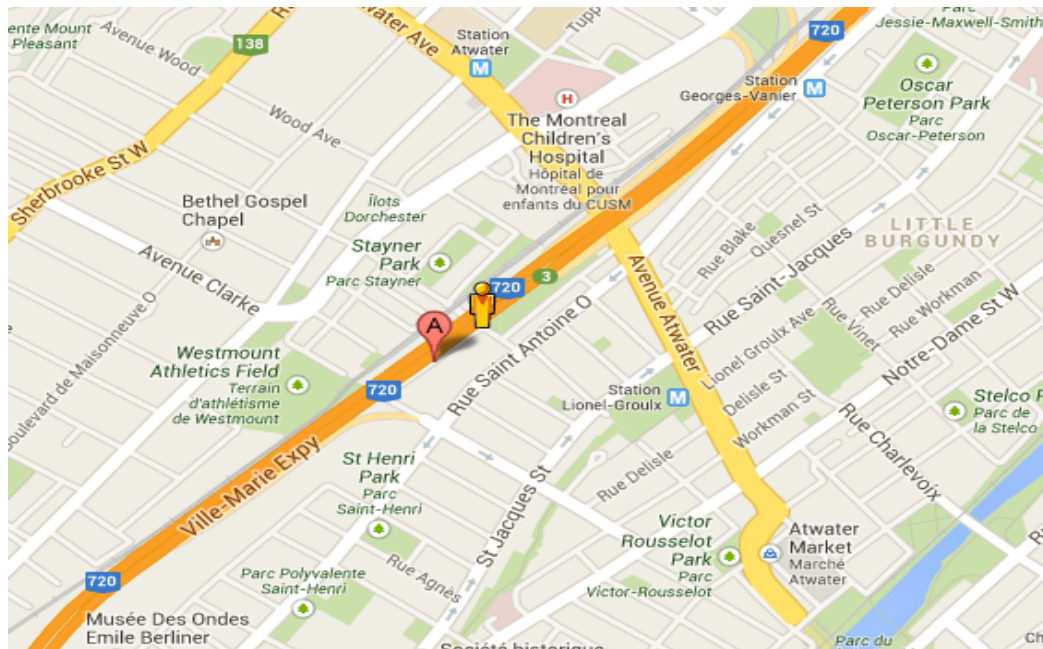


Figure 3.3: The location of Bridge Site for Field Demonstration



Figure 3.4: The Elevation of a Bridge Overpass

To illustrate crack quantification and change detection approach, several digital images were also collected during lab experiments designed for bending test of reinforced concrete beams as illustrated in Figure 3.5. For this experimental study, the design of reinforced the concrete beam was done by Rahmatian (2014) and the flexural testing was conducted at the Structural Engineering Laboratory at Concordia University. As of the present thesis, the crack patterns and their progression were monitored using crack scale and digital imaging.

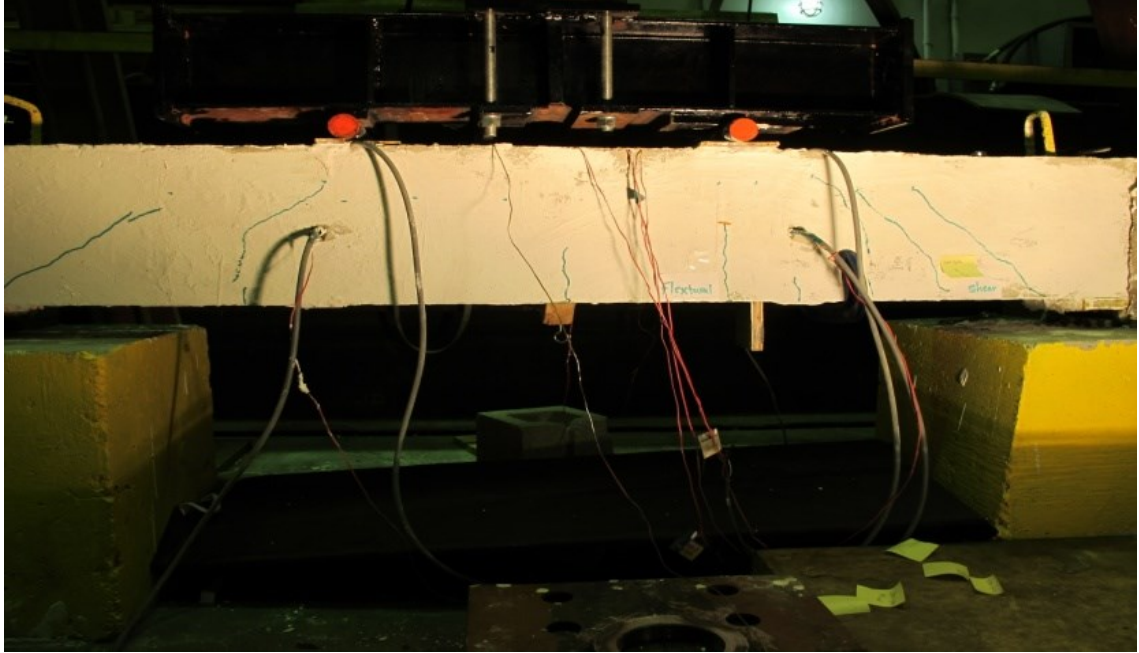


Figure 3.5: Images form Lab Observations

For image data acquisition, portable Sony cameras have been as used shown in Figure 3.6. For defect quantification, high resolution images are necessary with sufficient overlapping so that image stitching can be performed to get a single detailed image (Brown and Lowe, 2007). As far as possible, the high resolution digital images are taken orthogonal to surface of interest so that error due to camera manipulation can be minimized. The methodology also requires a single image showing entire face of a bridge element in order to build 3D model for bridge components to simulate on-site visual inspection. In order to accelerate the process of image acquisition, a framework of hybrid camera can be used. The hybrid camera consists of two cameras: one focusing on capturing the entire surface and another focusing on defects only. The details of using hybrid camera for image acquisition have been discussed in details by Nishimura et al. (2012).



Figure 3.6: Cameras used in for Image Acquisition

Targets

The dimension of objects in an image frame cannot be determined without a real world coordinate system with known scale. The image scale can be established by placing a target of known length in the image frame while performing photography. Generally, an artificial scale or natural scale can be included in image frames to highlight the object of interest, and also for image quantification purpose (Jáuregui et al. 2006). The natural objects such as sharp corners of beams and any visible objects in the image frame can be related to the scale of an image. Similarly, artificial targets are used when sufficient numbers of natural targets are not available. Any kinds of painted rods and colored card boards can be used as artificial targets (Jáuregui et al. 2006). Figure 3.7 shows a piece of paper of width 60 mm used as an artificial target.



Figure 3.7: Artificial Target in the image Frame

3.4 Digital image Processing

3.4.1 Pre-processing

After image acquisition with digital cameras, image pre-processing is necessary for image enhancement because real images contain noise. Noise is the unwanted element present in a picture frame which adds difficulties in processing image algorithms for the automation process. Generally, there are two image enhancement methods that can be applied: spatial domain operation, and frequency domain operations as shown in Figure 3.8 (Gonzalez et al., 2009). Spatial domain operation is divided into three parts based on the particular

needs. They are point processing, histogram based techniques and mask processing. For a particular given image, a combination of image enhancement algorithms may be required to produce representative images.

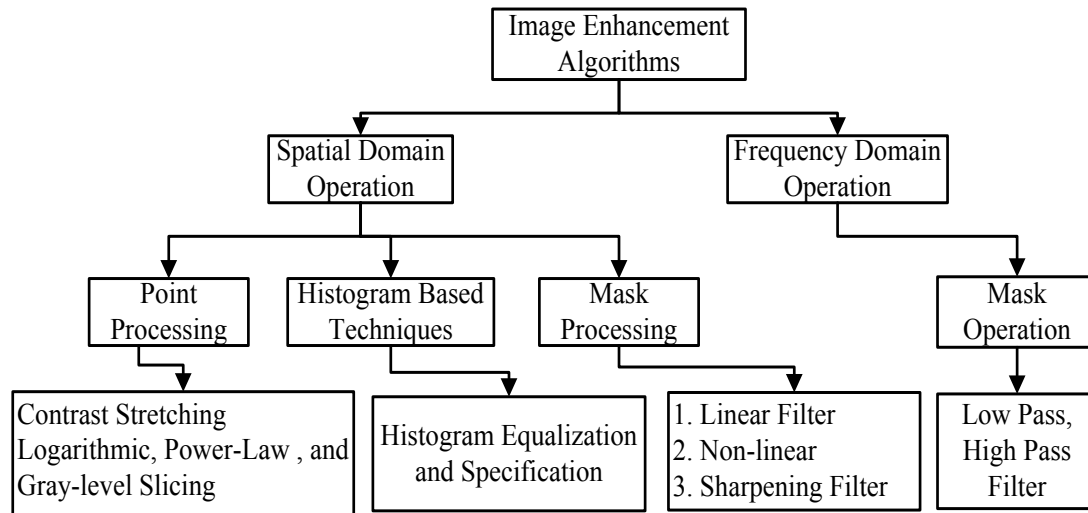


Figure 3.8: Image pre-processing techniques

As explained above, the main image acquisition device used in this research are digital cameras as shown in Figure 3.6. A conventional camera image is a 2D image, which is essentially a projection of 3D world scene. The perspective projection of a real object has been shown in Figure 3.9. The perspective projection of an image has two properties: a) foreshortening – the objects farther away from the viewer appears to be smaller, and line convergence – the lines parallel in the image frame appears to converge at a point (Solomon & Breckon, 2011). The elevation of the overpass bridge depicted in Figure 3.4 after correcting perspective errors has been shown in Figure 3.10. Further details of image pre-processing are described in Chapters 4, 5, and 6.

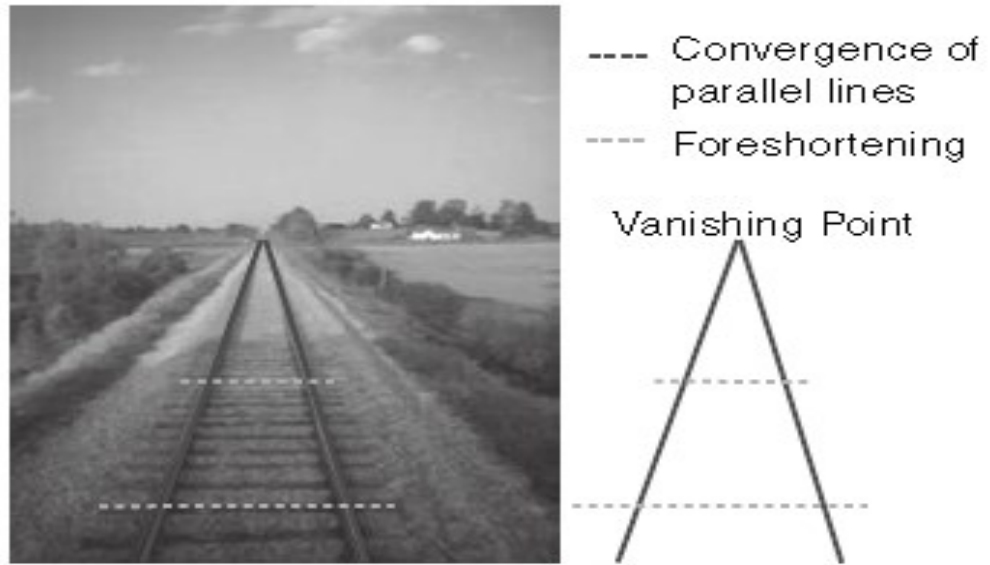


Figure 3.9: Effect of perspective projection model (Solomon & Breckon, 2011)



Figure 3.10: Corrected Image from Perspective Error

3.4.2 Segmentation

Digital images usually contain huge quantity of data with respect to pixel, as well as the intensity level associated with each pixel. However, all information present in an image may not be useful for a solution of a particular problem. Such extra information is called noise and need to be removed through the process of image segmentation. An overview of image segmentation algorithm is explained in Figure 3.11.

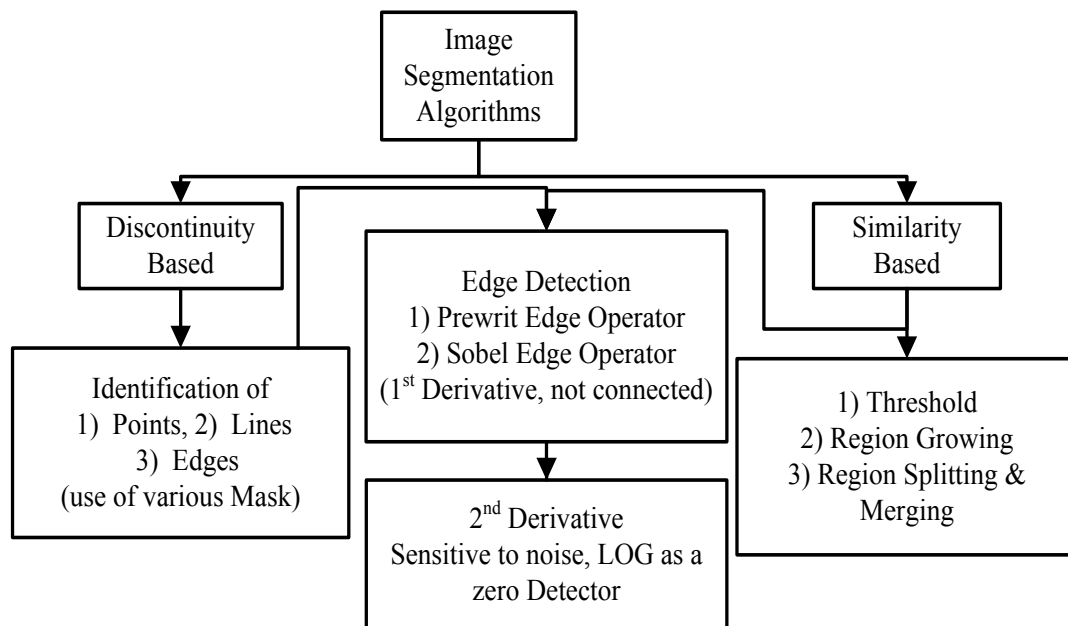


Figure 3.11: Image Segmentation Algorithms (Gonzalez et al., 2009).

Manual setting of threshold is considered to be more accurate than automatic thresholding; however, such process should be avoided, if possible, because different results are likely to be obtained at different time by different people (Russ, 1992). A number of automated thresholding methods have been developed over past decades and a summary of widely used methods can be found in (Parker 1997, Otsu 1979, Sezgin and Sankur 2004). As an

initial segmentation, canny edge detection is applied; however, the segmented result from this operation does not yield satisfactory results (Maini & Aggarwal, 2009). So, a number of additional mathematical morphology operations are designed for proper image enhancement which successfully separates objects and their backgrounds. The process starts with the proper selection of color plane which can better represent the class of defects. The details image segmentation sequences are explained in Chapter 4.

3.4.3 Morphology

The common applications of mathematical morphology in digital image processing can be classified into three groups: a) image pre-processing, for example, noise filtering, and shape simplification i.e. complicated structure can be broken into simple form, b) object quantification by finding out object area, perimeter, and etc., and c) enhancing object structure by dilation, erosion, opening, and closing operations (Biswas, 2008). The erosion, dilation, and their combinations are most widely used morphological operations which are usually processed from binary images (Coster and Chermant 1985, Dougherty and Astola 1999). An example of mathematical morphology is shown in Figure 3.12.

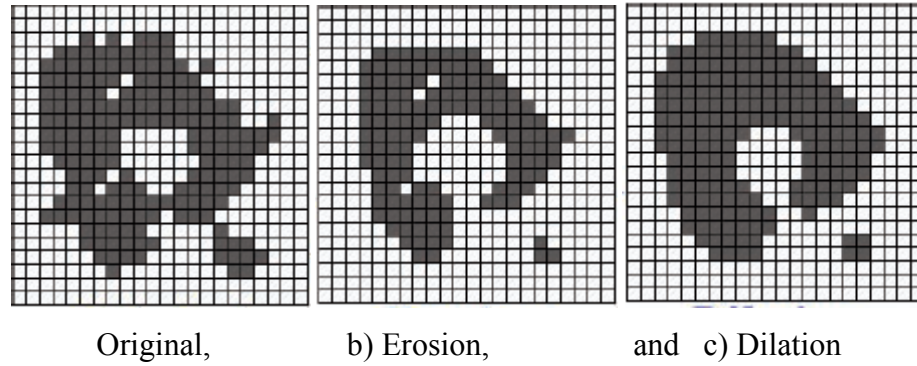


Figure 3.12: Combining Erosion and Dilation Processes (Maini & Aggarwal, 2009).

3.5 Data Processing and Condition Assessment

In this research, neural networks algorithms are used for data processing which is described briefly here.

3.5.1 Neural networks

After obtaining the feature attributes form digital image analysis, the features are processed using neural network to draw meaningful information which can aid in condition assessment of bridge components. Neural Networks were first introduced by McCulloch & Pitts in 1943 (Fausett 1994). They can be used as an effective tool for decision making purpose because they mimic the similar way of how human brain works (Anderson and Davis, 1995). The processes can be automated and the influence of subjectivity can be eliminated, and thus improving the reliability of asset management. Back propagation neural networks are adopted for data analysis for mapping bridge defects into element condition ratings. The superior performance of neural networks for condition assessment

of civil infrastructure has been discussed by several authors (Moselhi et al. 1994, Tamura and Tateishi 1997).

The outcome of neural networks processing is based on distribution of weight which is generally obtained by trial and error method. Although there are some guidelines in choosing initial parameters such as: a) activation and scaling functions, b) numbers of hidden layers, c) numbers of neurons in input, hidden, and output layers, and learning rate and momentum coefficients, the iterative process can only predict the satisfactory performance of mapping models. The details of neural networks design and implementation can be found in Chapter 5. The neural networks model for prediction of condition rating has been illustrated in Figure 3.13.

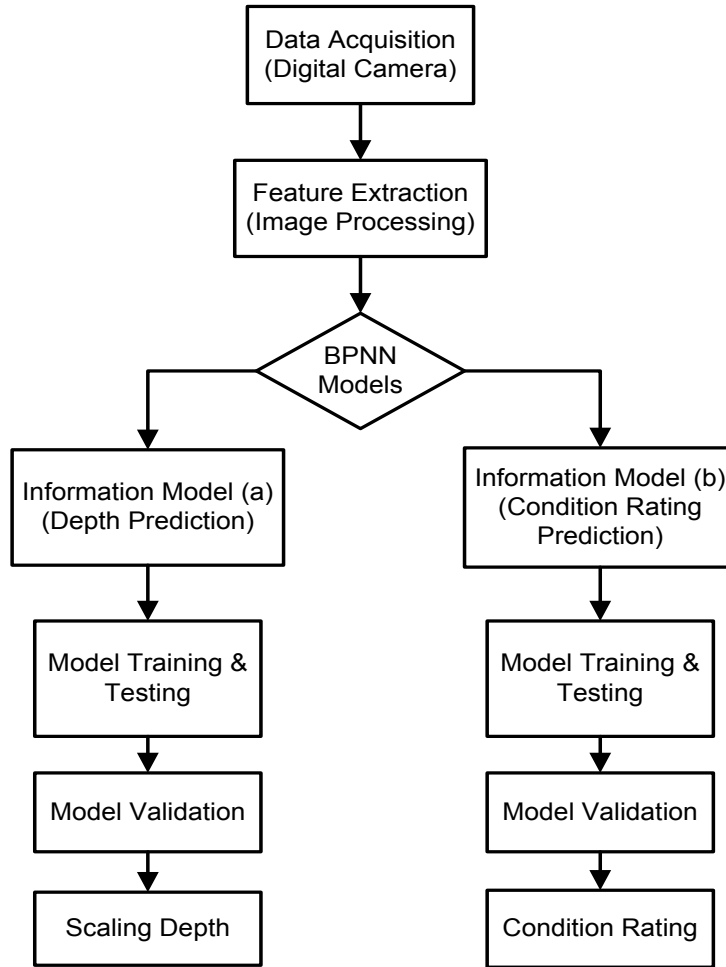


Figure 3.13: Neural Network Model for Condition Assessment (Adhikari et al. 2012a).

3.5.2 Spectral and Fractal Analysis

The changes in defect patterns or in element condition index during visual inspection of bridges are primary concerns for inspectors. This thesis presents a new approach for change detection of defects in bridges by identifying changes in texture patterns through spectral analysis of digital images. The commonly used method for change detection is image differentiation. This subtraction method requires images to be of same size, scale, and

rotation. However, no two images are same in real practice. Thus, image registration is required to align images and to produce change maps. This process is tedious and it is difficult often to achieve a good registered image. But, the change detection task can be readily modeled in frequency domain for texture patterns discrimination and also for quantifying their properties. The novel approach of change detection works by transforming digital images into Fourier spectrum. In new coordinate system, 1-D signature functions can be drawn which facilitates easy comparison of textures in different directions (Adhikari et al. 2013a). Similarly, the fractal analysis describes the surface disorder of defects by finding the fractal dimension (FD) using Box Counting Modeling algorithm. The proposed methodology provides useful tools for comparison of inspection history graphically and quantitatively. In practice, expensive sensors are used to detect subtle change in defect patterns (Adhikari et al. 2013d). The proposed method can be used to detect subtle changes in defect patterns using digital images at much lower cost. Enhanced methodologies of spectral and fractal analyses has been shown in Figure 3.14 and 3.15 respectively.

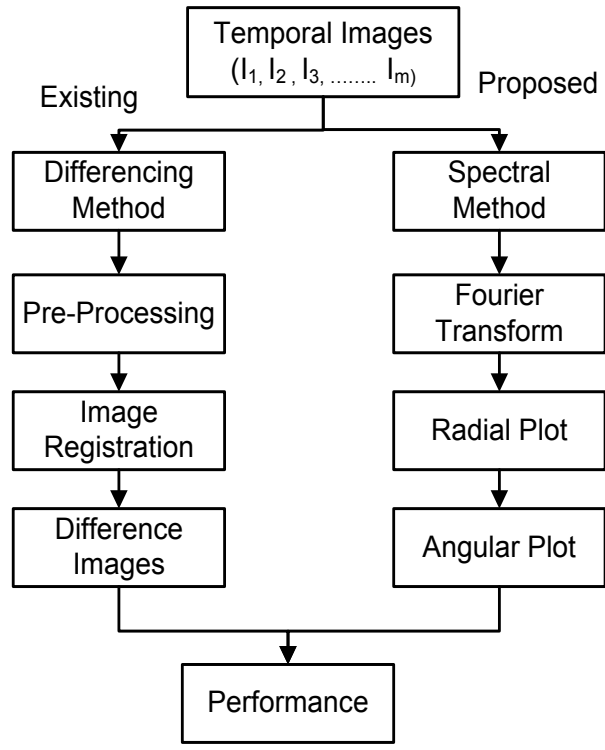


Figure 3. 14: Spectral Analysis of Digital Images (Adhikari et al. 2013a).

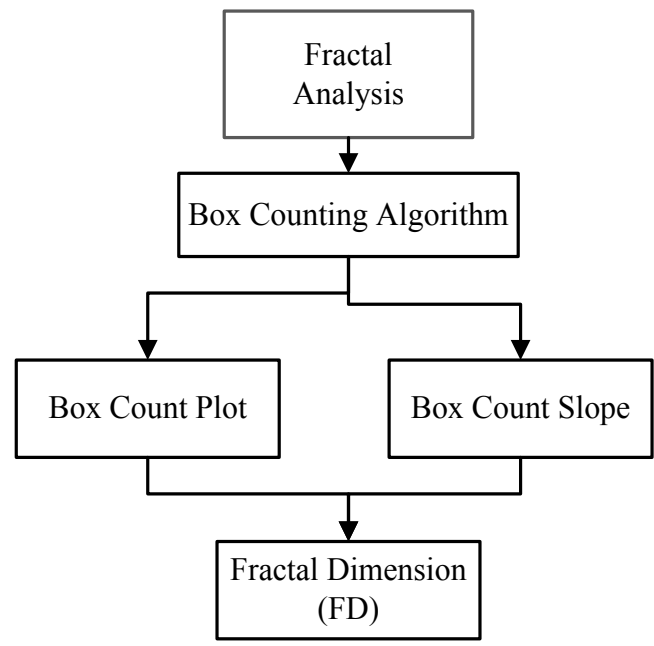


Figure 3. 15: Fractal Analysis of Digital Images (Adhikari et al. 2013d).

The condition assessment of reinforced concrete bridge module consists of three major modules: a) condition assessment based on crack analysis of concrete beams and slabs, b) condition rating assignment based on scaling defects, and c) recommendation based on change detection. The details of condition assessment module with 3D visualization are explained in Chapter 4. This thesis explores the aspect of condition assessment based on surface defects which can be tracked with digital images. In general, condition assessment of bridges depends on any changes in geometric properties of structures, environmental conditions, loading/boundary conditions, and change in material properties. Although the current structure health monitoring methods for bridges use level IV to assess in-service performance of structures with primarily focus on determining the damage extent and location (ISIS 2001), the detailed condition assessment of bridge structures including internal defects are outside the scope of this research.

3.6 Limitations

As outlined in this chapter, as well as described description found in Chapters 4, 5, and 6 along with the lab and field studies, the following limitations are identified during this research.

This thesis develops crack quantification algorithms which have utilized the digital images collected in lab during the bending test of reinforced concrete beams. Considering the camera limitations adopted for this work, the developed algorithms are suitable for the

crack width from 0.3 mm to 0.9 mm. The developed algorithms can be also applicable for crack quantification of hairline cracks provided higher resolution digital camera is used for crack data acquisition.

Another limitation of the quantification module is that most of the digital images are taken in similar environmental conditions. Several digital image processing techniques have used to isolate the required objects from their background. However, the effect of environmental effects on object segmentation has not been studied in this research. During the research, it has been realised that concrete crack detection and quantification problem is also dependent on the texture of the concrete surface.

This research develops a neural networks model for prediction of a crack length given the crack width for a reinforced concrete beam, which is 1.7 m in length having the cross section of 0.25 m x 0.15 m. It was found that the crack width is not directly proportional to the crack length/depth ratio for a given material and beam cross section. The behaviour need to be studied with different beam length with varying cross sections to simulate the real world environment.

The complete condition assessment of concrete structures involves studying more than seventeen defects as mentioned in FHWA (2006). So far, this research proposes automatic predication of condition rating for bridge elements based on scaling defect only. The condition rating model has been developed based on supervised learning of neural networks which is based on OSIM (2008). To develop such rating system for other defects,

it is necessary to have quantitative condition rating mapping information available in inspection manuals either in the form of images or numbers. Unfortunately, the current inspection manuals do not provide such information for all defects except crack, scaling, rusting, and so on. Based on the linguistic information, it is difficult, although not impossible, to develop automated condition rating models.

Chapter 4: Concrete Crack Analysis using Digital Images

4.1 General

The problems of cracking in reinforcement concrete structures are natural and can invite spectacular failure of entire structures (Rizkalla & Shahawi, 1982). There always exist constraints in reinforced concrete structures and hence cracking is unavoidable regardless the types of structures. Cracks not only provide access to harmful and corrosive chemicals inside concrete, but also allow water and de-icing salts to penetrate through bridge decks which can damage superstructures and bridge aesthetics (Krauss & Rogalla, 1996). In spite of significant research in addressing the problems of cracking in bridges, it still remains a challenging problem whether it is an old and newly constructed bridge (Ganapuram et al. 2012). Therefore, a rigorous study towards the evaluation of extent and severity of cracks is necessary for condition assessment of bridges, and to maintain database for bridge inspections for long-term analysis.

This chapter presents an integrated model considering crack as a major defect for condition assessment of concrete bridges in order to enhance the tasks of routine bridge inspection. The proposed integrated model consists of crack quantification, neural networks, and 3D visualization models to represent concrete defects in such a way that it mimics the on-site visual inspection.

Many attempts have been made to enhance traditional approaches of condition assessment of concrete bridges. Abudayyeh et al. (Abudayyeh et al. 2004) proposed a framework for automated bridge imaging system based on digital image processing and integrated with Bridge Management Systems (BMS) PONTIS (Gutkowski & Arenella 1998). The prerequisite to such automated models are the digital representation of defects i.e. the defects or change detection need to be defined numerically to automate the process. Several Non-Destructive Testing (NDT) techniques such as corrosion detection, alkali-silica reactions, and sulfate attacks exist to identify the existence and extent of deterioration in concrete structures in order to understand their behavior (OSIM 2008). However, the detection of extent and severity of internal defects in concrete components is laborious, time consuming, and often may not be reliable. Although this thesis discusses only external defects which can be tracked by digital images or visual observation, the internal defects may not often reflected on the concrete surfaces in the form of scaling, spalling and cracks. Those defects can be identified using Non-Destructive Test or Evaluation (NDT/NDE) and Structural Health Monitoring (SHM) techniques. The concrete surfaces show the combined effects of internal and external defects in the form of surface defects. Out of several defects in reinforced concrete structures, cracks play a vital role in determining the condition assessment of structural elements. For this reason, this work adopts concrete cracks as the major defect parameter for condition assessment of concrete elements. For crack analysis, crack quantification and identification of crack patterns are necessary to reveal the condition of bridges.

Crack width varies at each point along the length of cracks. From practical point of view, a long crack needs to be divided into several small segments and average width of each segment requires to be analyzed separately. The proposed crack quantification model evaluates crack length from crack skeleton perimeter which considers the tortuosity of cracks and the crack segments are obtained by subtracting key marks such as branch points from the crack skeleton itself. The existing work on crack length quantification is based on object-oriented bounding box which does not consider the tortuosity of cracks (Zhu et al. 2011). Also, the crack segmentation approach required searching of crack pixel connectivity. This approach needs input of at least one point to start searching of connected points and matching with orientation angle to decide whether the pixel in question belongs to same group or not (Zhu et al. 2011). If there exists multiple of crack skeletons (unconnected crack regions) in a same image frame, the existing approach of segmentation becomes time consuming. The proposed method is free of such issues. Additionally, the number of branch points serves as a good indicator of condition rating of concrete elements. The increasing numbers of branch points could be an indicator of decreasing integrity of structural elements.

Identification and detection of individual cracks are not sufficient in understanding the structural behavior. It is a challenging task to identify how the crack patterns will develop over time and what will be the severity of cracks on those locations. For this purpose, a method is developed for 3D visualization model of crack patterns measured through crack density defined as the total length of cracks divided by total surface area. Maksymowicz et al. (2011) developed 3D visualization models of defects based on digital image processing.

However, their models were supported by advanced graphical editor software to model defects from photos. The proposed integrated model is supported by 3D visualization of crack density by projecting digital images and neural networks models to predict crack depth necessary for condition assessment of concrete components. With the successful application of the proposed approach, the tasks of routine bridge inspection can be greatly enhanced by merging with automated bridge management systems.

4.2 Crack evaluation in Concrete Structures

The common forms of crack patterns experienced in reinforced concrete structures are longitudinal, transverse, diagonal, crack map, and random cracks (Schmitt & Darwin 1995). Transverse cracks are generally formed perpendicular to longitudinal axis of bridge decks under the transverse reinforced steel. Transverse cracks are typically full depth across sections and cracks spacing are 3-10 feet apart seen along the length of bridge deck (Krauss & Rogalla 1996). Field survey requires identifying the location and orientation of such cracks. Similarly, the cracks running parallel to longitudinal axis are called longitudinal cracks which appear just above the longitudinal reinforced steels. The latter cracks follow the paths of reinforcing steel in structural elements (Curtis & White 2007). Crack patterns also differ from one type of bridges to another. Skewed bridge decks are more prone to diagonal cracks as compared to straight aligned bridges (Feng et al. 2007). Another way of visualizing a crack pattern is Map Cracking. Improper curing and restraining volumetric change of concrete are the primarily causes of Map Cracking (Schmitt & Darwin 1995). There is a lack of appropriate methods for modeling and

visualization of crack patterns that can assist in quick and reliable decision making process. The crack survey described here is as per the protocol developed by the University of Kansas as a part of Pooled Fund TPF -5(051) Construction of Crack-Free Concrete Bridge Decks (Ganapuram et al. 2012, Pooled Fund 2009). The cracks considered in this protocol are greater than 0.2 mm because this size of cracks is visible with the naked eyes. The initial preparation of the deck surface is required before carrying out crack survey. The bridge deck might require cleaning with clear water so that the cracks are visible to the naked eyes. Then, a grid of 5ft by 5 ft. (as reported by Ganapuram et al. 2012) is marked on the deck surface to locate the position and dimension of cracks. This survey data is plotted on CAD drawings and overlaid on structural drawing. The obtained crack map can reveal important distinction between structural and non-structural cracks on the deck surface (Ganapuram et al. 2012). However, this procedure is time consuming and expensive. Hence, a fast and economical way of preparing a crack map using digital image processing is sought for 3D visualization of cracks.

4.3 Proposed Method for Analysis of Cracks

The developed method encompasses structured procedures for image capturing, image projection, crack segmentation, and data fittings by Neural Networks with a 3D visualization of crack patterns as shown in Figure 4.1. A set of algorithms such as crack identification and quantification are designed and developed based on branching concept of cracks. Additionally, a neural network model was developed that maps relationship between crack depth and crack width supported by 3D visualization models.

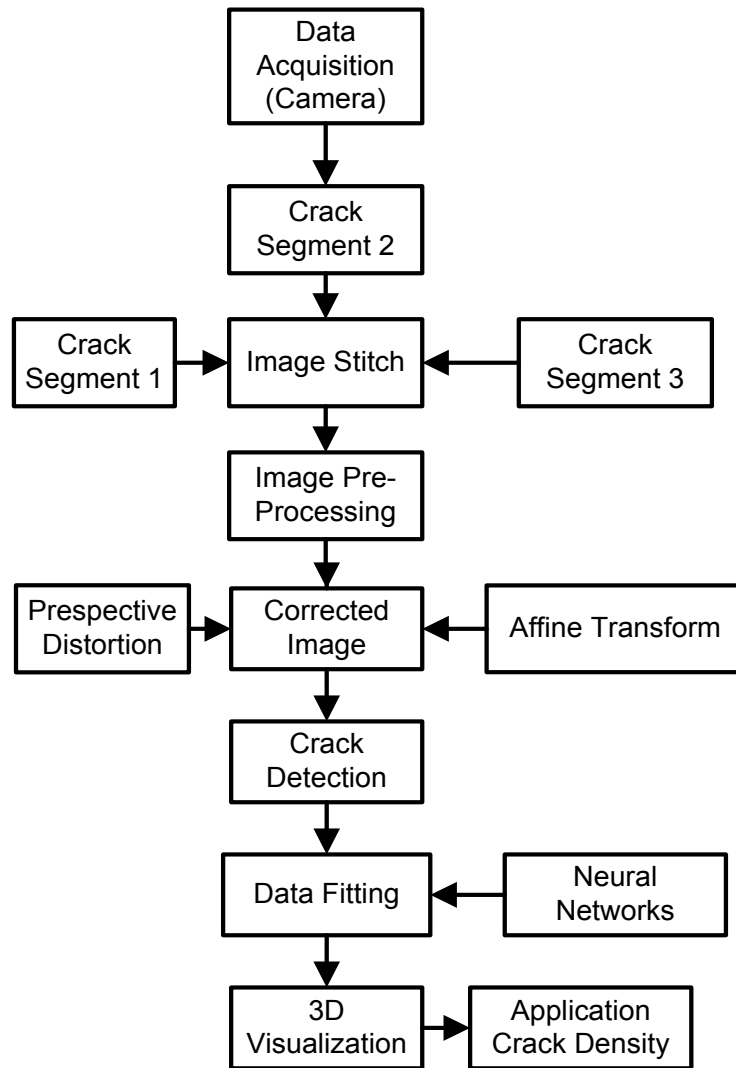


Figure 4.1: Proposed Method for Analysis of Cracks

4.3.1 Imaging Criteria for Data Acquisition

A digital image is 2D projection of 3D real world objects. The effectiveness of digital image analysis highly depends upon how 3D to 2D projections occurs. The image

projections can be broadly classified in two parts: perspective and orthographic projections. The camera coordinate in perspective projection can be defined by Equation 4.1 (Solomon & Breckon, 2011).

$$x = f * X / Z \text{ and } y = f * Y / Z \quad (4.1)$$

where, a 3D real world coordinate is represented by (X, Y, Z) , a camera coordinate is given by (x, y) , and f represents the focal length of a conventional camera as shown in Equation 4.1.

Scheffy et al. (1999) corrected the orientation of original images by removing warp and skew before tracing the cracks properties. Similarly, McRobbie (2008) showed a single pixel in an image taken perpendicularly to surface that would represent a smaller area than the same pixel in an image taken at an angle. Furthermore, the report lists various imaging criteria's such as minimum pixel resolution shall be 1 pixel/mm, camera position, elevation and bearing shall be recorded while taking images, and successive images shall be overlapped for image stitching problems. The orthography projection is defined mathematically by Equation 4.2 (Solomon & Breckon, 2011) as follows.

$$X = m * X \text{ and } y = m * Y \quad (4.2)$$

where, m is called the scaling factors. This projection is an affine transformation in which the relative geometric relationships are maintained. In practice, if the images are acquired

very close to scene, it can be considered as orthographic projection and is suitable for digital image analysis (Solomon & Breckon, 2011). However, in bridge inspection, it is not always possible to acquire images very close to the scene, and they need some sort of transformation to make the images orthographic. In general, a transformation matrix is composed of rotation, translation, and magnification as expressed by Equation (3) (Gonzalez et al. 2009).

$$\begin{pmatrix} x' \\ y' \end{pmatrix} = \begin{bmatrix} A11 & A12 \\ A21 & A22 \end{bmatrix} \begin{pmatrix} x \\ y \end{pmatrix} + \begin{pmatrix} b1 \\ b2 \end{pmatrix} \quad (4.3)$$

Where, x' , y' are the transformed coordinate of points (x, y) .

The coefficients $b1$, $b2$ relate to translation, $A11$, $A12$, $A21$, $A22$ correspond to rotational and scaling parameters.

For affine transformation, all elements of the projection vector is equal to 0. To illustrate the perspective error, synthetic images of different length and width were drawn and the developed algorithms was tested on the images as shown in Figures 4.2a and 4.2b. Figure 4.2a was taken by rotating the image by 10 degrees and Figure 4.2b was taken at 45 degrees. The analysis showed that errors increased significantly, up to 40%, in oblique images.

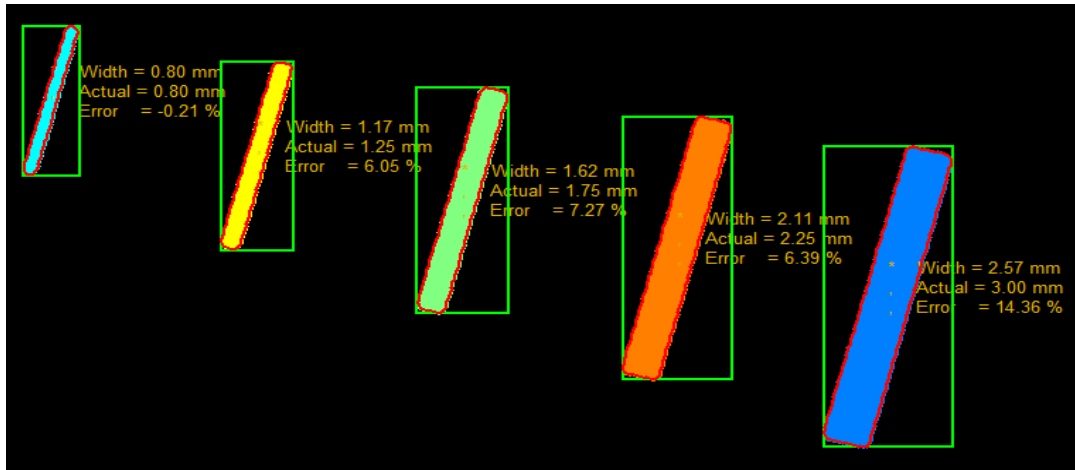


Figure 4.2: (a) Images rotated by 10 degrees

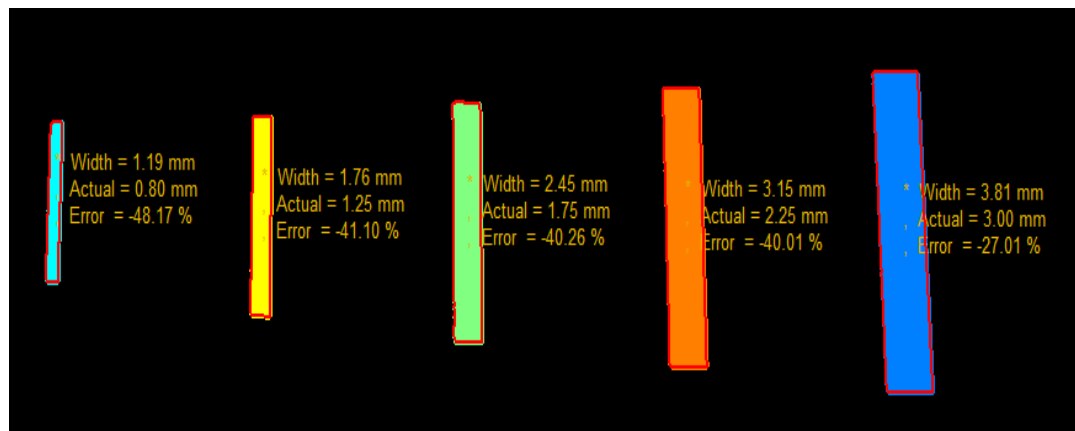


Figure 4.2: (b) Images at 45 degrees (oblique view)

Projective transformation can be considered as a tool to project images on 2D planes such that the geometric relationships within each image are not destroyed. The complete workflow for this projective transformation has been shown in Figure 4.3, based on (Solomon & Breckon, 2011).

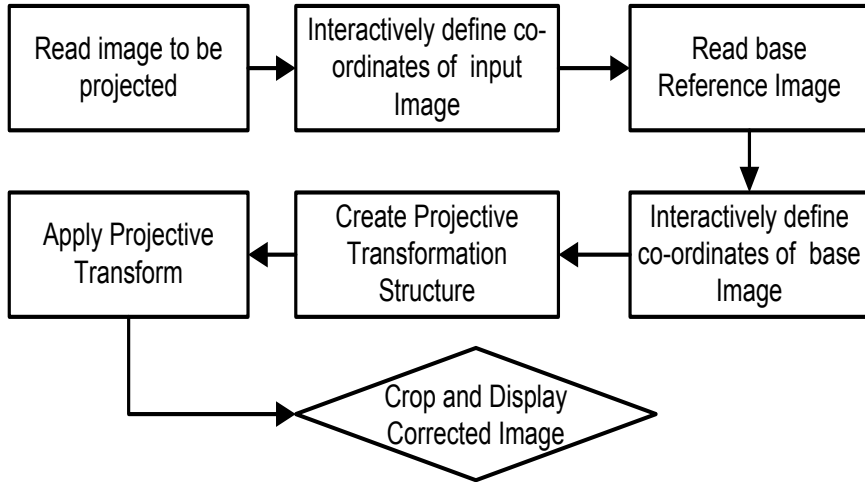


Figure 4.3: Projective Transform Work Flow

The synthetic image displayed in Figure 4.2b was corrected against the perspective error and displayed in Figure 4.4. The errors in crack width calculation from the corrected image are within an acceptable range from inspection aspect of concrete elements in comparison to visual inspection.

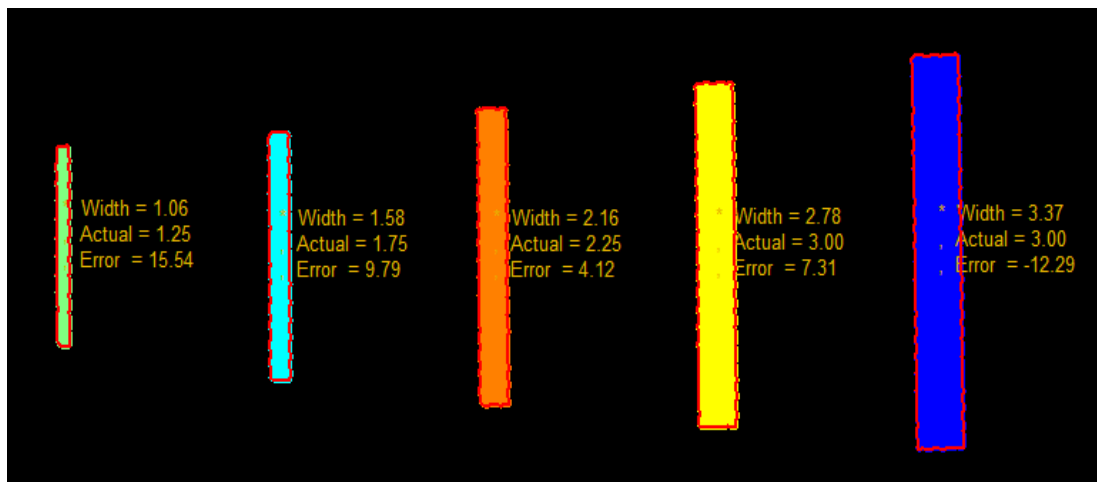


Figure 4.4: Image after Projective Transformation (corrected Image)

The tests on five such synthetic images show that the orthogonal images have the least perspective and parallax errors. The Figure 4.4 shows the estimated width of cracks and the actual width of cracks measured manually. The results show that error increases up to 48% by taking the images at 45 degree angles from horizontal plane (perspective error). In bridge inspection, it is not always possible to take images in orthogonal views and it needs to apply geometric transformations to correct such errors. After applying orthogonal transformation, the error was reduced to below 15% on the test images which is acceptable in many cases for bridge inspection purpose in comparison to visual inspection of bridges shown in Figure 4.4.

4.3.2 Image Stitching

This research adopts the image stitching algorithm developed by Brown and Lowe, 2007. In this process, a set of images of different parts of an object are stitched or combined together based on the invariant features extracted from those images and matching them. This algorithm works on feature-based registration which is invariant to rotation, zooming, and illumination change in input images. The additional details about the image stitching problem can be found in Zhu et al. 2011, and Brown & Lowe 2007.

In this work, each photo frame must include either a natural or artificial target for scale calibration to get pixel value in millimeter. After image acquisition, pre-processing is required for proper image enhancement. Generally, there are two image enhancement methods considered: spatial domain, and frequency domain operations. Spatial domain

operation is divided into three parts: point processing, histogram based techniques and mask processing (Biswas 2013). The adoption of particular algorithm is an application dependent. The preliminary study of image stitching and image preprocessing is explained in Adhikari et al. (2012a).

4.3.3 Discrete Crack Detection and Analysis

Practically, it is not feasible to develop a generic algorithm to extract object properties from digital images (Laptev et al. 2000). There is always human intervention at some point in the automation process and an acceptable level of human intervention shall be defined based on accuracy, efficiency, and repeatability (Paul 2000). The developed algorithms for retrieval of crack properties are shown in Figure 4.5. The process starts with reading digital images and selecting a suitable color plane for crack identification. Then, image preprocessing and image morphology are carried out to find image skeletons and branch points associated with an image frame. After identifying the desired objects in the image frame, objects attributes such as crack length and width are labeled for visualization. The detection and analysis of cracks starts with reading images, exploring red, green, and blue (RGB) color planes and segmenting by suitable edge detection algorithms.

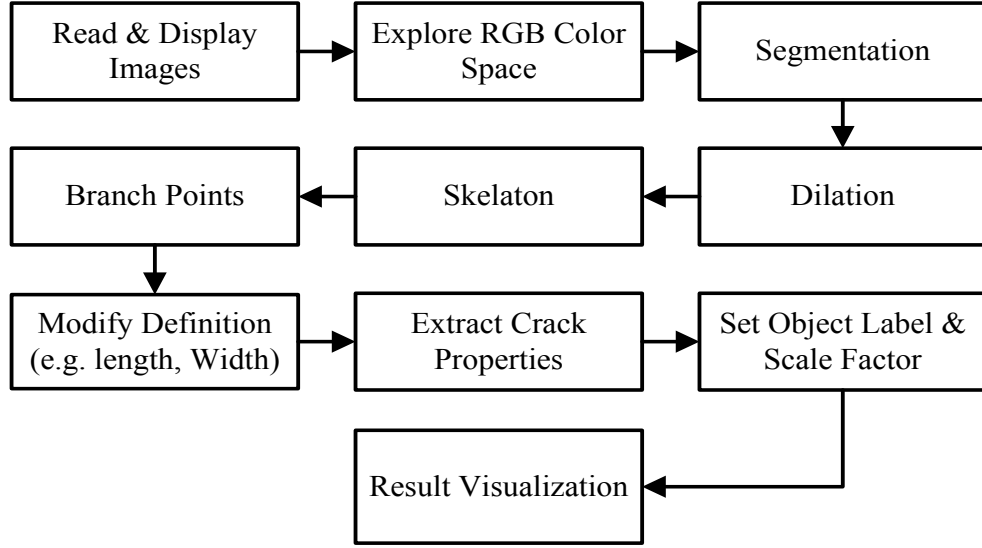


Figure 4.5: Crack Detection Algorithm

4.3.4 Skeletonization of cracks

Skeletonization is an important step to retrieve crack segments which show different paths at their branching points. This can be described mathematically by distance measure in image processing domain (Biswas 2013). In digital domain, the commonly used algorithms for distance measures are Euclidean Distance, D4 distance, City Block distance, Manhattan Distance, and Chase Board Distance. Considering three points $p(x, y)$, $q(s, t)$, and $z(u, v)$, the Euclidean Distance, D4 distance, and D8 distance can be calculated using Equations 4.4, 4.5, and 4.6 respectively (Biswas 2013).

$$D_e(p, q) = [(x-s)^2 + (y-t)^2]^{1/2} \quad (4.4)$$

$$D_4(p, q) = \text{abs}(x-s) + \text{abs}(y-t) \quad (4.5)$$

$$D_8(p, q) = \max[\text{abs}(x-s), \text{abs}(y-t)] \quad (4.6)$$

From the skeleton of an image, the following crack descriptors which can be easily obtained are defined: length of the segment, points of at least 2 branches, points of at least 3 branches, and number of branch points, and width profile.

4.3.5 Crack Length and width

The above approach divides a given crack in various segments subtracting branch points from the crack skeleton. The estimation of crack length is based on the perimeter of crack skeleton. Practically, cracks in concrete elements have less number of pixels as compared to their background and have large length to width ratios. Hence, half of the perimeter of crack skeleton is a good approximation of crack length. The area of a crack object in binary images is found by the summing area covered by each pixel. After getting the length and area of a crack object, its average width can be calculated by dividing total area by length of the crack segment. The process has been described in Figure 4.6d. Then each crack segment is labeled and the crack properties are retrieved. However, additional criteria need to be defined to clean up the noise present at the final stage to discriminate among the cracks (Richard et al. 2001). For example, the additional criterion for length estimation is that a crack must not have a length smaller than 20 pixels. This limit is application dependent and can vary from one problem to another. The developed algorithms are tested on real images shown in Figure 4.6. The images in Figure 4.6a, 4.6b, and 4.6c show crack detection, branch points, and estimation of crack length respectively.

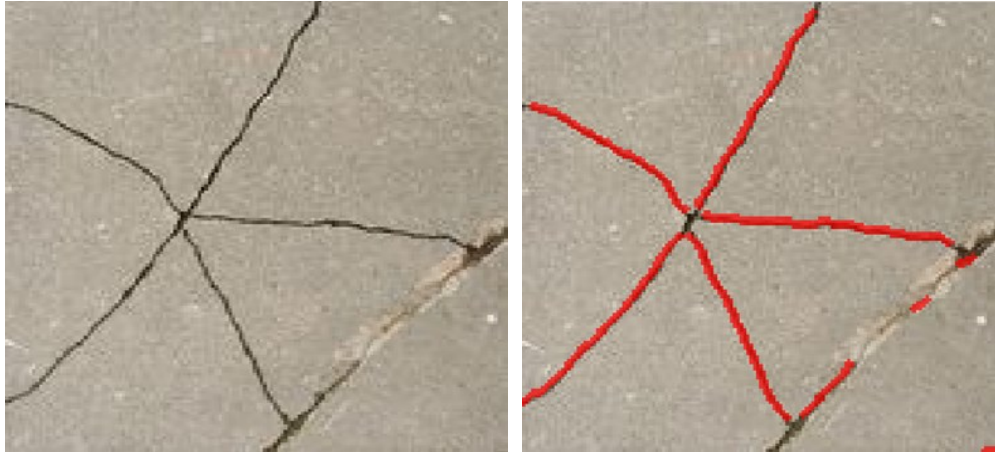


Figure 4.6: Original crack image, (a) Crack Detection

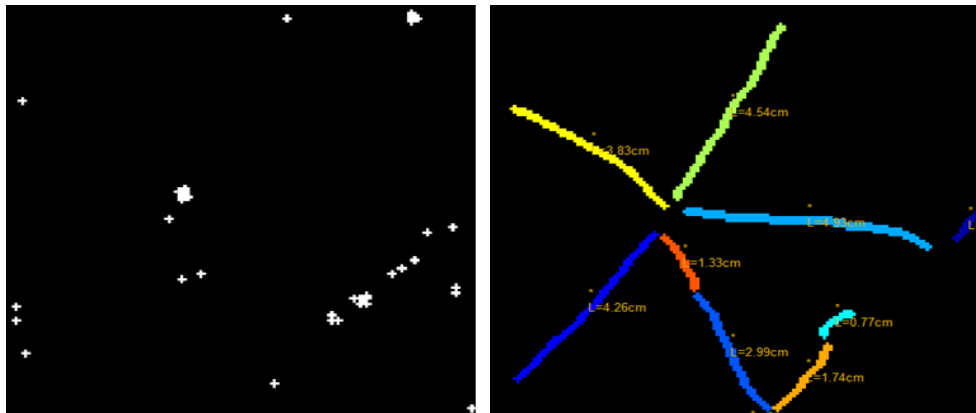


Figure 4.6 (b): Branch Points,

Figure 4.6 (c): Crack length

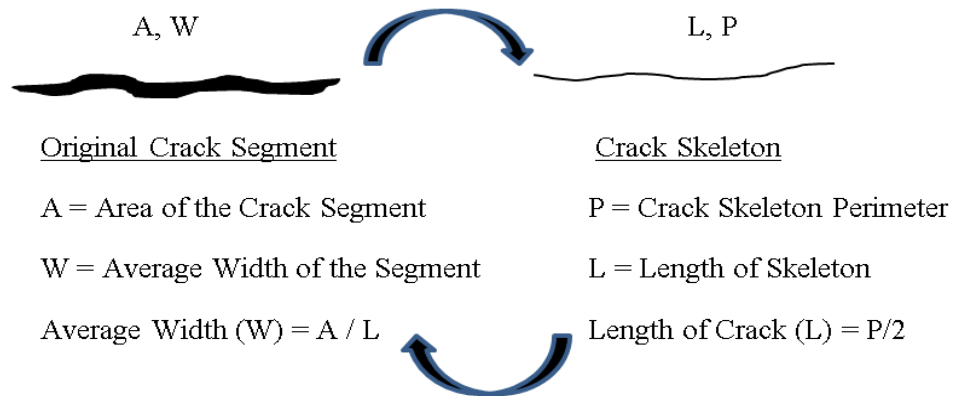


Figure 6(d): Estimation of Crack Length and Width

Images from Lab Experiments

Due to a great variability in observing the crack-depth and crack-width, the accurate assessment of the condition of a structural member are is possible only at a statistical level (Gilbert 1992). The experimental setup is shown in Figure 4.7 where a numbers of digital images were collected for data analysis. The details of cross sections and structural reinforcing bars details are shown in Figure 4.7a. When tensile strength of a concrete member reaches its maximum allowable value, the flexural cracks appear the stiffness of the member reduces. These cracks are called primary cracks which penetrate spontaneously to a certain depth. It was observed that the height of a primary crack immediately after cracking is significant and remains constant under increasing loads to some extent. However, the width of such a crack increases gradually with load and time. The images were collected during experiment at different levels of the applied load.

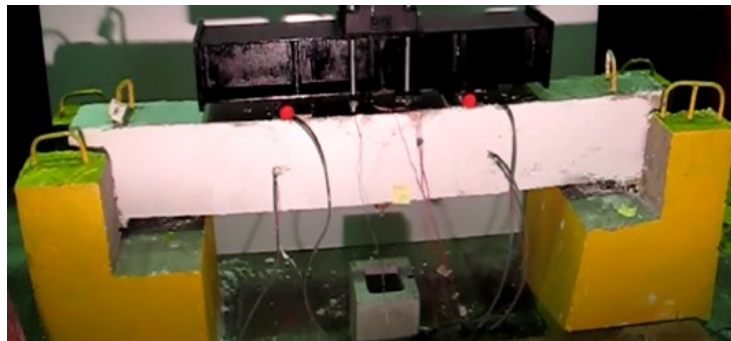


Figure 4.7: Experimental setup for beam loading under bending

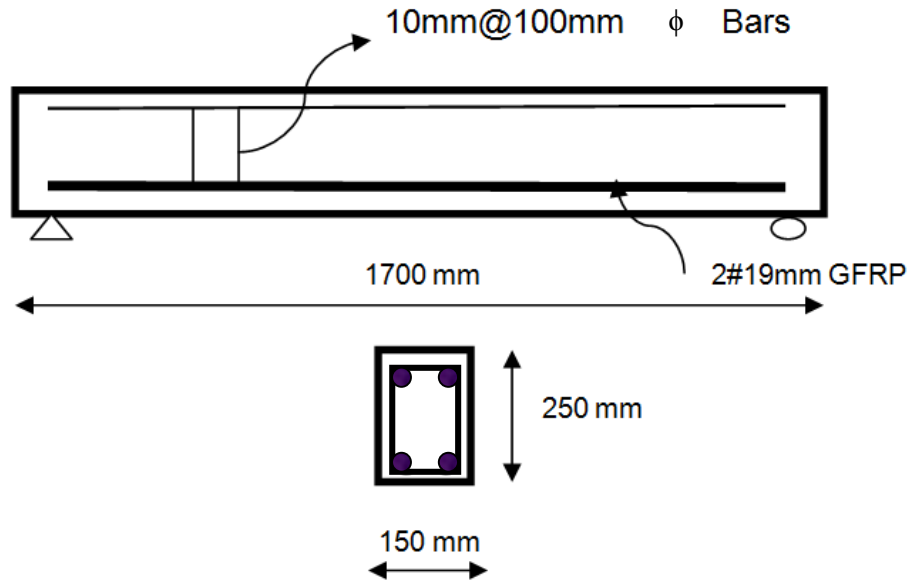


Figure 4.7a - Cross-section and reinforcement details.

For crack detection, a camera was focused at the critical crack point just below the point of application of loads, while another camera was used to take different images covering crack patterns of the whole beam. At images taken at different stages were later retrieved and their length and width were calculated separately. To check the accuracy of crack width obtained from developed algorithms, a crack scale shown in Figure 4.8 was used to measure the actual crack-width. For illustration, the original image was rotated to 90 degree to fit the paper size and space. The obtained crack width using the developed algorithms at 115 KN load was found 0.89 mm as shown in Figure 4.8a and 4.8b. The actual width measure is 0.9 mm in Figure 4.8.



Figure 4.8: Use of Crack Scale for Width Measurement

American Concrete Institute (ACI) (Richard et al. 2001) and Ontario Structure Inspection Manual (OSIM 2008) assign permissible limit of crack-width in various weather exposure conditions as shown in Tables 4.2 and 4.3. These limits are important for condition assessments of reinforced concrete structures. The result of tracking of cumulative crack-depth and width (width in mm *100, to plot in same graph) of a particular flexural crack under various loading stages are summarized in Figure 4.9 and Table 4.1. The developed algorithm has also been shown in detail in Appendix B as implemented in MATLAB.



Figure 4.8(a): Crack Edge Detection

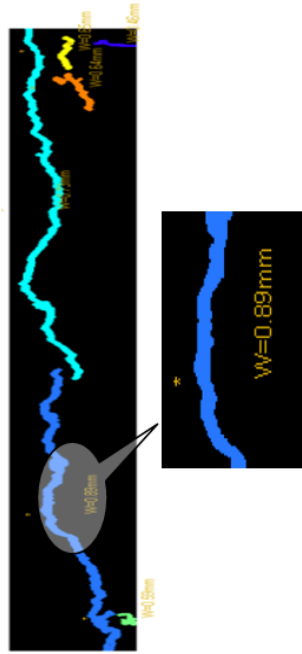


Figure 4.8 (b): Crack width

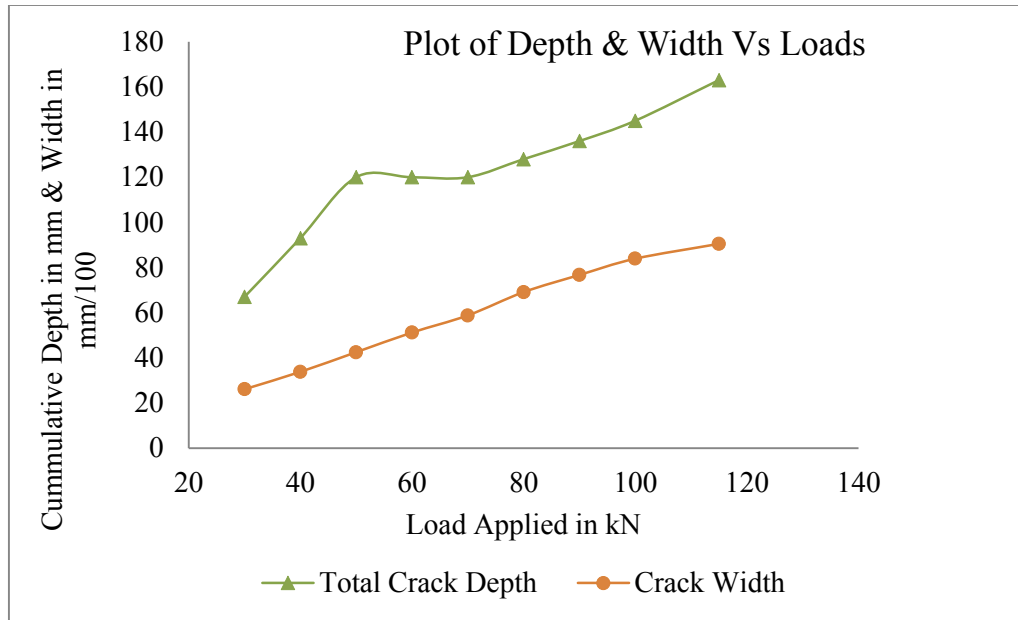


Figure 4.9: Plot of Cumulative Crack Depth and width

Table 4-1: Evaluation of Crack Width and Depth

| Image No | 0045.tif | 0046.tif | 0050.tif | 0083.tif | 0092.tif | 00100.tif |
|-----------------------------|----------|----------|----------|----------|----------|-----------|
| Load in KN | 30.00 | 50.00 | 70.00 | 90.00 | 100.00 | 115.00 |
| Proposed Crack Width in mm: | 0.30 | 0.37 | 0.58 | 0.75 | 0.86 | 0.89 |
| Measured Crack Width in mm: | 0.23 | 0.30 | 0.50 | 0.77 | 0.85 | 0.90 |
| % Error: | 30.43 | 23.33 | 16.00 | -2.60 | 1.18 | 1.11 |
| Measured Crack Depth in mm: | 67.00 | 120.00 | 120.00 | 136.00 | 145.00 | 163.00 |

Table 4.2: ACI 224R-01, 2008 Permissible crack width in Reinforced concrete structures

| Exposure Condition | Maximum Allowable Width |
|----------------------------|-------------------------|
| Dry Air | 0.016 in (0.406 mm) |
| Humidity, Moist Air, Soil | 0.012 in (0.305 mm) |
| Deicing Chemicals | 0.007 in (0.178 mm) |
| Sea Water | 0.006 in (0.152 mm) |
| Water Retaining Structures | 0.004 in (0.101 mm) |

Table 4.3: OSIM (2008), Crack Classification for Reinforced Concrete Structures

| |
|--|
| Hairlines Cracks – less than 0.1 mm wide |
| Narrow Cracks – 0.1 mm to 0.3 mm wide |
| Medium Cracks – 0.3 mm to 1 mm wide |
| Wide Cracks – greater than 1 mm wide |

4.3.6 Data Fitting for Crack Depth vs Crack Width

Marsi (2000) showed a method to predict the level of damage by neural networks constructed using the data from vibration measurements of structures. A back-propagation neural network and computational mechanics approach were used by Liu et al. (2002) to classify type, location, and the length of cracks. Similarly, Xu and Humar (2006) used the modal energy-based damage index to determine location of damages and an ANN to

determine the extent of damages in structures. In this thesis, a neural network was trained to predict depth of crack given width of crack. The proposed neural networks model is a supervised model having input attribute as crack-width and output attribute as crack-depth. One hidden layer was used with 10 neurons. The total of 101 crack patterns was obtained from digital images to train networks with 39 patterns defined as testing and validation sets. The training algorithms work flow chart for this network explained in Figure 4.10.

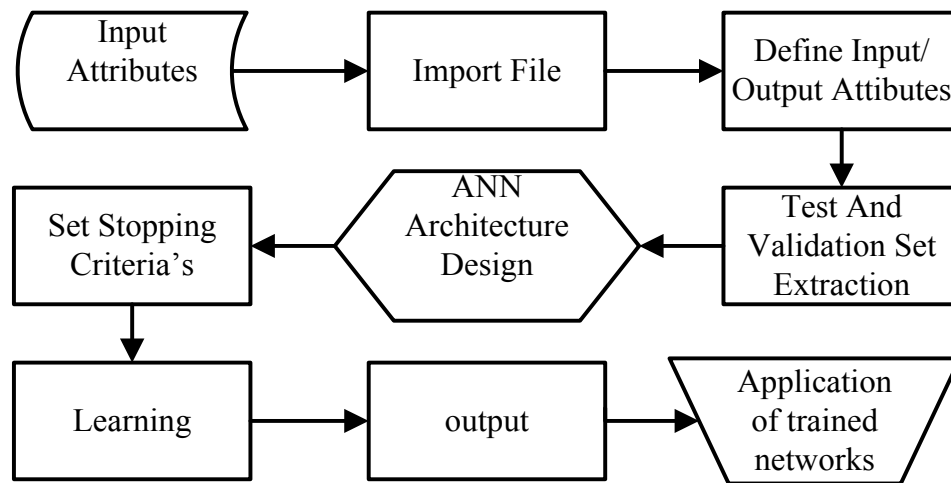


Figure 4.10: Neural network Training Flow Chart

After defining the training, testing, and validation sets for the network, the actual training of the neural network was started. The training stopped at 12th epochs since the validation error was constant after 6th epochs as shown in Figure 4.12. The fitted data of the rest of the patterns are displayed in Figure 4.11 with the distribution of error at each point.

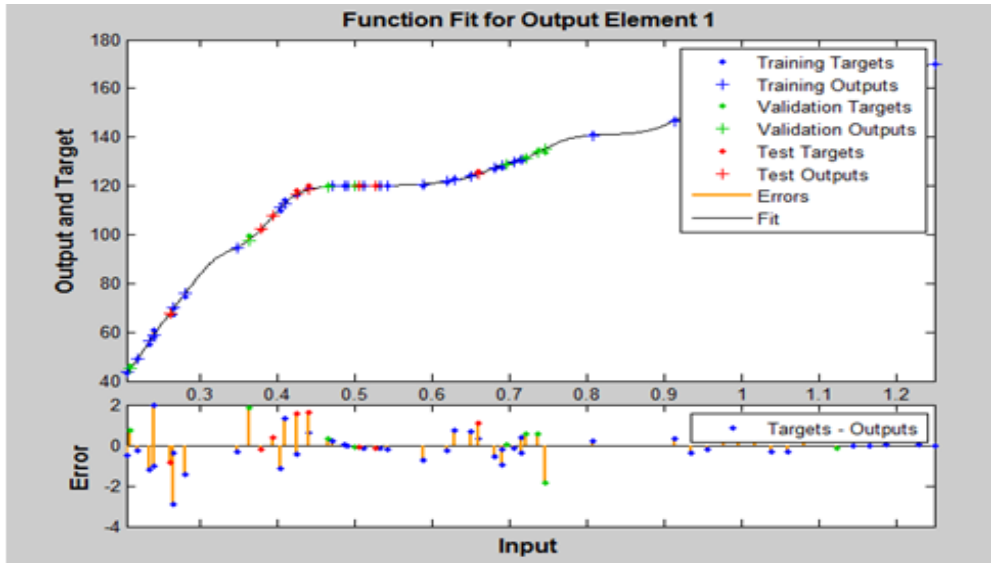


Figure 4.11: Data Fitting by Neural Networks

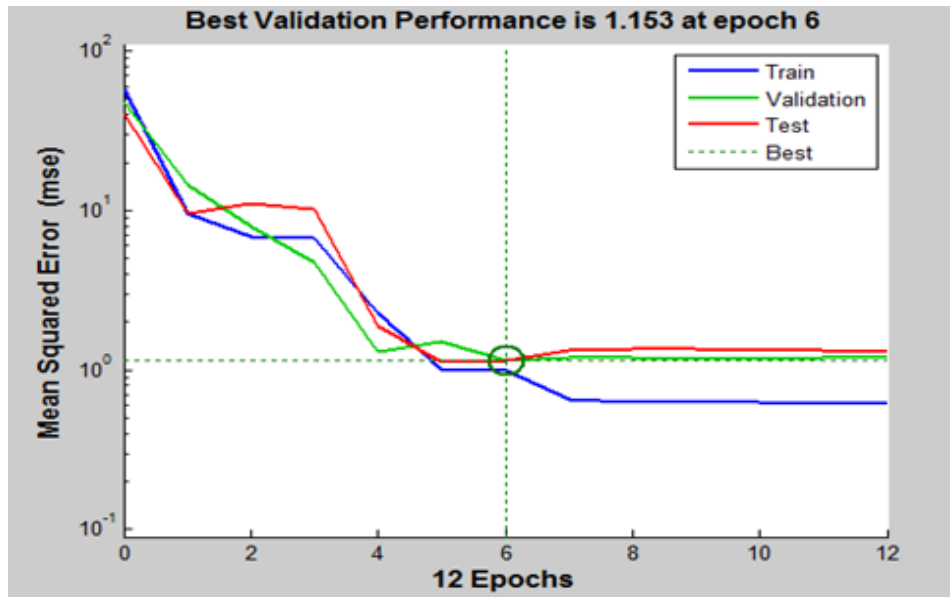


Figure 4.12: Error in Training, Validation, and Test Sets

Next the trained networks were tested with test data to evaluate the performance of the model shown in Figure 4.13. This Figure shows the data fitted with 39 data patterns which were not exposed to the network during the training phase. The predicted data points and test data points matched with an acceptable degree of accuracy as shown in the plot of the residual and histogram. The residual error was calculated using Equation 7 (MATLAB R2012a):

$$\begin{aligned} \text{Error_Percentage} \\ &= (\text{abs}(\text{Residuals}) / \text{Test_Data}) * 100 \end{aligned} \quad (4.7)$$

where, $\text{Residuals} = (\text{Forecast_Data}) - (\text{Test_Data})$

The residual plot showed the distribution of data very close to zero line. Most of the data points were distributed with + 5 to – 5 which was also clearly seen in residual histogram plot at top right of the Figure 4.13.

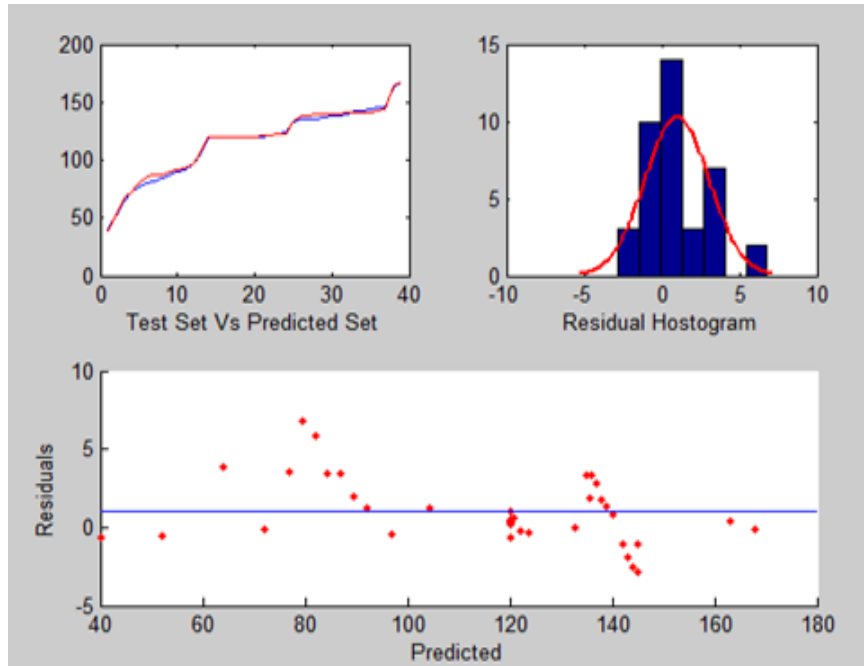


Figure 4.13: Performance Evaluation of Trained Networks

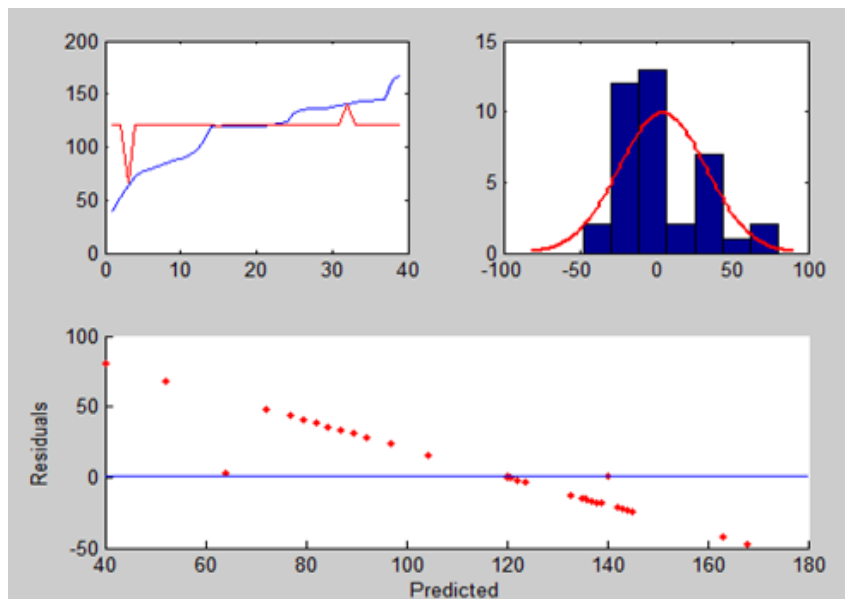


Figure 4.14: Comparison with Boosted Decision Tree

The above trained model was compared with Boosted Decision Tree algorithms and the results are presented in Figure 4.14, which show that the predicted data and the test data are not fitted well, and the residuals plots are very scattered from + 90 to – 50 as shown in bottom of Figure 4.14. This comparison shows the model developed by neural networks is superior as compared to boosted decision tree models.

The results successfully demonstrate the crack quantification model. The work adopts a new approach of crack segmentation method based on key features in an image frame called branch points, crack length estimation based on crack skeleton perimeter which considers the tortuosity of crack instead of estimating crack length from object-oriented bounding box, and the average crack width considering the entire characteristics of crack pixels instead of seeking how many points need to be considered to obtain the average crack width. First, this approach overcomes the limitation of manual input of at least one skeleton point to start searching of the crack connectivity to define the crack segmentation boundaries (Zhu et al. 2011), and is efficient even when multiple unconnected crack skeletons are present in the same image frame. Previously, the length of a crack was approximated from a bounding box enclosing the crack skeleton. Although the maximum and minimum crack width could be successfully estimated using existing methods, the average crack-width could not be determined, which is one of the important pieces of information required for condition assessment and billing purpose to prepare contract documents.

To demonstrate the proposed method, 101 images retrieved from the experimental set up as illustrated in Figure 4.7 were utilized. A part of the result of crack analysis performed over these images from developed algorithms is illustrated in Table 4.1. The depth of a crack represents the perpendicular distance from top of a crack tip to the bottom of the beam surface. The width of cracks obtained at various loading stages was displayed in Table 4.1 and the results were compared with the actual crack width measured from a crack scale in Figure 4.8. The results showed that developed algorithms works well for crack width greater than 0.3 mm, however, errors are not acceptable when crack-width is less than 0.3 mm. Since the OSIM and ACI mention that for visual inspection purpose, a crack width less than 0.3 mm falls in narrow crack class and may not be documented (OSIM 2008, ACI 2008). So, the developed algorithms are suitable for inspection of cracks in reinforced concrete structures with the camera used in this work. The limitation of the crack-width accuracy can be improved by using high resolution cameras.

4.4 3D Visualization and Crack Density

Alan (2011) proposed a new framework for object recognition process using BIM. This system supports the storage and retrieval of objects of interests in his model. Ryan (2012) showed his work in evaluating surface defect detection capability of terrestrial LiDAR for reinforced concrete bridge decks by generating 3D model from Point Cloud. Likewise, El-Omari and Moselhi (2008) integrated 3D scanning and photogrammetry in order to enhance the accuracy of data collection from construction sites. The above approach requires point cloud to be matched with digital images to identify members and defects on

elements. In this paper, the 3D visualization is developed manually by projecting digital images as well as the image texture. The automated process of 3D visualization model is possible by integrating 3D point clouds with digital images (Adhikari et al. 2013c). However, further works are required in quantification of defects based on such models. For better 3D models, at least four images are required at the four sides of an object. However, a 3D model can also be developed just from a single image taken at 45 degree so that at least three corners can be seen from a single position.

The images shown in Figure 4.15(a) and 4.15(b) have been used here to develop the 3D models of a beam, and Figures 5.15 (c), (d) show the crack pattern on the front and back faces of the beam, respectively. Based on these models, specific parameters such as crack densities are calculated to differentiate the severity of cracks and cracking patterns.



Figure 4.15(a): 2D images of GFRP-Reinforced Concrete beams

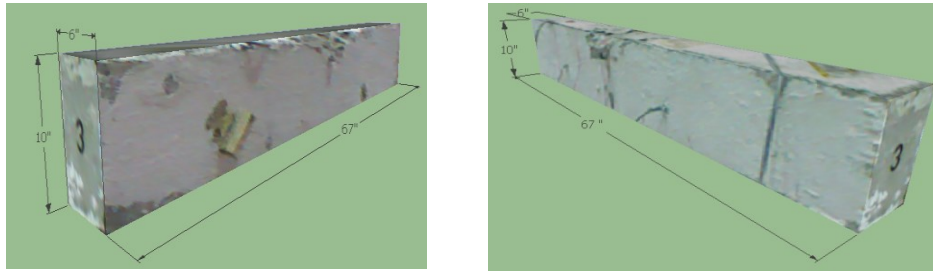


Figure 4.15 (b) 3D Visualization Model of a beam

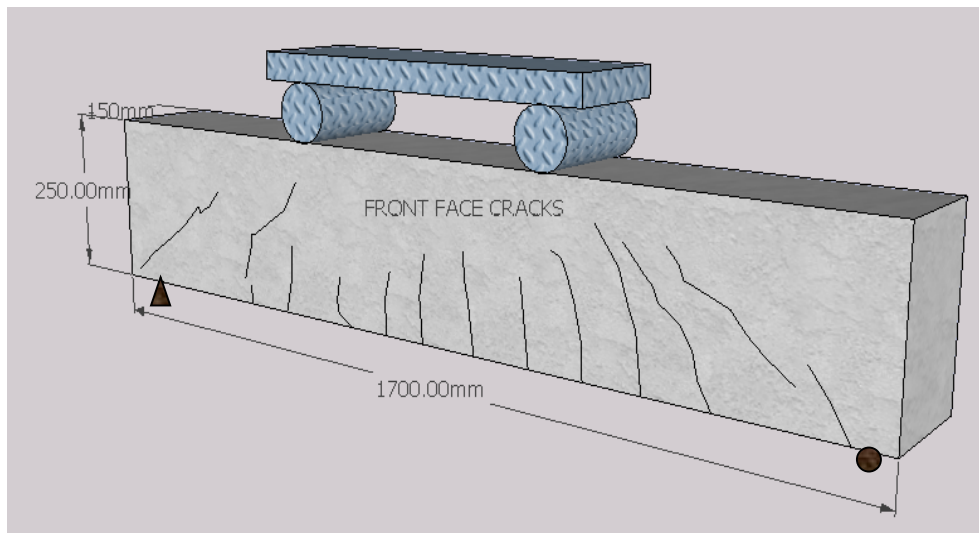


Figure 4.15(c): 3D visualization, Front Face Crack Density = 0.0066 mm/mm²)

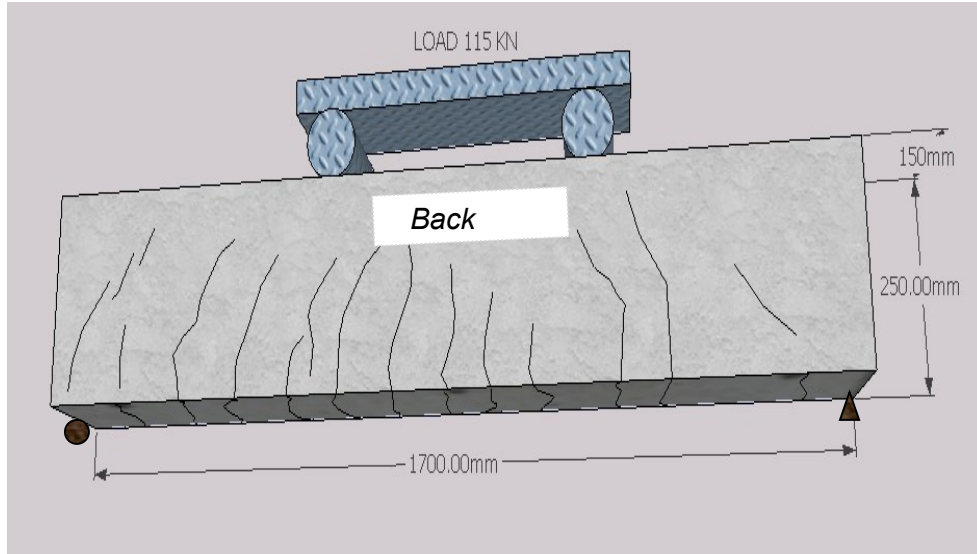


Figure 4.15 (d): 3D visualization, (Back Face Crack Density = 0.0058 mm/mm², Bottom Face Crack Density = 0.0085 mm/mm²)

4.5 Discussion

Displaying the information from visual inspection in the form of a 3D model is an important aspect visualization of the condition of a structure or a part of the structure. Based on digital images, 3D models were developed as shown in Figures 4.15. The cracks patterns in the Figures 4.15 were observed under the load at 115 KN. The model was developed by projecting images by finding matching lines in x and y directions. Crack density can be visualized from these models showing as crack density of 0.0066 mm/mm² for front face, 0.0058 mm/mm² for back face, and 0.0085 mm/mm² for bottom face. The crack patterns are important to identify during bridge inspection which includes the types of cracks, location of cracks, crack width and depth, and crack spacing. In this research, neural

networks model was trained to predict the depth of cracks given the crack width. Such information will be important for decision making about integrity of structural members and for repair and maintenance purpose. The trained networks performance was acceptable with Mean Absolute Percent Error (MAPE) equal to 1.66%. The plot of residuals showed normal distribution centered on zero. The data fitting algorithms were tested with Boosted Decision Tree method and Mean Absolute Percent Error (MAPE) was found to be 24.88%. Also, the residuals in this case are wide spread as shown in Figure 4-14. The analysis showed that neural networks data fittings are superior over boosted decision tree model. The remaining part of this result discusses how the images can be photographed so that numerical errors for defects could be minimized.

The 3D visualization of cracks is demonstrated in Google Sketch up software in displaying the crack density of concrete elements under flexural loads. In the past, researchers have used several commercial software systems to develop 3D visualization model, such as Mesh Lab, Rhino, TrueSpace, and Photosynth (McRobbie et al. 2010). However, this kind of software becomes obsolete after few years and it is difficult to get an updated version. Some authors have used advanced graphical software to model defects and quantify them for bridge inspection purpose (Maksymowicz et al. 2011). Hence, easily accessible and comprehensible model sought to be developed for proper visualization of defects. This work adopted Google Sketch Up software which has the capability to project texture from digital images directly on models to simulate on-site visual inspection (Google Sketch). This approach does not require field measurement survey for 3D visualization (Ganapuram et al. 2012).

4.6 Summary

This chapter proposed an integrated model based on digital image processing to enhance the fundamental tasks of routine bridge inspections. The integrated model consists of crack quantification, neural networks, and 3D visualization models for condition assessment of concrete structures. Crack length is estimated from its crack skeleton perimeter. Since the aspect ratio of crack length to crack width is large and crack skeleton is a single pixel connected path, this approximation is reasonable for estimation of crack properties.

The integrated model also consists of the neural networks models to predict crack depth given crack width. The importance of 3D visualization model has been demonstrated by developing 3D models based on digital images which mimic the on-site visual inspection. The visualization model is demonstrated in terms of crack density which is one of the crack parameter required for industry experts. The proposed integrated model can be integrated with BMS to enhance the reliability of decision making process for the condition assessment of concrete bridges.

Chapter 5: Image-based Automated Element Condition Rating

5.1 Introduction

To ensure effective management of civil infrastructure, it is necessary to identify the critical components of structures, and evaluate their performance in order to verify that they are safe under current service loads and satisfy service requirements. In general, the performance of bridges is evaluated by two approaches. The first approach is based on reliability analysis of bridge structures considering the load and resistance models of infrastructure (Frangopol et al. 2008a & 2008b). In recent years, the tracking of real time performance of structures is made possible by using Structural Health Monitoring (SHM) technique utilizing several types of sensors (Humar et al. 2006, Lee et al. 2007). However, the application of SHM sensors is found to be expensive as compared to visual inspections (Orcesi & Frangopol (2010)). The second approach of bridge performance evaluation is based on visual inspection which is widely accepted by the governments in most jurisdictions, as well as by other agencies (AASHTO 2001). This current research adopts the second approach in developing condition assessment models for concrete bridges, while augmenting it through new methods developed based on digital image processing and artificial neural networks.

This Chapter proposes an automated prediction of condition rating for bridge elements using artificial neural networks. To illustrate the concept, the approach considers scaling defect as a candidate defect in reinforced concrete structures. The guidelines used here for

assigning a condition rating are based on Ontario Structure Inspection Manual (OSIM 2008). Recently, Hinzen (2013) showed that a systematic comparison of building damage evaluation is possible with Google street view data. The study demonstrated that the Google street view resolution was enough to detect structural damages, as well as in identifying cracks as reported by the author. The work by Hinzen (2013) shows the importance of digital image application for condition assessment of civil infrastructure. However, the application of digital image processing for automatic prediction of condition rating for structural components is yet to be developed.

Abudayyeh et al. (2004) proposed an imaging data model for monitoring and generation of inspection report of bridges based on digital images. The developed model was integrated with PONTIS to enhance the reliability of visual inspections. Although the imaging data model demonstrated the capability of producing inspection reports automatically based on stored information, the process of assigning condition rating for the structural components was done manually.

5.2 Proposed Framework

The proposed framework encompasses a structured procedure for evaluating an element condition index after predicting condition rating for elements as illustrated in Figure 5.1. In order to obtain a bridge condition index, the approach integrates the condition rating of individual elements according to their weights or element importance factors. The process starts with developing a 3D model of the inspected bridge for visualization purpose. Before

performing defect quantification, the recorded images need to be corrected if they contain noise, perspective, and parallax errors as discussed in Chapter 4.

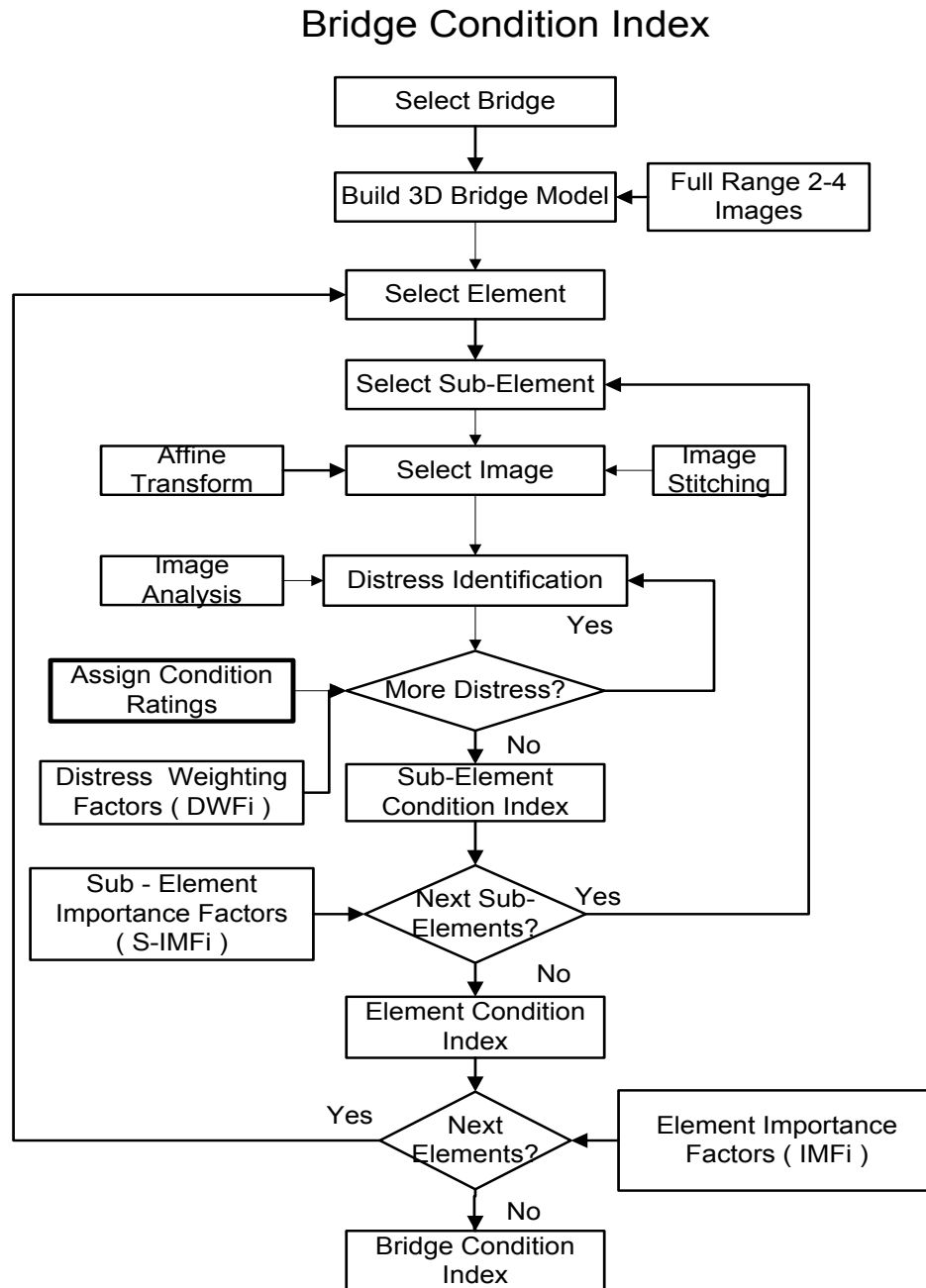


Figure 5.1: The Proposed Framework

A detailed procedure for prediction of condition rating based on neural networks is shown in Figure 5.2. The condition rating according to OSIM guidelines is based on the severity of scaling defects which are defined by the depth of scaling defect. Evaluating the scaling depth is a time consuming task. Therefore, in this work, the depth of scaling is estimated by digital image processing as explained here.

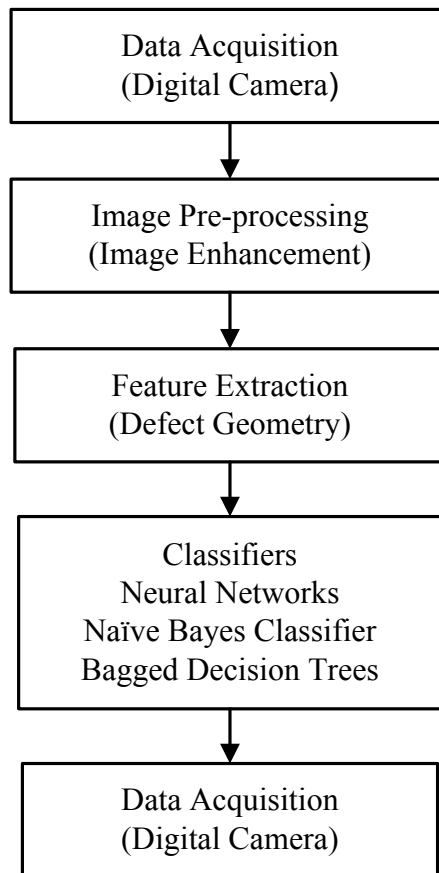


Figure 5.2: Work Flow Diagram for Automated Condition Rating

The variation in Red, Green, and Blue (RGB) color profile is measured to quantify the depth perception from digital analysis of the retrieved images. The major components of the proposed methodology comprise data acquisition, image preprocessing, attributes

extraction, and development of neural networks models for automated labeling of condition rating for structural elements.

5.2.1 Feature Extraction

A commercially available digital camera is used for data collection of reinforced concrete bridge surface defects. For defect identification, close-range photographs are required with proper focus on defects. Each photograph frame shall include either a natural or artificial target for calibrating the dimensions. In general, natural objects such as the details of beams, and columns can be used as natural targets. In case of insufficient natural objects, an artificial target can be placed in the vicinity of area of interest (Jauregui et al. 2006). An example of use of artificial target has been shown in Figure 5.3.



Figure 5.3: Artificial Target

Collected images are processed through spatial and frequency domain operations in order to enhance the feature extraction. Depending on situations, one can use high pass filter or low pass filter to filter for image enhancement using frequency domain operations (Xu et al. 2012 and Adhikari et al. 2012b). In this work, both domains of image pre-processing are used for image enhancement as explained in Figure 3.7 in Chapter 3.

Feature extraction can be done either at global or local level depending upon the task requirements. In this work, the scaling defect attributes are estimated by selecting a Region of Interest. Various attributes considered for mapping of scaling depth and prediction of condition rating based on defects severity are listed in Figure 5.4.

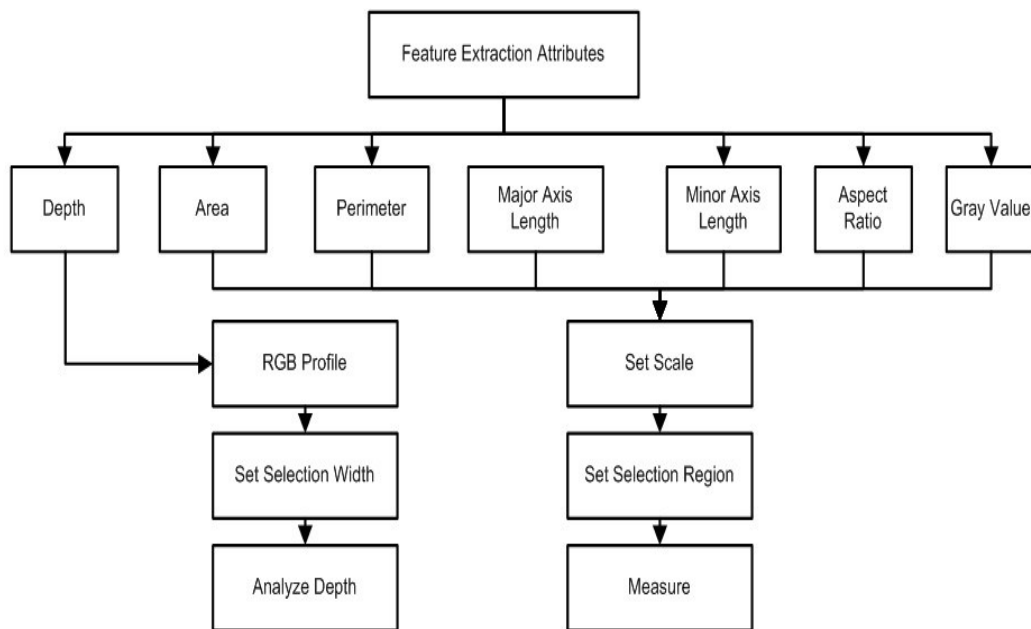


Figure 5. 4: Attributes Feature Extraction

The perception of distance based on light intensity was first discovered by Leonardo Da Vinci saying that among bodies equal in size and distance, that which shines the more brightly seems to the eye nearer (MacCurdy 1938). After this statement, a number of studies are done to validate the hypothesis concerning the intensity of light and object distance relationship (Samonds et al. 2012, Coules 1955, and Ashley 1898). This research adopts the property of intensity variation of light with depth as shown in Figures 5.5a and 5.5b. It is evident from the 3D visualization of color profile that brighter the intensity the lower the depth perception. The sectional RGB color profile is shown in Figure 5.6 which is used for quantifying the depth perception. Several RGB profiles are obtained by varying the selection width shown in Figure 5.7. To filter such noise, the width of line is increased from 1 to 30 units leading to smooth intensity variation with pixels distance.

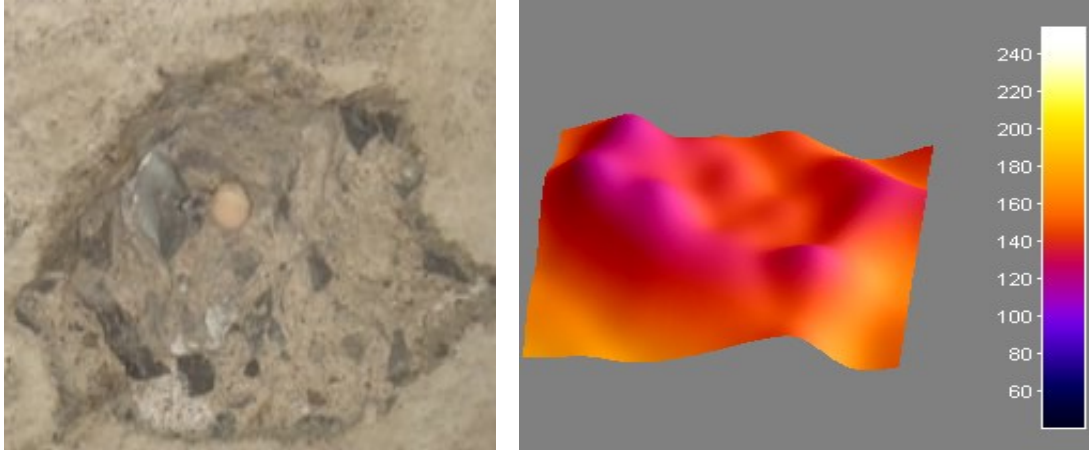


Figure 5.5 (a): Scaling Defects region of Interest

Figure 5.5(b): 3D Visualization of Scaling Defects

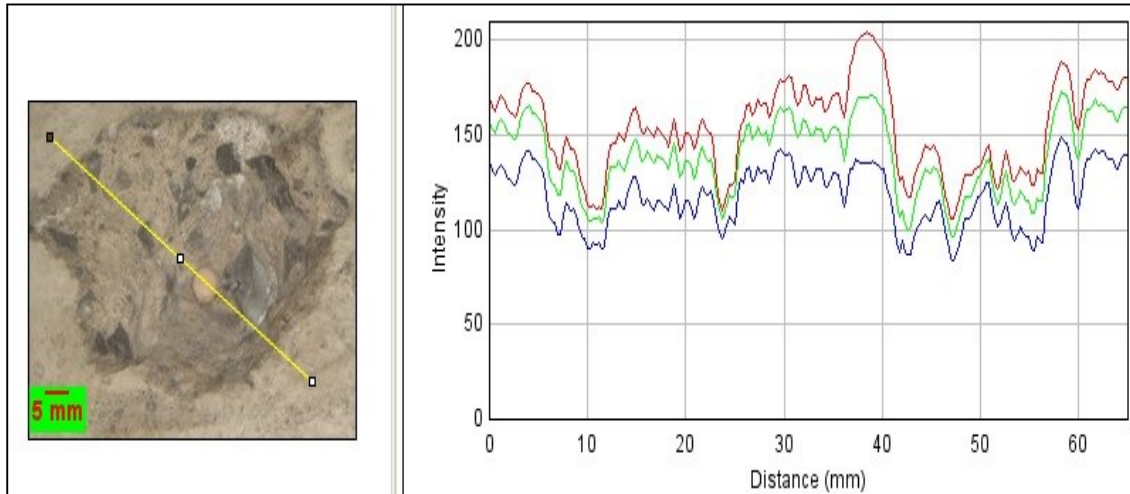


Figure 5. 6: RGB profile with line width of 1 Unit

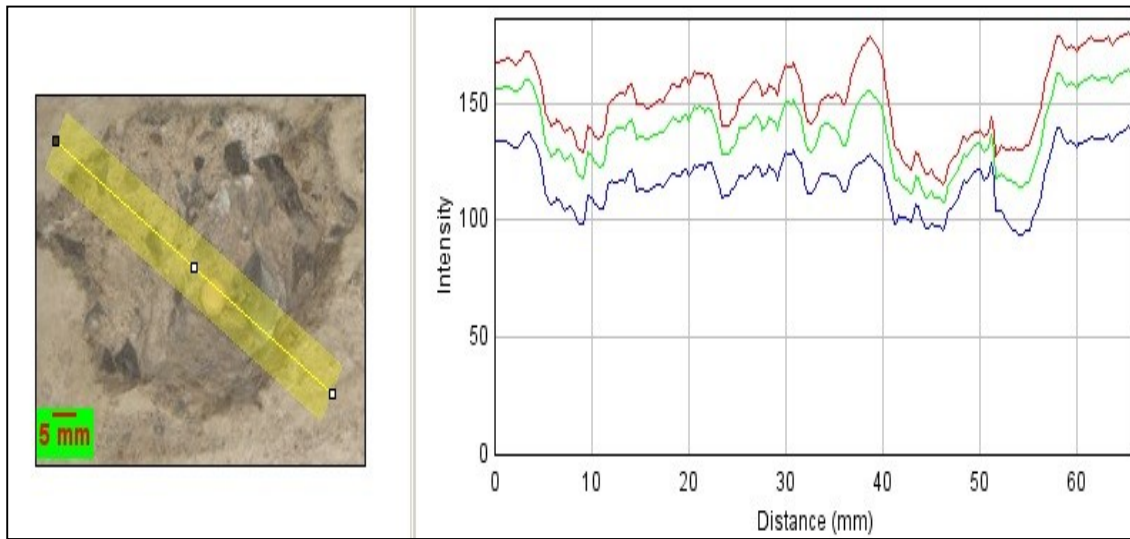


Figure5. 7: RGB profile with line width of 30 Units

Based on the above description, 19 images have been processed to obtain the intensity of color variation along the selected sectional profile. Some of the sample images used in this research are displayed in Appendix A. The difference in intensity is correlated with the real scaling depth shown in Figure 5.8.

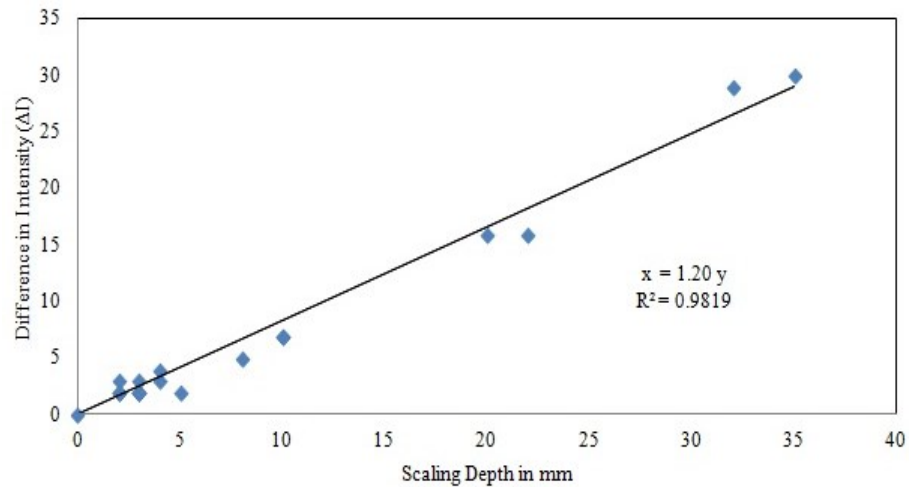


Figure 5.8: Scaling Depth Estimation from RGB Profile

5.2.2 Artificial Neural networks (ANN)

The neural networks are the ideal choice of algorithm when the solution cannot be represented by a flowchart (Heaton Research 2013). In general, the solution of the problem is difficult to predict when it depends on various parameters and final solution is highly dependent on selected factors. The neural networks are ideal choices for prediction of condition rating because condition ratings of bridges depend on a number of parameters. The following two training parameters are important for training the neural networks.

- 1) Learning rate: it determines to what degree the calculated change will be to the NN weight matrix. High learning rate can cause instability to the networks whereas setting low learning rate may take forever to train NN.
- 2) Momentum: It determines the influence of previous iterations to the current

iterations. It is useful in avoiding the situation when there is chance to trap in local minima.

While choosing multi-layer perceptron architectures, the number of neurons assigned to a layer is important. In general, the number of neurons is decided on trial and error method. For the initial guess, one can use the number of neurons in a layer based on rule of thumb. For example, the number of neurons in a hidden layer may be taken as two-third the size of input layers plus the size of output layers (Heaton Research 2013). Sometimes multi-layer perceptron and back propagation terms are used interchangeably. However, they have their own significance. Back propagation means propagation of errors in backward direction shown in Figure 5.9. Multi-layer perceptron has two types of signals. One is the functional signal which flows in the forward direction and the other is the error signal which flows in the backward direction.

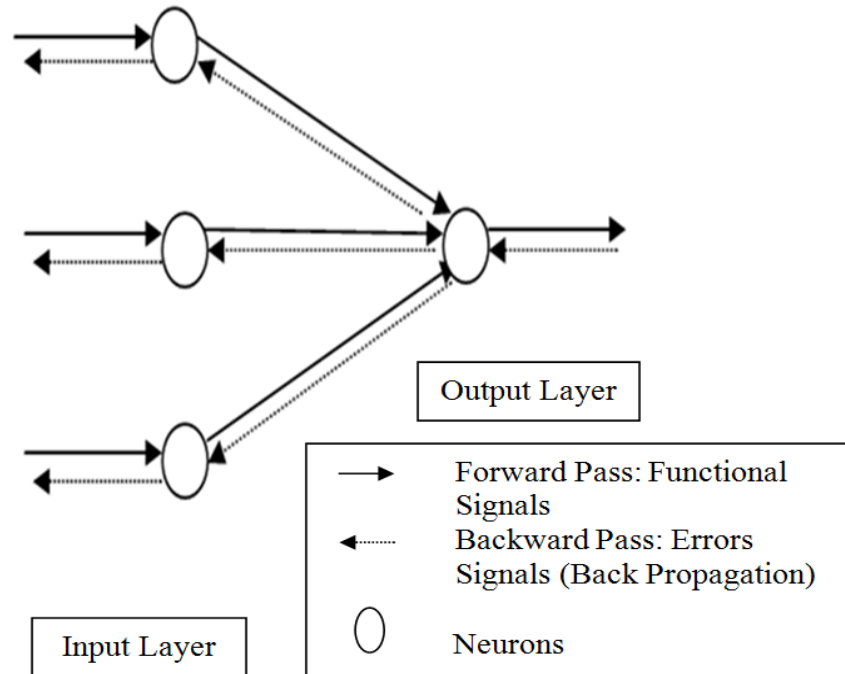


Figure 5.9: Forward and backward pass for Back Propagation Algorithm

Back Propagation Algorithms are explained in Appendix C.

5.3 Data Analysis and results

The proposed methodology for automated prediction of condition rating is implemented in MATLAB (MATLAB R2012a) and Neuroshell (Ward Systems, 2013) in Windows Vista Enterprise 32 bit operating System. The desktop consists of Intel ® Core ™ 2 Duo CPU, E6550 @ 2.33 GHz. A commercially available SONY-DSC T5 digital camera of 5.1 mega pixels with optical zoom 3X is used for image acquisition. Also, commercially available software called ImageJ is used for extracting digital information of an image and 3D visualizations (ImageJ 1.45s).

5.3.1 Check for Normal Distribution

In this work, seven input parameters were retrieved from the selected digital images as shown in Figure 5.10. The simplest model for such mapping problem is to use discriminant analysis. However, in that case, the data set should follow a normal distribution. The distribution of input data is shown in Figure 5.9.

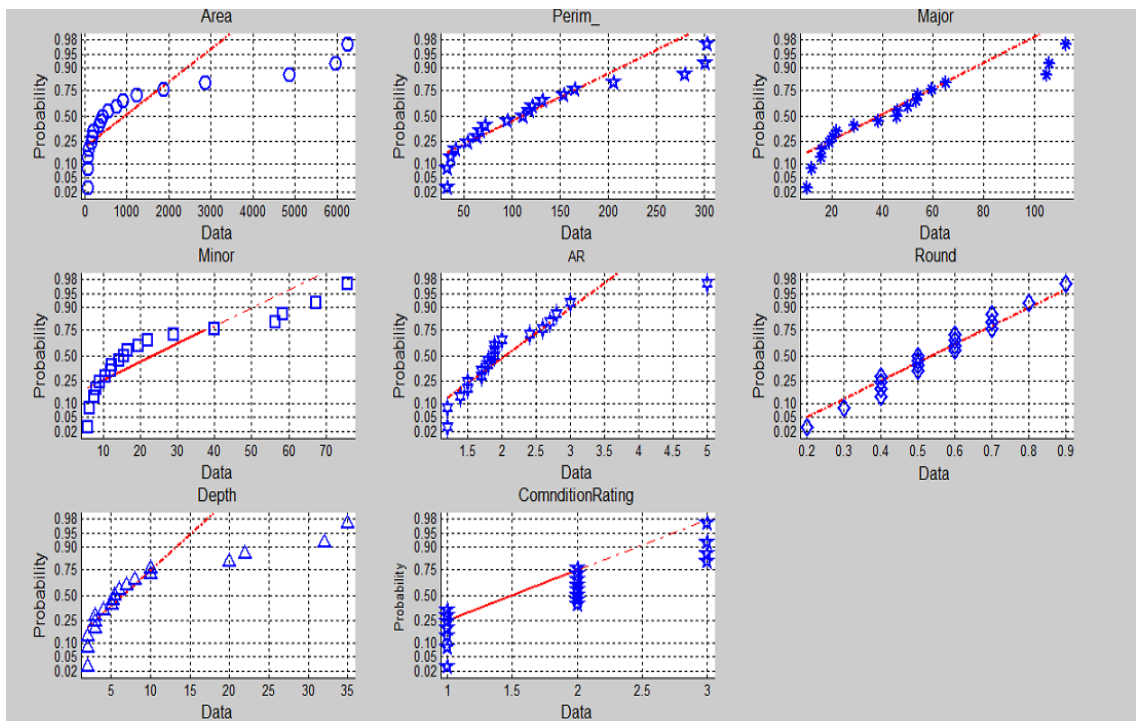


Figure 5.10: Check for Normal Distribution of input parameters

The plots in the above Figure 5.10 clearly show that the data points are not following the red lines and are not normally distributed. So, the discriminant analysis for such problem

is not deemed a good choice; and hence, neural networks are chosen for the classification purpose, which is explained in next section.

5.3.2 BPNN Models

Back propagation neural networks (BPNN) models are developed for mapping of elements condition rating based of their scaling depth. The following two models are constructed: model (a) to predict scaling depth, and model (b) to predict condition rating based on scaling depth shown in Figure 5.11. Model (b) contains an additional attribute of depth as an input variable in data patterns to predict element condition rating. The data sets are collected from the bridge located in Montreal, Quebec. Digital photographs are taken from close range so that defects are magnified. Table 5.1 summarizes the condition state rating grades as mentioned in OSIM (2008), where condition rating 1 indicates a light damage, and 3 indicates a severe damage. The input data used in the BPNN models are normalized between 0 and 1 using the Equation 5.1.

$$X_{ni} = (X_i - X_{min}) / (X_{max} - X_{min}) \quad (5.1)$$

where, X_{ni} is the normalized value of X_i ; X_i is the i^{th} value of a data series with X representing the raw data; X_{min} is the minimum value of X in the sample set; and X_{max} is the maximum value of X in the sample set.

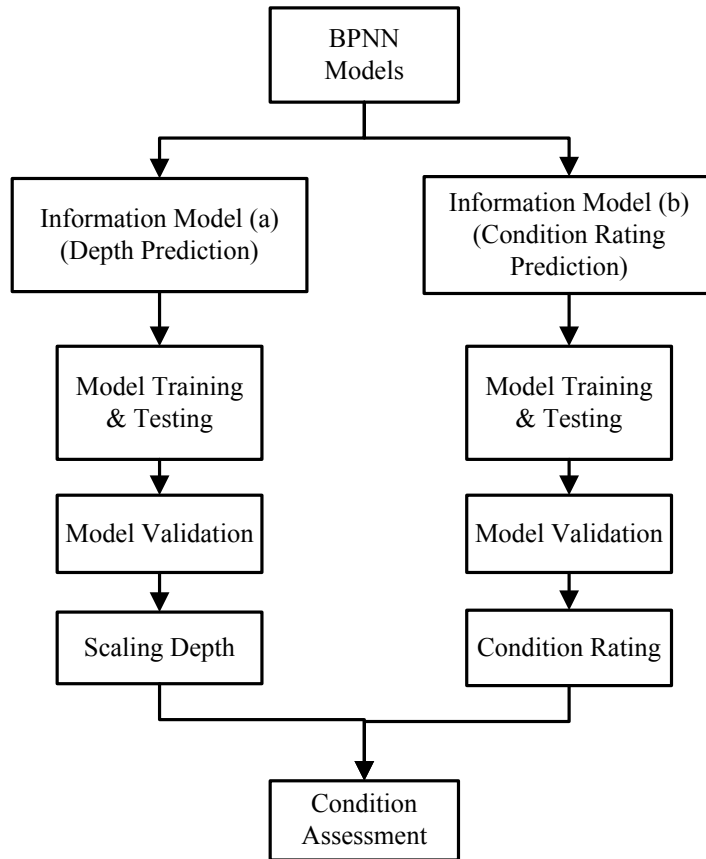


Figure 5.11: BPNN Models

Table 5.1: Description of Condition State Rating based on OSIM (2008) guidelines

| Condition State Rating for Scaling Defect | | |
|---|---------------|--------------|
| Local Flaking/Loss of Surface Portion of Concrete or Mortar due to Freeze or Thaw | | |
| Light (1) | Medium (2) | Severe (3) |
| Up to 5 mm Depth | 6-10 mm Depth | > 10mm Depth |

5.3.3 Training and validating of the BPNN

The modeling process for the neural networks as explained in Figure 5.12 consists of the development of ANN architecture, and design and training modules. The architecture of the network consisted of five layers of neurons with one input layer (the number of input neurons is equal to number of attributes in each pattern), 3 hidden layers, and one output layer (the number of output neuron is one). The detailed information about the design of neural networks architecture is shown in Table 5.2. The important parameters for training such as training rate, momentum, and initial weights are chosen to be 0.2, 0.2, and 0.3, respectively. It requires a trial and error approach to fix these parameters to get the desired output. A total of 19 data patterns are prepared consisting of 60% training set, 20% testing set, and 20% validation set. The validation data sets are also called production set which is not presented to the networks during training module. These data sets are later used to validate the model.

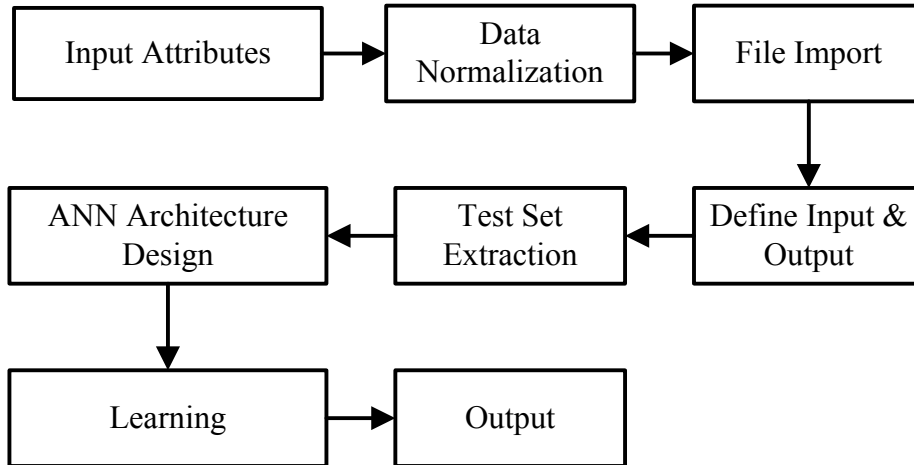


Figure 5.12: Neural Network Modeling Process

Table 5.2: Neural Networks design criteria

| Slab Number | Number of Neurons | Activation Functions | Learning Rate | Momentum | Initial Weight |
|--|-------------------|----------------------|-------------------------------------|----------|----------------|
| 1 | 7 | Linear (0,1) | 0.2 | 0.2 | 0.3 |
| 2 | 2 | Gaussian | 0.2 | 0.2 | 0.3 |
| 3 | 2 | Tanh | 0.2 | 0.2 | 0.3 |
| 4 | 3 | Gaussian comp | 0.2 | 0.2 | 0.3 |
| 5 | 1 | Logistic | 0.2 | 0.2 | 0.3 |
| Training | | | | | |
| Stop training when one of these is true about the training set | | | Average error< | | 0.0002 |
| | | | Epochs since minimum average error> | | 1,000 |
| Stop training when one of these is true about the test set | | | Calibration interval (events) | | 200 |
| | | | Events since minimum average error> | | 20,000 |

Table 5-3: Performance of Model (a) and Performance of Model (b) respectively

| Patterns processed | 19 | Patterns processed | 19 |
|---------------------------|------|---------------------------|------|
| R squared | 0.70 | R squared | 0.98 |
| r squared | .79 | r squared | 0.98 |
| Mean squared error | 0.02 | Mean squared error | 0.01 |
| Mean absolute error | 0.14 | Mean absolute error | 0.03 |
| Min. absolute error | 0 | Min. absolute error | 0.00 |
| Max. Absolute error | 0.27 | Max. Absolute error | 0.16 |
| Correlation coefficient r | 0.89 | Correlation coefficient r | 0.99 |
| (a) | | (b) | |

Table 5.4: Contribution factors for Model (a) and Contribution factors for Model (b) respectively

| Ranking | Parameter | CF | Ranking | Parameter | CF |
|---------|-----------------|------|---------|----------------------|-------|
| 1 | Depth | 53% | 1 | Length of Major Axis | 27.6% |
| 2 | Length of Minor | 9.6% | 2 | Area | 23.8% |
| 3 | Aspect Ratio | 8.8% | 3 | Length of Minor Axis | 19.6% |
| 4 | Roundness | 7.6% | 4 | Aspect Ratio | 12.2% |
| 5 | Length of Major | 7.2% | 5 | Perimeter | 9.9% |
| 6 | Perimeter | 6.8% | 6 | Roundness | 6.7% |
| 7 | Area | 6.7% | | | |
| (a) | | | (b) | | |

The accuracy of the developed model is evaluated by applying the validation data sets and measuring their performance in terms of statistical parameters. The BPNN depth prediction model shows the accuracy 89 %, whereas the BPNN condition rating prediction model shows the accuracy of 99 % expressed in terms of correlation coefficients as shown in Table 5.3 and Table 5.4 respectively. Likewise, contribution factors (CF) are evaluated to measure the importance of an input variable contributed for outputs in comparison with other input variables as shown in Table 5.4. A largest number of contribution factors indicate that the particular variable has contributed the most in entire training process of networks. However, a variable having a low value of contribution factor does not mean that it shall not be included in the model.

A comparison of the estimated depth obtained from the BPNN model and the actual one for all data points is presented in Figure 5.13. Similarly, the predicted condition rating for the selected sample images after training the neural networks is plotted with the actual condition rating according to the OSIM (2008) guidelines is shown in Figure 5.14.

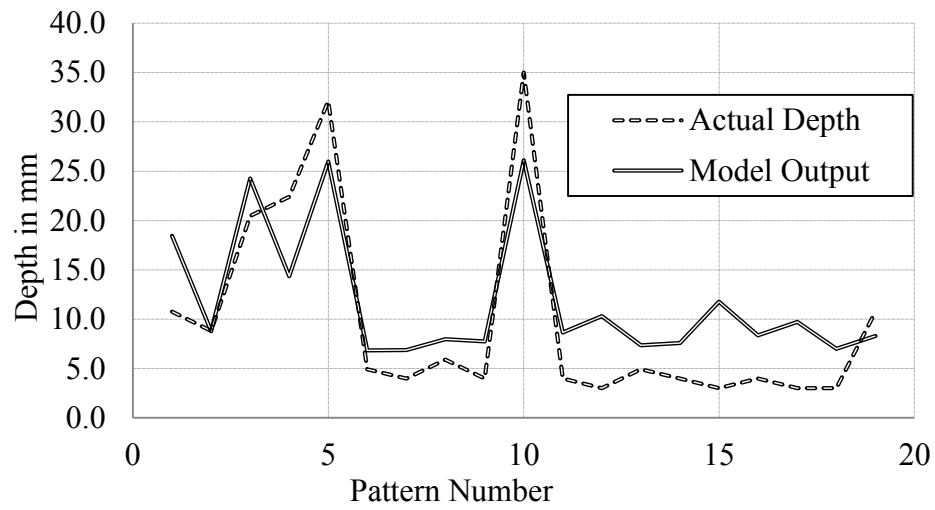


Figure 5.13: Prediction of Actual Depth Vs Model Output

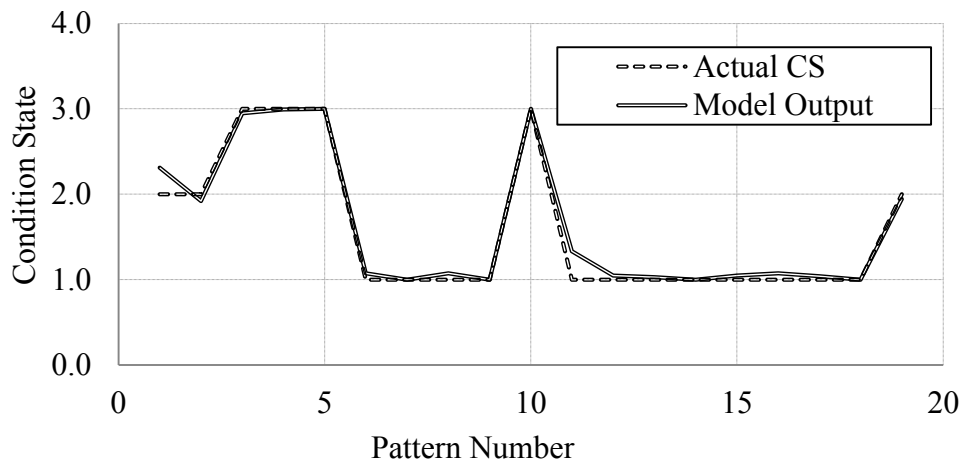


Figure 5.14: The Actual Condition State Rating Vs Model Output

5.3.4 Comparison with other classifiers

The choice of classifier is largely dependent of the characteristics of data input. Since the selected input attributes are dependent on each other, the choice of neural networks appears to be the best classifier for this problem. There is no assumption for the input data for the training of neural networks, and hence expected to perform better than other classifier. The results of a few commonly used classifiers, such as Naïve Bayes Classifier and Bagged Decision Tree Model are compared here.

Naïve Bayes Classifier

Bayes' rule is given by Eq. 5.12,

$$P(H|E) = \frac{P(E|H) \times P(H)}{P(E)} \quad (5.12)$$

The basic idea of Bayes's theorem is that the probability of an event (H) can be predicted based on some evidences (E). A prior probability of H or $P(H)$ is the probability of an event before the evidence is observed. A posterior probability of H or $P(H|E)$ is the probability of an event after the evidence is observed. It also classifies data in two steps:

- 1) Training Steps: The method determines the probability distribution based on the training sample assuming that the feature is conditionally independent for the given class.
- 2) Prediction Steps: The method calculates the posterior probability of the data set which is unseen to the model; and then classifies the test sample based on the largest posterior probability.

The independency of the data sets is an underlined assumption for Naïve Bayes Classifier. To check the accuracy of the Naïve Bayes Model, Bayes Error is calculated using statistical tools and was found as 66%. The Bayes error shows that only 34% of the test data sets are correctly classified and 66% of test sets are wrongly classified. The analysis is tested for the importance of each parameter and the process indicated that only two input parameters Major Axis Length and Depth are important for this problem.

Bagged Decision Tree Model

Bagged Decision Tree is another type of machine learning algorithm which can improve the classification accuracy and stability of the training process. It reduces variance and avoids data over fitting problems. This method has better capability than Naïve Bayes Classifier and it can also measure the feature importance of input parameters. The bagged decision tree algorithm has been performed on the previous data set and out of bag error was found as 37% which shows better accuracy in condition rating prediction than Naïve Bayes Classifier which has 66 % error. Also, the input parameter importance factors are calculated as shown in Figure 5.15. It shows that feature number 5 (Aspect ratio) and 6 (Roundness) did not contribute to classification problem. The highest contributing factor for this classification is depth, which has a contribution of more than 65%.

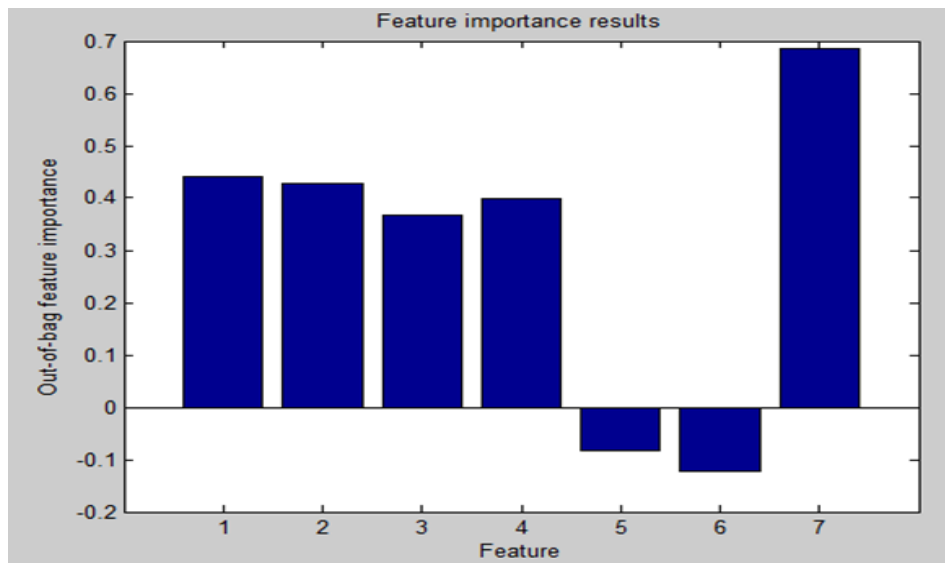


Figure 5.15: Out of Bag algorithms (Feature Importance factors)

Table 5.5: Comparison of results from different classifiers

| Classifier | Naïve Bayes Classifier | Bagged Decision Tree | Artificial Neural Network |
|----------------------|------------------------|----------------------|---------------------------|
| Accurately Predicted | 34 % | 63 % | 99 % |

Table 5.5 summarizes the results of different classifiers. The results show that the prediction capability of neural networks is better than other classifiers showing 99% of predicting accuracy. The Naïve Bayes Classifier shows only 34% of data was classified correctly, whereas Bagged Decision tree is able to correctly classify 63% of input data. The neural networks do not have any underlying assumptions on the requirements in input data during training process except that during a complete cycle of back propagation (forward pass and backward pass), the input data pattern shall not be changed. For other classifiers,

there are fundamental assumptions associated with specific requirements in input data which might be the reasons of poor accuracy. The statistical features of the trained BPNN models are shown in Tables 5-3 and 5-4.

5.3.5 Element Condition Index

3D visualization

3D modeling provides a better understanding of objects as well as several features can be derived from such models without going to bridge sites. This work utilizes a direct method of photo projection to generate 3D models with help of Google Sketch up (2008). Figure 5.16 illustrates the result of 3D modeling which shows overall dimensions of bridges and texture projected on elements.

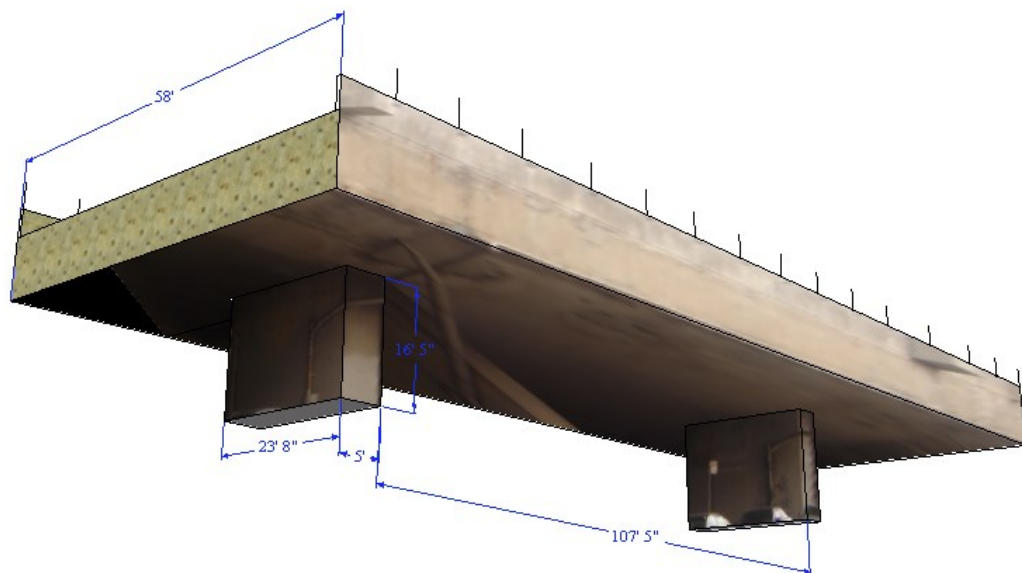


Figure 5.16: Fly over pass at the intersection of street Selby and Greene near Lionel Groux Metro

Distress Quantification

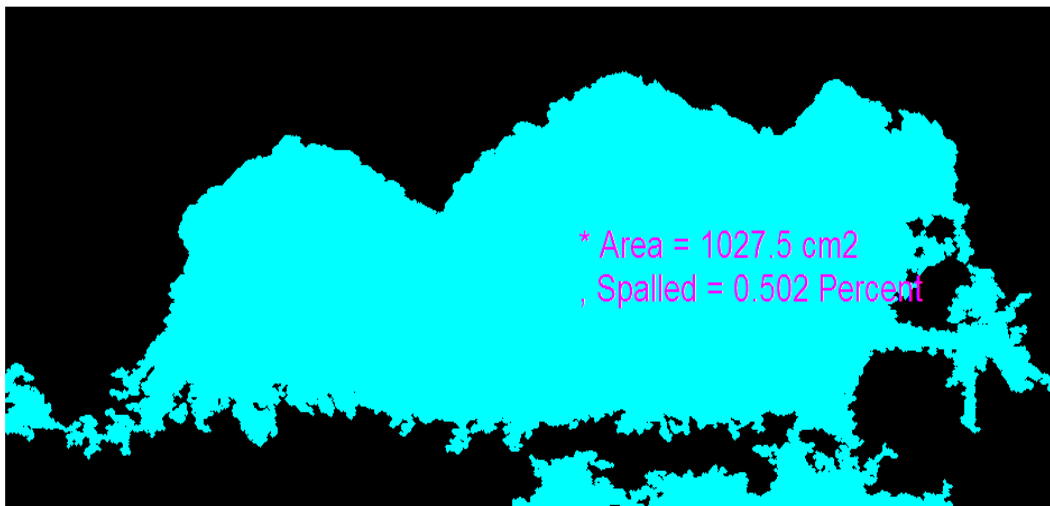
Evaluation of an element condition index requires estimation of percentage defect in structural components. For example, the element condition rating for concrete decks without overlay as defined in PONTIS are as follows: 1 (no spall, Delaminations, and temporary patching), 2 (the combined distress is 2% or less of the total deck area), 3 (the combined distress is more than 2% but less than 10% the total deck area), 4 (the combined distress is more than 10 % but less than 25% the total deck area), 5 (the combined distress is more than 25% the total deck area) (Minnesota Bridge Inspection Manual, 2009). Hence, it is important to determine the percentage of defects to assign an appropriate condition rating as shown in Figure 5.17.



(a)



(b)



(c)

Figure 5.17: (a) Detection of the spalled area, (b) defects identified as an object, and (c) object leveling and quantification.

Table 5.6: Condition Assessment of a Deck Slab

| S.N. | Area (m ²) | Percentage Defects (%) | Condition Rating |
|-------------------|---------------------------|---------------------------|------------------|
| Deck Slab (18*32) | 576 | | |
| Spalled | 5.2 | 0.92 | 2 |
| Exposed Reinforce | 5.2 | 0.92 | 2 |

A set of equations (5.13, 5.14, and 5.15) are proposed for evaluation of element condition index which utilizes the information of condition rating obtained from digital image processing.

$$BCI = \{ \sum_{i=1}^N W(i) * ECI(i) \} / \{ \sum_{i=1}^N W(i) \} \quad (5.13)$$

$$ECI(i) = \{ \sum_{j=1}^n W(j) * SCI(j) \} / \{ \sum_{j=1}^n W(j) \} \quad (5.14)$$

$$SCI(j) = [\{ \sum_{k=1}^d m * W(k) \} / d] * 100 \quad (5.15)$$

where,

BCI = Bridge Condition Index, W (i) = Element Weight Factors,
 ECI (i) = Element Condition Index, W (j) = Sub-element Weight Factors,
 SCI (j) = Sub-element Condition Index, W (k) = Distress Weight Factors,
 N = Number of Bridge Components, m = Material Factors, Concrete =1.0,
 n = Number of Sub-element Components, d = Number of distress,

The weights of element and sub-element, and distress weight factors were adopted from Wakchaure and Jha, 2012. The distress weight factors are calculated from Equation 5.16:

$$W_k = [1 - (\text{Condition State} \# - 1) * (1 / (\text{State Count} - 1))] \quad (5.16)$$

The identified spalling defect is found to be 0.92 %. Based on this information, the condition ratings are assigned for the deck is 2.

Table 5.7: Evaluation of Bridge Condition Index

| S. N. | Component | Distress Type | Condition State No. | W _k | SCI(j) | W(j) | ECI(i) | W(i) | BCI |
|-------|-----------------|-------------------|---------------------|----------------|--------|------|--------|------|-----|
| 1 | Substructure | | | | | | 100 | 26 | |
| | Pier | Nil | 1 | | 100 | 26 | | | |
| 2 | Super-structure | | | | | | 75.00 | 15 | |
| 2a | Deck Slab | Spalling | 2 | 0.75 | 75.00 | 15 | | | |
| | | Exposed Reinforce | 2 | 0.75 | | | | | |

91

* Identified Defects

For an element having 5 condition states such as Condition State numbers 1, 2, 3, 4, and 5, the weights obtained from Equation 6 are 1, 0.75, 0.5, 0.25 & 0.0 respectively. Table 5.7 explains the procedure of calculating bridge condition index using the above equations. For

demonstration purpose, two types of defects are identified: spalling and exposed reinforced. Based on identified defects, the bridge condition is found to be in good condition as the derived bridge condition index number is 91.

5.4 Summary

This Chapter presents an automated prediction of condition rating models based on the severity of defects captured by using digital cameras and processing data with neural networks. The proposed method considers scaling defects to demonstrate the mapping of condition rating based on OSIM, 2008. The model contains 5 layers of neurons; one input layer, three hidden layers, and one output layer with several types of activation functions in each layer. The production data set, which has not been presented to the network during training of neurons, is later used to validate the model. A comparison of the estimated depth output by the BPNN model and the actual one for data points are plotted, and the acceptable accuracy has been observed showing a correlation coefficient of 89%. Similarly, the predicted condition ratings after training of neural networks are plotted with the actual condition rating obtained according to the OSIM (2008) manual, and the accuracy of the prediction of condition rating has been observed 99 % as a correlation coefficient.

A case study example has been demonstrated for evaluation of bridge condition index based on identified defects. This procedure can reduce inspections time as inspectors need only to take engineering photographs, and analyze them to determine the distress level in order to assign element condition rating. Once element rating is available, it can be summed

at bridge level to find bridge condition index. Since the proposed method is fast and less expensive, the frequency of inspection can be altered to provide additional safety to bridges by recognizing the effect of extreme loadings and defects propagation.

Chapter 6: A Study of Defect Propagation

6.1 General

This chapter proposes a novel approach of change detection based on non-dimensional set of parameters obtained from spectral and fractal analysis of digital images. Radke et al. (2005) conducted a systematic survey on the state-of-the-art for change detection based on digital images taken from close field of view. However, their work was demonstrated in general terms without emphasising on a particular area of application. Previously, authors worked in evaluating for change detection for condition assessment of civil structures based on comparison of multi-temporal remote sensing data (Singh 1989, Coppin & Bauer 1996). The key aspect of change detection in those studies was based on remotely sensed data from satellites or flying airplanes. To address the problem of change detection in concrete structures for bridge inspection, this thesis proposes a set of scale-invariant shape descriptors obtained from Fourier and fractal analysis of digital images. In the process of change detection, it is necessary to establish a base image from where percentage change can be measured. For this purpose, two types of images are used in developing the concept; real crack images from testing of reinforced concrete beams in laboratory environment, and fractal images generated through fractal tree algorithms simulating the base crack and its propagation.

6.2 Periodic Detection of Defects

The change detection process has many engineering applications. It can be used to monitor the Earth surface such as it changes due to construction, deforestation, floods, forest fires and other kinds of activities (Carlotto 1997). High resolution 3D scanning techniques were used to measure internal damages and crack growth in a small mortar cylinder at different levels of deformation and loadings (Landis et al. 1999). In recent years, the concept of change detection through digital images has been extensively used for medical diagnosis. Such techniques also have valuable applications to find subtle changes between MRI (Magnetic Resonance Imaging) scans for assessing the progression of diseases over time (Bosc et al. 2003). Change detection approach answers some of the fundamental questions such as, 1) how fast the changes are taking place; and 2) what is the trend of changes (EL Shehaby et al. 2012). However, there are a number of limitations for a successful application of change detection in engineering fields. For examples, the lack of a priori information about the shape of changed areas, absence of a reference background, differences in lighting conditions, and the alignment of multi-temporal images are important ones (Townshend et al. 1992).

6.3 Fractal Damage Characteristics

Fractal geometry has abilities to model irregular shapes and to measure fractal dimension more accurately than dividing the region into regular geometry (Mandelbrot 2008). Recently, fractal theory has been extensively used in many engineering field and the

application has been also tested on analysis of concrete structures (Carpinteri 1994). For example, fracture surfaces of rock were measured by fractal dimension which basically characterize the topology of rock surfaces (Zhou and Xie 2003).

Berke (Berke 2005) introduced a new mathematical tool for estimating spectral fractal dimension (SFD). Fractal dimension (FD) estimation is primarily based on a binary image which did not consider the color associated with original image. He showed that SFD had higher number than FD. Similarly, fractal theory based on mono-fractal and multi-fractal was suggested for online non-destructive damage assessment of reinforcement concrete structures (Maosen et al. 2006). They showed that fractal theory and conventional damage parameters are linearly correlated with commonly used physical parameters such as natural frequency, average carbonized depth, and residual material intensity.

Likewise, Carpinteri et al. (2009) used fractal analysis for evaluation of damages in concrete structures. They found that single fractal dimension did not adequately describe a crack network since two crack domains might have the same fractal dimension having significantly different properties. This emphasises that apart from fractal features, other feature attributes need to be considered for defining the system properly. These studies suggest that comparison of multiple defects with fractal dimension may not be a good tool. However, it can be used as a tool for change detection. Fadi (2010) developed a framework to automate the detection, localization, and characterization of subsurface defects inside bridge decks based on ground penetrating radar (GPR) images. The developed algorithms

were based on a fractal-based feature extraction to detect defective regions, estimate the depth of defects, and classify defects in concrete structures.

6.4 Methodology

A new algorithm for change detection is developed which can quantify changes in element condition state based on fractal and spectral analysis of digital images shown in Figure 6.1. Two types of experiments are performed in analyzing digital images for deriving defect parameters. In the first experiment, eight sets of images are captured during bending test of a reinforced concrete beam at different loading stages as discussed earlier. In the second experiment, four sets of artificial crack images are generated simulating the notion of cracks observed at different inspection time. The proposed method requires high-resolution images to capture defect propagation over time. To achieve such high-resolution images, two cameras are used to collect digital images. The first camera is placed orthogonal to the defect surface and focuses only on the crack of interest, whereas the second camera is placed next to the first one focusing on the entire concrete surface. The details of using hybrid camera for image acquisition had been discussed in details by Nishimura et al. (2012).

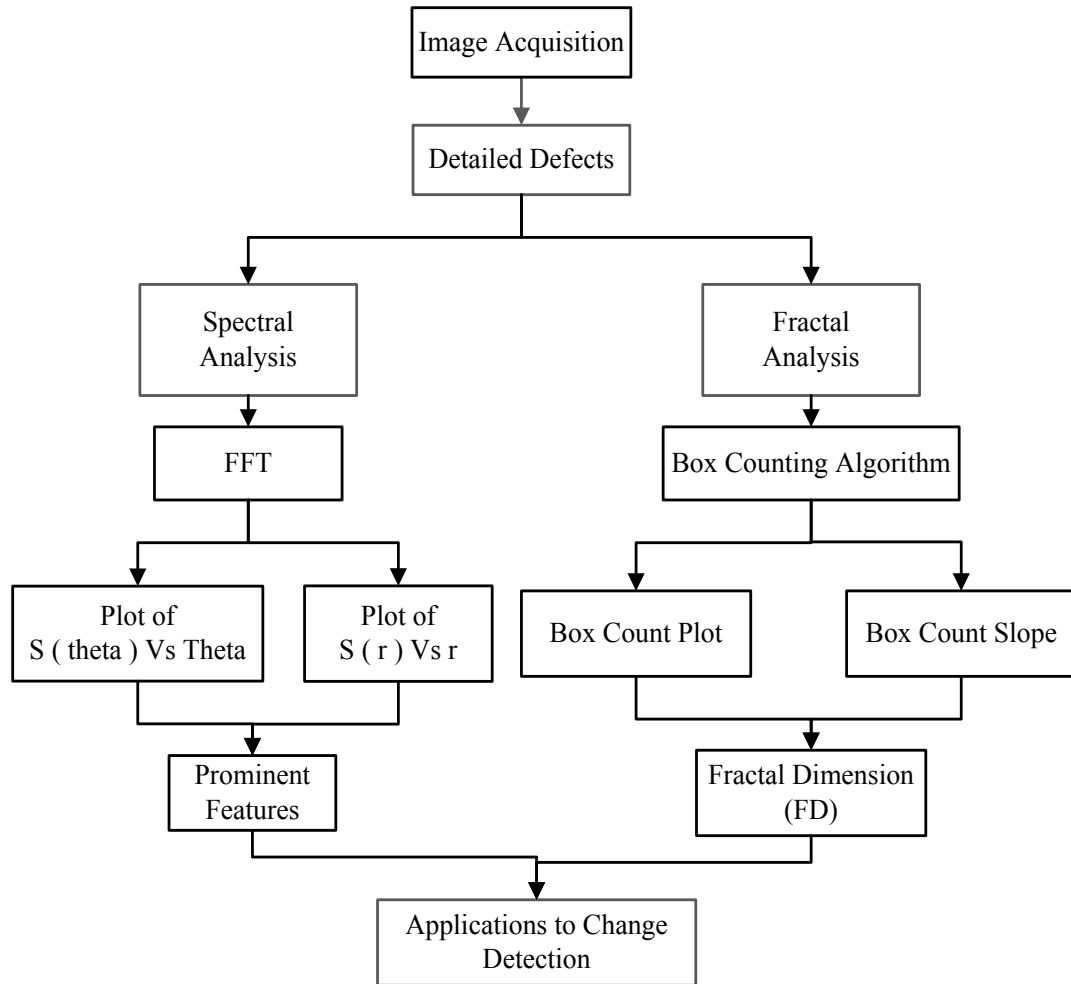


Figure 6.1: Proposed Change Detection Algorithm

6.4.1 The Fractal Analysis of digital images

Before carrying out fractal analysis of digital images, it is necessary to have a reliable method for defect quantification based on digital image processing. The crack quantification model used in this Chapter is taken from Adhikari et al. 2014. The segmentation approach adopted for the procedure is Canny Edge Detection algorithm because the performance of Canny algorithm has been observed superior over Sobel,

Prewitt, Robert, and LoG (Laplacian of Gaussian) in many scenarios (Maini and Aggarwal (2009)).

The concept of fractal was introduced by Mandelbrot (2008) to describe the irregular structures of many natural objects and phenomena. The typical fractal dimension for fractal dust lies between 0- 1, for fractal signal between 1- 2, and for fractal surface between 2- 3 (Turner et al. 1998). Fractal and Euclidean dimensions are equal to 1 for a straight line; however, for a line inscribed in a plane, the fractal dimension varies from 1 to 2 depending upon the tortuosity of crack and how crack fills the entire plane.

6.4.2 Computation of Fractal Dimension

Fractal dimension obtained from fractal analysis has many different applications in Civil Engineering, including rock surface study due to fracture (Lee et al. 1990, Kulatilake et al. 1997), the study of cracks in concrete (Farhidzadeh et al. 2012, Carpinteri et al. 2012), and condition of crack propagation in reinforced concrete structures (Sun et al. 2011). In these studies, authors have used various algorithms for estimating fractal dimensions by introducing Bounding Box method, Spectral Fractal Dimension, Hurst method, Fractional Brownian Motion method, and to name a few. The popular method for estimating fractal dimension in civil engineering application is the Bounding Box method because it is easy to use and requires selection of box size for a given image frame (Kulatilake et al. 1997, Farhidzadeh et al. 2012, Liaw & Chiu 2009). For condition assessment of reinforced concrete structures, the crack patterns are important surface pointers indicating the health of entire structures. To assess the health of concrete structures based on crack patterns, a

Damage Index (DI) based on fractal dimension using bounding box algorithm was proposed as shown in Equation 6.1 (Farhidzadeh et al. 2012). However, the process required the redrawing of cracks manually ignoring the crack width to get the crack pattern of the entire surface considered for analysis.

$$DI = \frac{D_i - DI}{2 - DI}, \quad 0 \leq DI \leq 1 \quad (6.1)$$

where,

D_i = represents the fractal dimension of i^{th} inspection, and

DI = represents the fractal dimension of first inspection when cracks appears to be visible.

Although the bounding box algorithm is simple and easy to use, it is not suitable for the time sequence data analysis (Ashkenazy et al. 1999). In such case, the more popular method of estimating fractal dimension is by using Hurst exponent H , and the fractal dimension D can be estimated from Equation 6.2 (Biagini 2008).

$$D = 2 - H \quad (6.2)$$

In further discussion of different algorithms, Fractional Brownian Motion (FBM) algorithm is suitable for describing the time dependent random events such as change in water level profile at the sea coast hitting on a wall, and weather patterns prediction. In fbm process, if the Hurst parameter corresponds to $1/2$, it is called constant process and random process is independent with variable increments. But when the Hurst parameter $H > 1/2$, the process is called positively correlated and when the Hurst parameter $H < 1/2$, the

process is called negatively correlated (Biagini 2008). Berke (2005) used spectral characteristics to evaluate fractal dimension taking into account of color layers associated with the given image frame. To demonstrate spectral fractal dimension, he took two digital images; one black and white image (8 bits) and another color image (24 bits). He calculated the fractal dimension of both images using bounding box method and was found as 1.99, whereas the spectral fractal dimension for the color image was increased to 2.49 considering the color layers in the image (Berke 2005). Based on the literature review, it was found that the problem in hand with the characterization of concrete surfaces, the bounding box method is more suitable which has been adopted for this research and the detailed algorithm has been explained in next section.

6.4.3 Box-counting of 2D images

To demonstrate the concept, a square box is considered having side length ϵ and N is the number of box required to fill the square space, then Equation 6.3 can be used to develop the relationship for estimating FD for any object (Banerjee 2009).

$$N(\epsilon) \equiv (1/\epsilon)^2 \quad (6.3)$$

For triangle,

$$N(\epsilon) \equiv \frac{1}{2} * (1/\epsilon)^2$$

For Circle,

$$N(\epsilon) \equiv \pi/4 * (1/\epsilon)^2$$

In general, it can be concluded that the idealized objects converges to

$$N(\epsilon) \equiv k * (1/\epsilon)^2$$

where, k is a constant. By taking log on both sides of the above expression, the following relation can be derived,

$$\ln N(\epsilon) = \ln(k) + 2 * \ln(1/\epsilon)$$

$$2 = \ln N(\epsilon) / (\ln(1/\epsilon)) - \ln(k) / (\ln(1/\epsilon))$$

In the above relation, the number 2 represent the dimension of a regular plane shape, which can be replaced by the fractal dimension, FD, for an object of an irregular shape. Since, the second term in the above relation vanishes to zero as ϵ tends to infinity, the expression for FD of an object can be simplified as follows in Equation 6.4.

$$FD = \ln N(\epsilon) / (\ln(1/\epsilon)) \quad (6.4)$$

The proposed workflow approach for estimation of fractal dimension is illustrated in Figures 6.2, and 6.3. Figure 6.3 (a) explains the process of size selection and Figure 6.3 (b) shows the derivative of the above plot to visualize fractal behaviour along the curve.

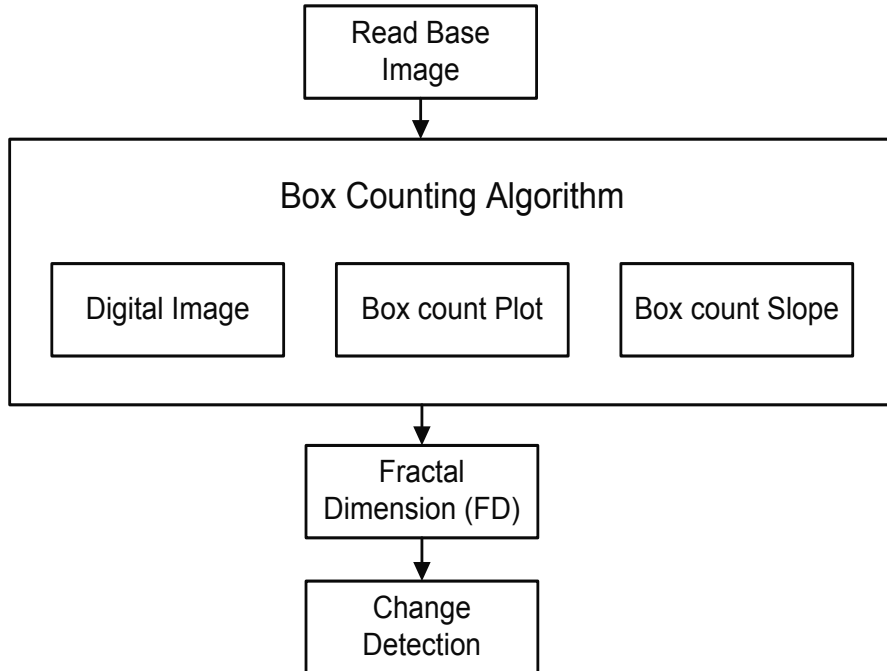
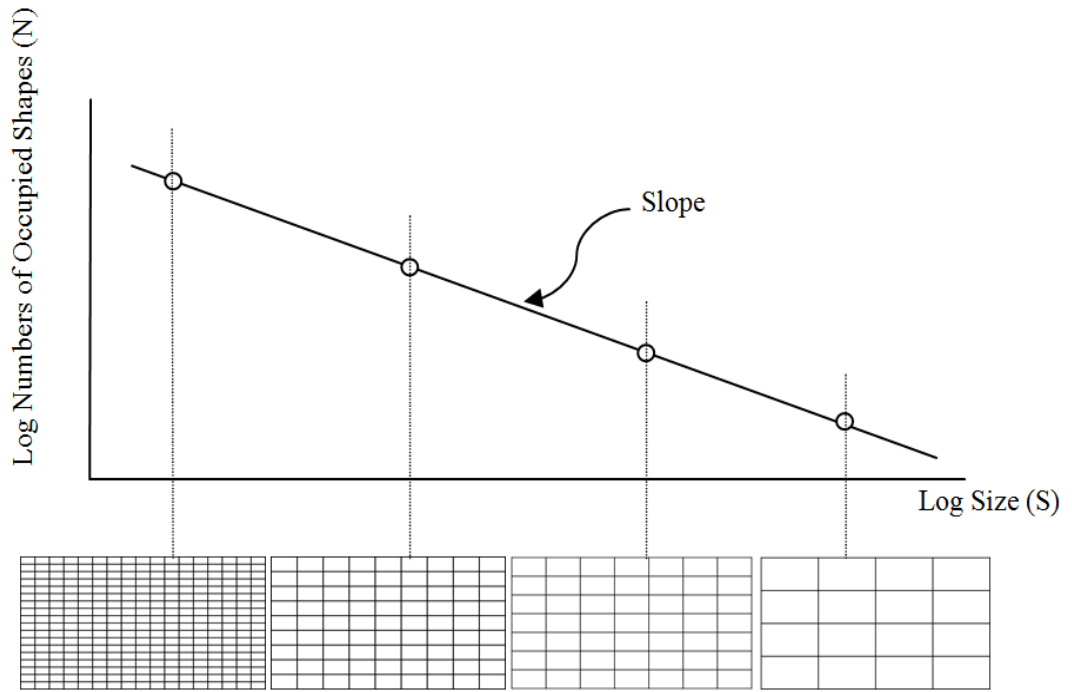
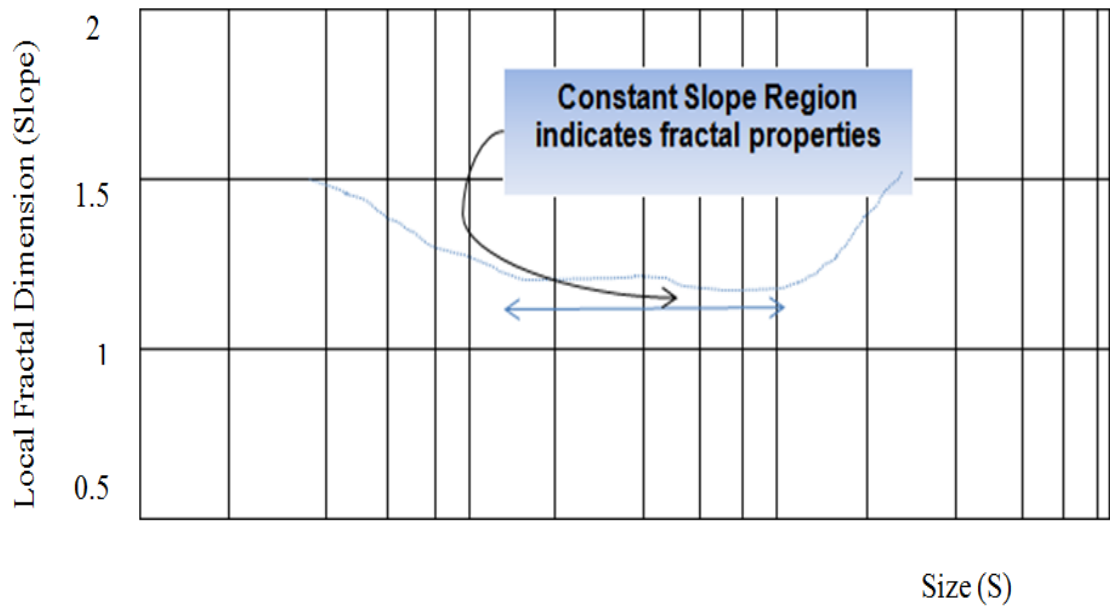


Figure 6.2: Box Counting Work Flow Diagram



(a)



(b)

Figure 6.3: Box Counting Modelling Process

6.5 Spectral Analysis

Figure 6.4 illustrates the work flow diagram for the change detection procedure in spectral domain. Spectral descriptors can provide quantitative information of images taken at different times to classify and rank them. For this operation, we need to convert the original images into frequency domain by Fast Fourier Transform (FFT). The FFT spectrum reveals information about the principal direction of texture contained in the images. Also, the location of the fundamental peaks provides information about the fundamental periods associated with the texture of the given images. Such method is useful for discriminating between the periodic and non-periodic texture patterns, and for quantifying differences among periodic patterns.

Spectral descriptors can provide quantitative information of images to classify and rank them taken at different times. The Fast Fourier Transform (FFT) of the selected image is shown in Figure 6.5. For convenient, Fourier Spectrum is converted to Polar Co-ordinates. These procedures yields a function $S(r, \theta)$ called spectrum function and r and θ are variables in polar coordinate system (Gonzalez et al. 2009). Two important relationships are derived from this frequency plot.

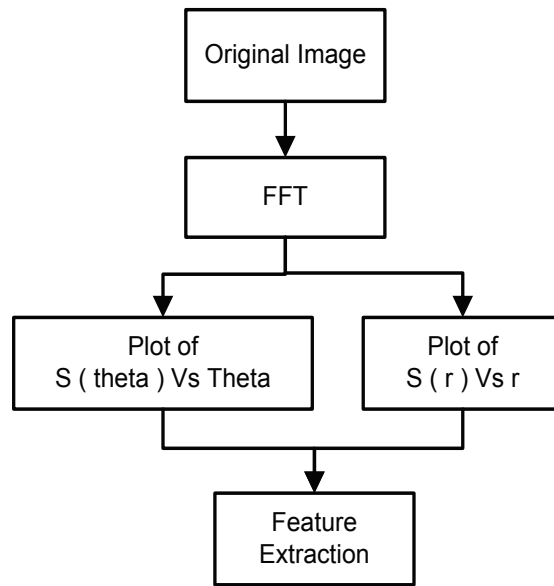


Figure 6.4: Spectral Change Detection

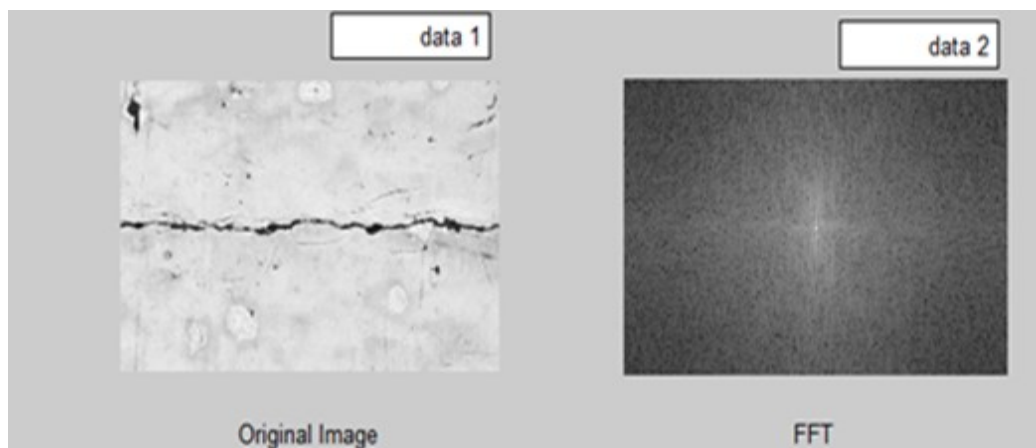


Figure 6.5: Fourier Transform of Digital Images at Time T1

A global description is obtained by integrating these functions as shown in Equations 6.9 and 10 (Gonzalez et al. 2009):

$$S(r) = \text{Sum} [S_{(\theta)}(r)] \quad (6.9)$$

where, (θ) varies from 0 to π .

$$S(\theta) = \text{Sum} [S_{(r)}(\theta)] \quad (6.10)$$

where, (r) varies from 1 to $R_0/2$, R_0 = the radius of a circle centered at the origin.

The result of the above equations is a pair of coordinates $[S(r), S(\theta)]$. The plot of these coordinates provides the information of variation in spectral energy contained in texture form. Typical descriptors can be retrieved from the functions $S(r)$ and $S(\theta)$ which can characterize their behavior quantitatively. Typical descriptors include location of the highest value, the mean and variance of both the amplitude and axial variations, and distance between mean and the highest value of the function as shown in Figure 6.6 (a) and (b).

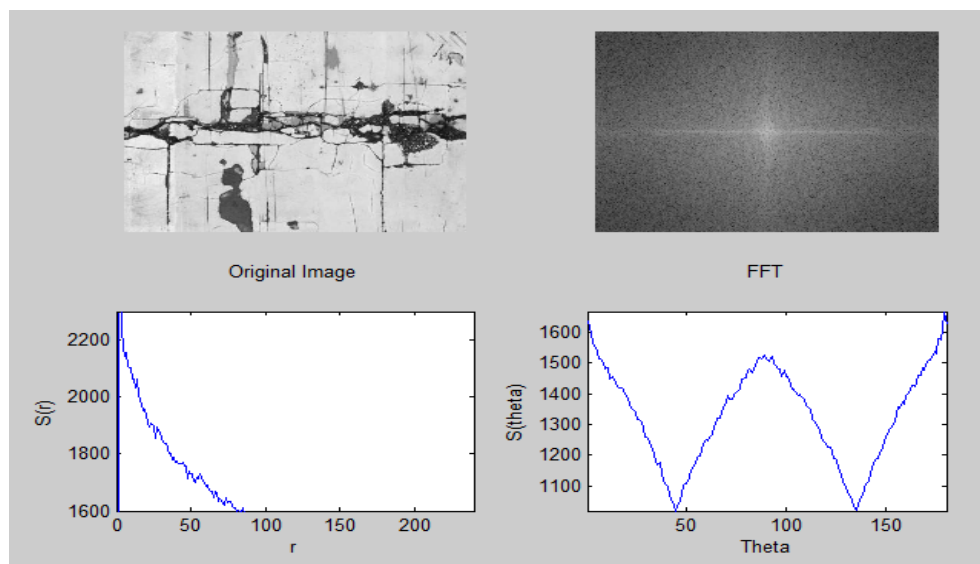


Figure 6.6: (a) Fourier Transform, Radial, and Angular Plot of Digital Images at Time T2

The distribution of energy in the radial direction between these two cracks varies from 100 to 150 and the texture variation in angular direction showed significant difference in the peak values from 1350 to 1600 as illustrated in Figure 6.6 (b). These digital values are the numerical representation of digital images which can be used as features to compare the extent of damage at different times.

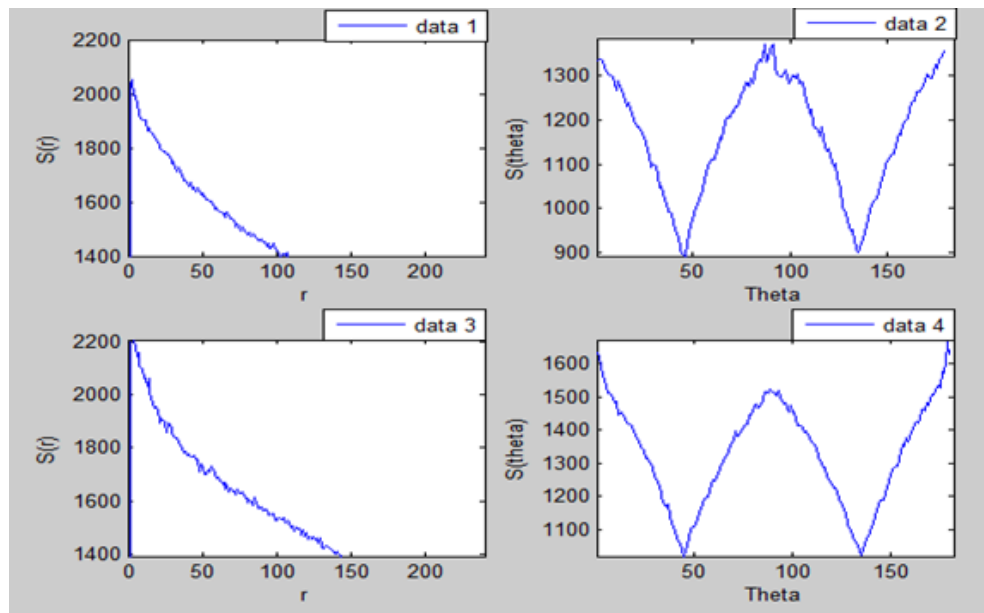


Figure 6.6 (b): Comparison of Descriptors at Time T1 and T2

6.6 Analysis and Results

In this experiment, a crack is tracked with a digital camera at various stages of loadings during the flexural behavior of reinforced concrete beams shown in Figure 6.7, and its

fractal dimension at each loading step is evaluated using box counting algorithm. In the second experiment, several crack patterns are developed to compare the fractal dimension simulating various images taken at different periods of time.

6.6.1 Analysis for isolated cracks

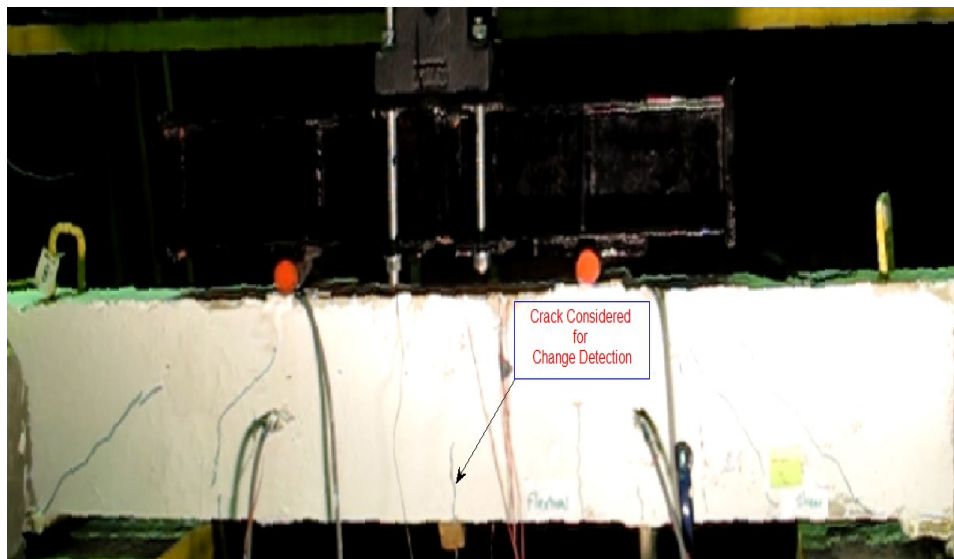


Figure 6.7: Crack Tracking in Lab Environment

The maximum crack width indicated in Figure 6.8 is evaluated using developed algorithms in previous chapter 4 and verified the results with the help of a crack scale. The crack image at 30 KN load is considered as a base image, and the crack image at 115 KN is represented as a final image. These crack images are used for estimating change detection based on spectral and fractal analysis of digital images which produce unique numbers to represent

the surface abnormalities. Figure 6.9 demonstrates the procedure for evaluating fractal dimension of a digital image based on box counting algorithm. It is clear from the 2D box-count plot of Figure 6.9 that all range of box-size increments for the crack image at 90 KN load do not follow the fractal dimension properties, and hence fractal dimension is evaluated by plotting the local dimension represented by a constant slope region.

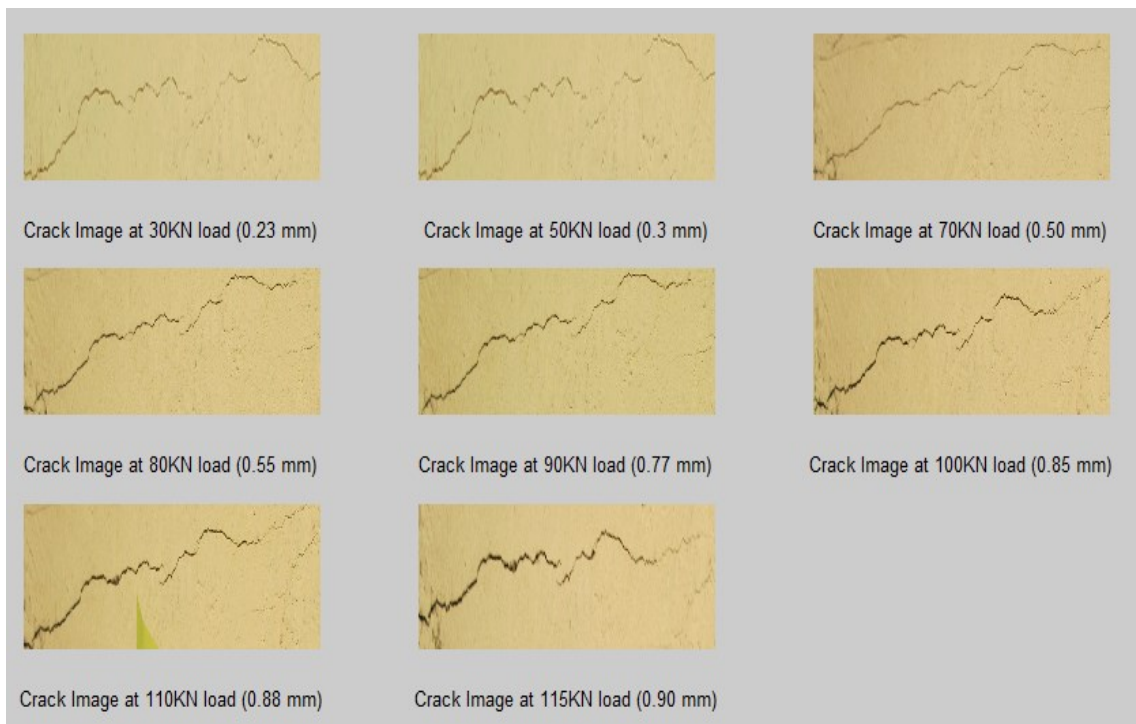


Figure 6.8: Cracked Images at Different Loads

Similarly, the cracks are processed for evaluating spectral parameters representing the surface defects in terms of surface texture. The adopted procedure for spectral analysis is already demonstrated in Figure 6.4. In spectral analysis for these crack images, the best parameter to represent the surface defects is found as peak value of radial plot which

shows the total energy variation in radial direction. It is clear from the Figure 6.10 that the peak value of radial plot for 100 KN load is 2272.

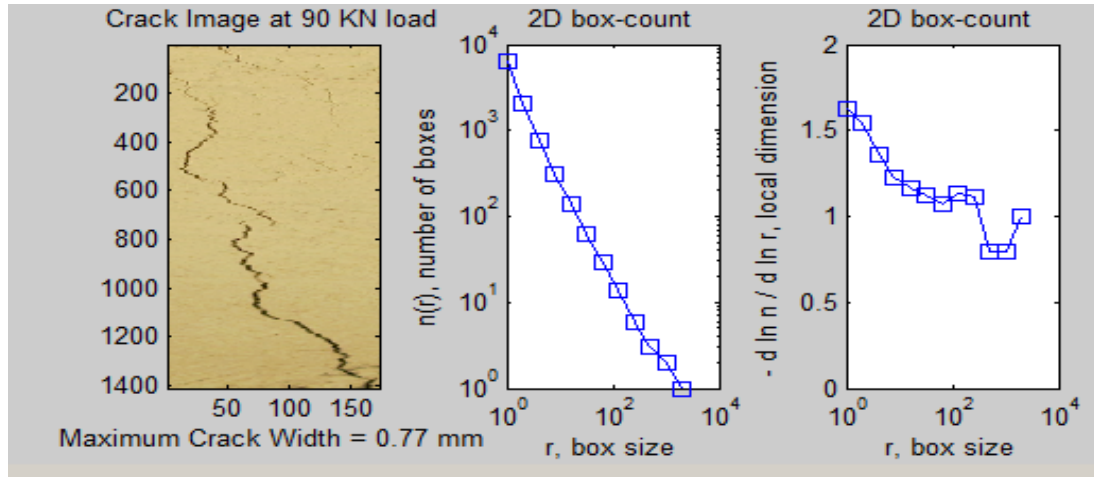


Figure 6-9: Estimation of Fractal Dimension

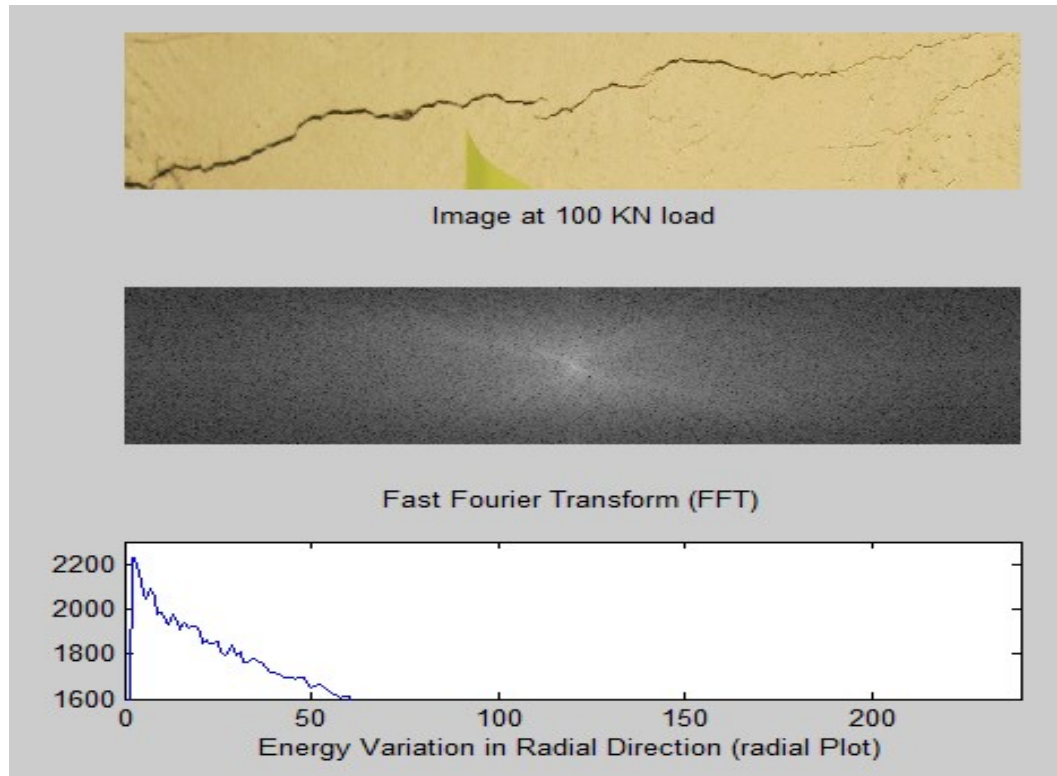


Figure 6.10: Estimation of Spectral Parameter

The obtained parameters from spectral and fractal analysis of the crack images are displayed in Table 6.1. Then, based on these information, the percentage change is calculated considering the base image as 30 KN load. The maximum detected change from fractal and spectral analysis are 23% and 24%, respectively which showed a close match in defect quantification. Also, the damage index (DI) as illustrated in Equation 6.1 proposed by Farhidzadeh et al. (2013) is evaluated and displayed in Table 6.2. The maximum damage index relating to image at 115 KN is found as 0.21. From visual inspection point of view, crack width of 0.9 mm is not critical; however, the crack width is wide enough for moisture penetration inside the beam which can result in corrosion of the

reinforcements (OSIM 2008). The result of damage index is 0.21, which is much lower than 1.0 representing the complete damage of the beam. The crack density (total crack length/total surface area) does not have significant change throughout the experiment because it is based on the crack length which does not change much in this particular experiment. The reason is that the beam has compressive tendency above the neutral axis and does not allow the crack to grow further, however, the change detection can be observed based on growing width of cracks.

6.6.2 Analysis for crack patterns

To illustrate the concept of change detection, several crack patterns are generated using fractal tree algorithm. The generated crack patterns are demonstrated in Figure 6.11 where crack 1 represents the base image crack pattern, and the crack 4 represents the final image crack pattern. The crack patterns are generated by changing the number of iterations (n) and affine transformation parameters (translation, rotation, and scaling) to fractal tree algorithms. The generated cracks from $n = 1$ to 4 are considered as crack propagation from time T1 to T4. A sample MATLAB code for the algorithm is shown in Appendix C.

Table 6.1: Spectral and Fractal Analysis of digital images

| Image Description | Fractal Analysis (FD) | % Change | Spectral Analysis (Radial Peak Value) | % Change | Damage Index (DI) |
|----------------------|-----------------------|----------|---------------------------------------|----------|-------------------|
| Base Image at 30KN | 0.960 | 0 | 1898 | 0 | 0.00 |
| Crack Image at 50KN | 1.039 | 8 | 2105 | 11 | 0.08 |
| Crack Image at 70KN | 1.078 | 12 | 2192 | 15 | 0.11 |
| Crack Image at 80KN | 1.084 | 13 | 2228 | 17 | 0.12 |
| Crack Image at 90KN | 1.121 | 17 | 2231 | 18 | 0.15 |
| Crack Image at 100KN | 1.142 | 19 | 2272 | 20 | 0.17 |
| Crack Image at 110KN | 1.172 | 22 | 2348 | 24 | 0.20 |
| Crack Image at 115KN | 1.183 | 23 | 2349 | 24 | 0.21 |

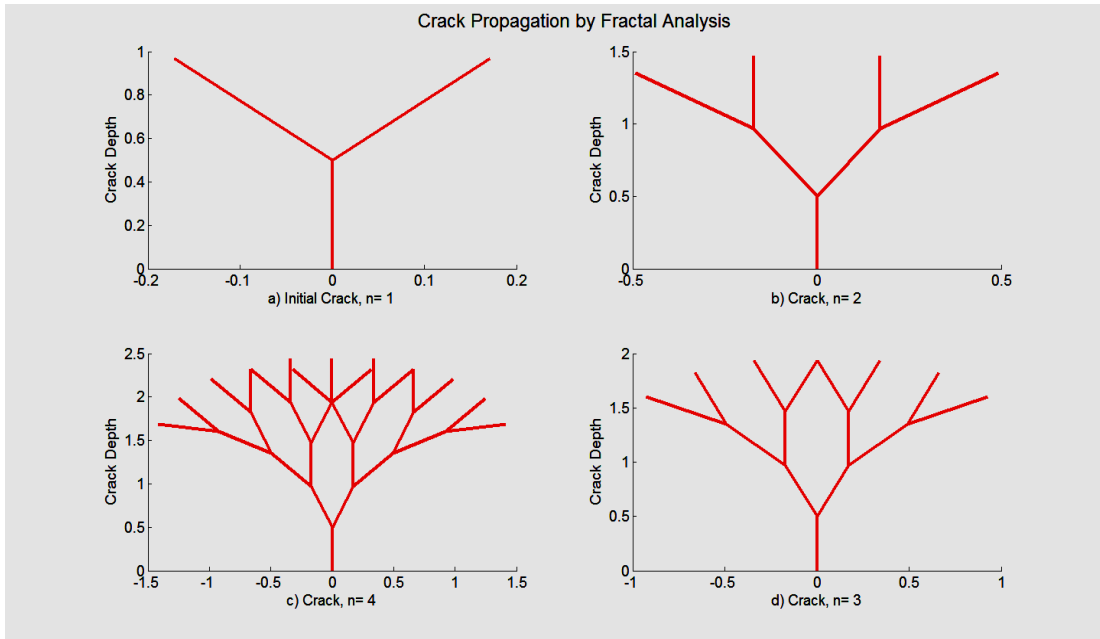


Figure 6.11: (a) Fractal images generated by Fractal Tree algorithms simulating cracks from Time T1 to T4

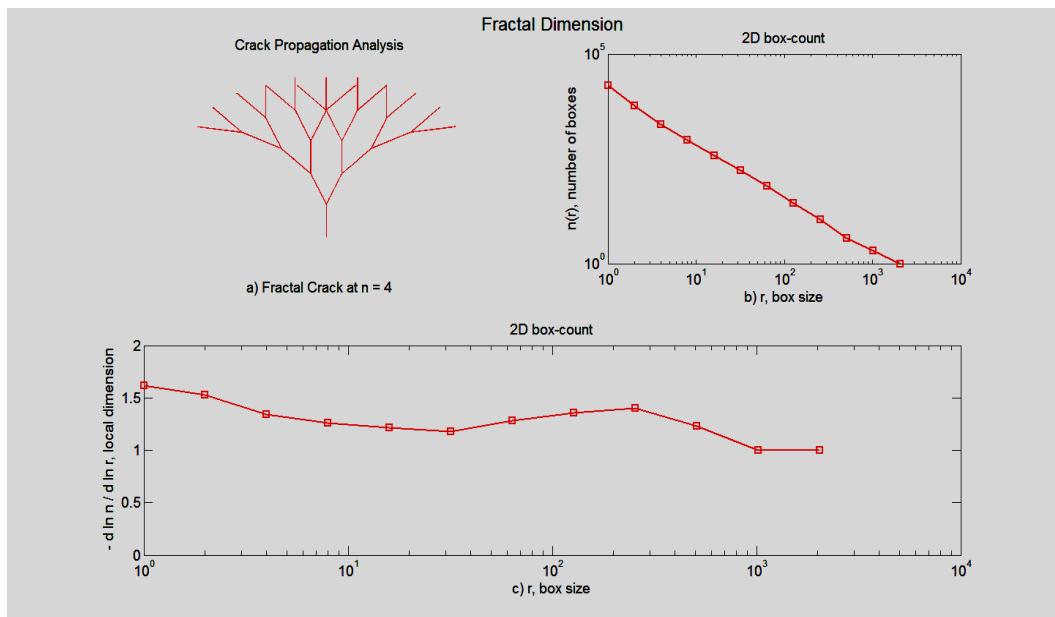


Figure 6.12: Estimation of Fractal Dimension using Box Count Algorithms

The result of the fractal analysis for crack patterns is shown in Figure 6.12 for the representative crack at $n = 4$. Figure 6.12 (b) shows the plot of box size against the number of box required to fill the given object space and Figure 6.12 (c) represents the derivative of the above plot representing the fractal dimension. The fractal dimension is evaluated for all the crack patterns and their plots are displayed in Figure 6.13.

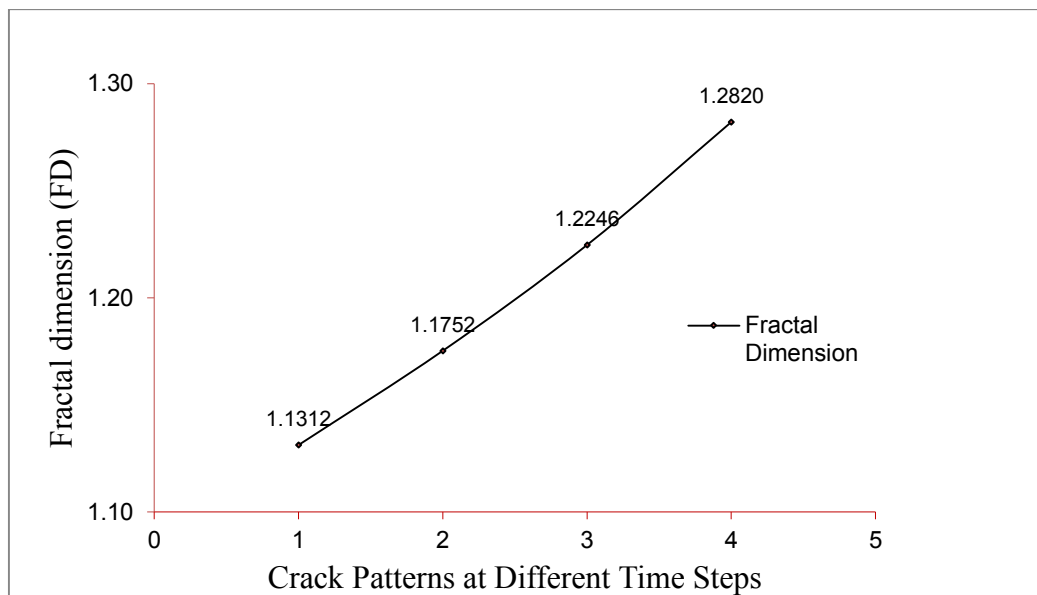


Figure 6.13: Change Detection by Fractal Analysis of Concrete Surfaces

The fractal-generated cracked images are converted to real images by photographing the images at different camera resolution shown in Figure 6.14. The printed cracks are imaged at camera resolution 3.591 pixels/mm, 2.07 pixels/mm, and at camera zoom 2x with

resolution 3.44 pixels/mm. The Min FD and Max FD represent the minimum and maximum fractal dimension obtained from standard deviation of plotted fractal dimension.

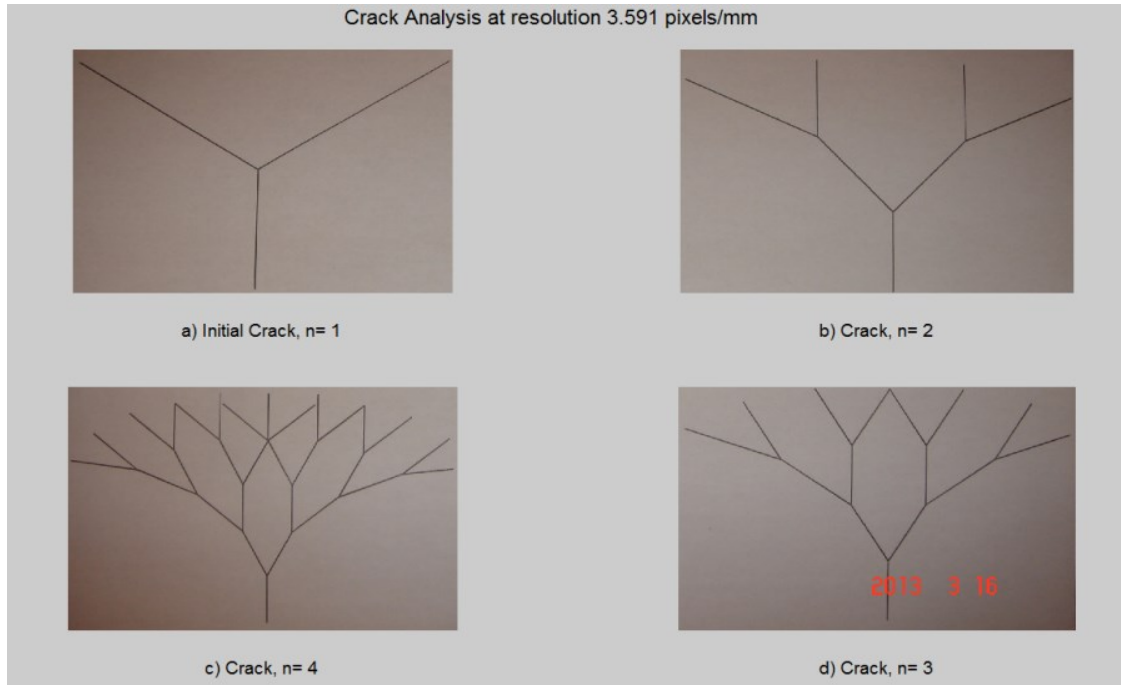


Figure 6.14: Experimented at different resolutions (Resolution 3.591 pixels/mm)

Due to camera quality and environmental lighting conditions, it is not possible to get the same results of defects based on fractal dimension. However, the change detection trends are similar. The results in Figure 6.15 shows that fractal dimension (FD) of cracks at camera resolution 3.59 pixels/mm is very close to FD of fractal generated cracks (taken as reference FD). However, the errors (deviation of FD from reference value) increase as the camera resolution is decreased to 2.07 pixels/mm. The errors further increase by zooming the camera although keeping image resolution at 3.44 pixels/mm. These errors are

All the results are summarized in Table 6.2 showing the comparison of results from fractal analysis, spectral analysis, and traditional approach of crack density (Ganapuram et al. 2012).

Table 6.2: Change Detection based on Spectral Analysis and Fractal Analysis

| Fractal Analysis | Crack # 1 | Crack # 2 | Crack # 3 | Crack # 4 |
|-----------------------------|-----------|-----------|-----------|-----------|
| No. of Cases (n) | 1 | 2 | 3 | 4 |
| Fractal Dimension (FD) | 1.13 | 1.18 | 1.22 | 1.28 |
| % Crack Growth | | 3.87 | 8.21 | 13.26 |
| Spectral Analysis | | | | |
| Spectral Mean Values | 1618.00 | 1656.00 | 1743.00 | 1798.00 |
| % Crack Growth | | 2.35 | 7.73 | 11.12 |
| Traditional approach | | | | |
| Length (mm) | 390.00 | 500.00 | 716.00 | 1105.00 |
| Area (mm ²) | 45135.00 | 45144.00 | 45144.00 | 45144.00 |
| Crack Density (%) | 0.86 | 1.11 | 1.59 | 2.45 |
| % Crack Growth | | 28.31 | 83.95 | 184.15 |

The crack #1 is considered as the base crack for result comparison. The results of fractal analysis and spectral analysis match very closely to 3 %, 8 %, and 12 % for Crack 2, 3, and 4 respectively considering Crack 1 as the base crack image. However, using the traditional Euclidean distance-based approach of obtaining crack density for the comparison purpose, the difference is found to be 28%, 84%, and 184% for the crack images 2, 3, and 4 respectively considering the base crack image as Crack 1. These results are too far away from that obtained from the spectral and fractal analyses. These analyses concluded that the Euclidean distance measurements are unable to capture the surface information contained in the form of texture properties.

6.6.3 Comparison with manually segmented images

To compare the efficiency of spectral change detection, two images are analyzed separately by choosing different threshold values manually and percentage changes between these two images are found. Figure 6.17 (a) presents an original image taken at time T1 and the binary image obtained by global image threshold using Otsu's method (Otsu 1979). After this operation, the image is labeled with different color as shown in Figure 6.17 (b) and the number of pixels contained in each object are counted and displayed. Similarly, the process has been repeated for another image taken at time T2 with the threshold value of 0.5 and leveled as shown in Figure 6.8 (a) and 6.18 (b).

Table 6.3: Change Analysis based on image registration

| Image Size | Threshold | Threshold |
|------------------|-----------|-----------|
| | (0.5) | (0.8) |
| | 298 x 448 | 298 x 448 |
| Image at Time T1 | 246* | 1532 |
| Image at Time T2 | 2300 | 14853 |
| % Defects at T1 | 0.18 | 1.15 |
| % Defects at T2 | 1.72 | 11.13 |
| % Change | 1.54 | 9.98 |

*image pixels

The same images are analyzed in frequency domain using spectral analysis of digital images and the results are shown in Table 6.4. Here, the mean values of radial and angular plots are of interest to find the change in successive images. The analysis shows that average percentage change detection found from spectral analysis is 10.75 % which is higher than the maximum threshold value of 0.8. Hence, it has been observed that spectral method completely avoids image registration process, provided superior results than traditional approach of image subtraction method.

Table 6.4: Change Detection based on Spectral Analysis

| | Image at T1 | Image at T2 | % Change |
|----------------------|-------------|-------------|----------|
| Mean of Radial Plot | 1386* | 1537 | 10.89 |
| Mean of Angular Plot | 1055 | 1167 | 10.62 |

* is a number obtained from Spectral Analysis indicating mean of radial plot at time T1.

6.6.4 Median Filter for Temporal Change Detection

To monitor change detection, digital images of an object are required at different periods of time. For illustration purpose, mask processing techniques are used to smooth images to get different extents of damage. The general operation of mask processing can be defined by Equation 6.11 (Gonzalez et al. 2009).

$$G(x, y) = T [f(x, y)] \quad (6.11)$$

where, T is a transformation function which operates on original image $f(x, y)$ to produce modified image $G(x, y)$. The size of the mask can be considered as [3 x3], [5 x5], or [7 x7] depending upon the degree of roughness or smoothness required. The first column of Figure 6.19 shows the same images at different damages levels using different mask, the second column shows the plot of radial energy variation, and third column shows angular variation of texture contained in images. The statistical values are summarized in Table 6.5.

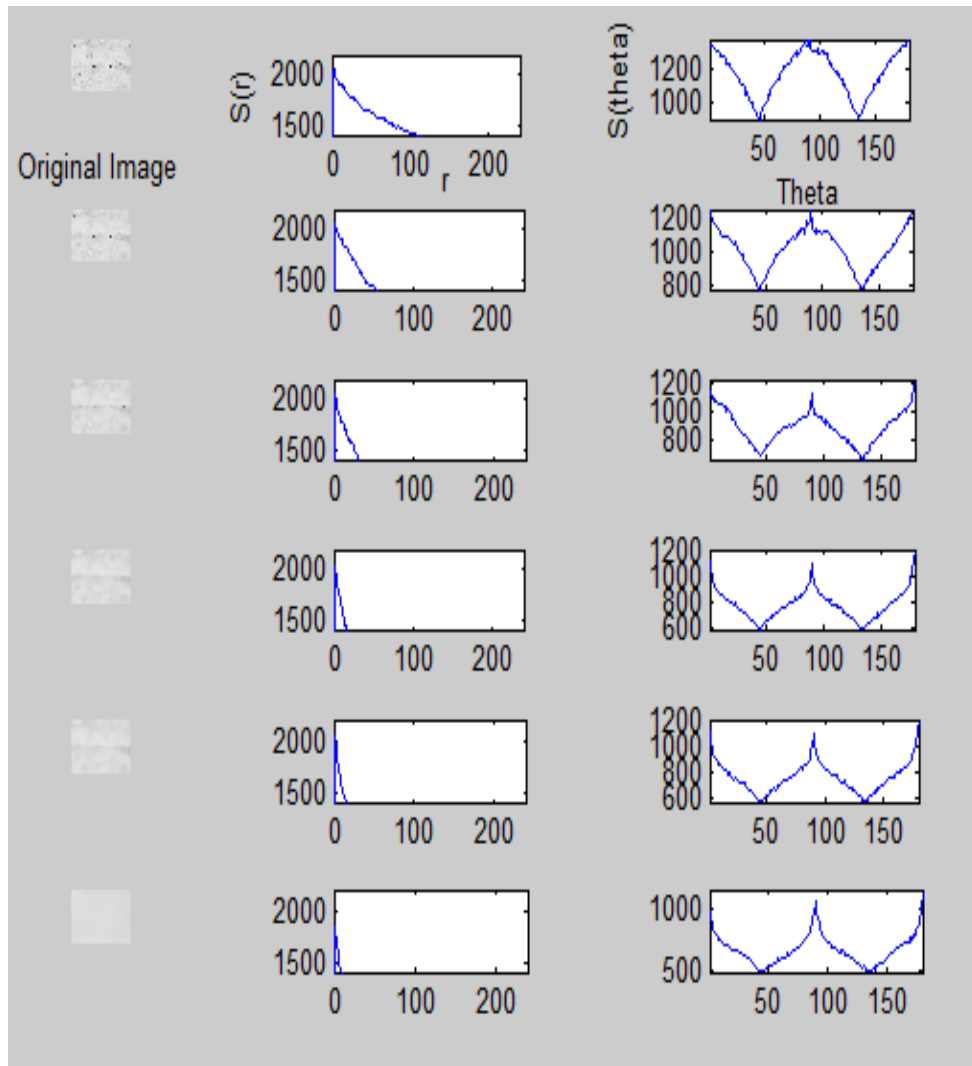


Figure 6.19: Temporal change detection

Table 6.5: Extraction of Descriptors from Spectral Analysis

| Images Descriptions | Radial Change | Angular Change |
|---------------------------------|---------------|----------------|
| Original crack (6) | | |
| Peak | 2052 | 1372 |
| Mean | 1537 | 1167 |
| Smoothed Image (5 Pixels) (5) | | |
| Peak | 2052 | 1236 |
| Mean | 1333 | 1017 |
| Smoothed Image (10 Pixels) (4) | | |
| Peak | 2048 | 1221 |
| Mean | 1157 | 885 |
| Smoothed Image (15 Pixels) (3) | | |
| Peak | 2037 | 1214 |
| Mean | 1008 | 777 |
| Smoothed Image (20 Pixels) (2) | | |
| Peak | 2029 | 1207 |
| Mean | 958 | 760 |
| Smoothed Image (100 Pixels) (1) | | |
| Peak | 1826 | 1165 |
| Mean | 865 | 671 |

6.7 Summary

This Chapter describes the development of new algorithm for periodic detection of changes in concrete defect and demonstrated its application utilizing digital images from laboratory environment as well as fractal generated images. The procedure extracts a set of dimensionless metrics pertinent to spectral and fractal analysis of digital images. The result shows that the maximum changes after the fractal and spectral analysis for the selected

images captured at 30 kN load to 115 kN load are 23% and 24% respectively measured from a base crack image at 30 kN load. Furthermore, Damage Index (DI) is also calculated based on the fractal dimension analysis of digital images, and the maximum value DI found is 0.21. The change of DI equal to 0.21 indicates safe operating condition for bridge components because the complete failure of concrete beams will happen at DI equal to 1.0. However, the correlation of such parameters with the performance history of bridge components needs to be studied further which is outside the scope of this work.

The second part of the spectral and fractal analysis is tested on different crack patterns generated through fractal tree algorithms. The results of fractal and spectral analysis match closely to 3%, 8%, and 12% change in cracks #2, #3, and #4 respectively where crack #1 is considered as the base defect. However, the tradition approach of obtaining crack density for comparison purpose is found to indicate the change level of 28%, 84%, and 184% for crack images #2, #3, and #4 respectively where crack #1 is considered as the base image. Also, the result of the spectral analysis of digital images is tested with the result of different threshold values. The detected change for the selected images taken at time T1 and T2 is 1.54% at threshold 0.5 and 9.98% at threshold 0.8. The change detection parameter obtained from the spectral analysis is 10.6% which neither required a threshold value nor an image registration process. The proposed method overcomes the limitations of the existing subtraction method by simply bypassing image registration processes and demonstrates the value of superior features of the developed algorithm.

Chapter 7: Conclusions and Future Work

7.1 Conclusions

Civil infrastructure systems are deteriorating at an alarming rate because of increased load (e.g. traffic on bridges and roads), aging, material degradation, environmental effect, and to list a few. To effectively manage infrastructure, reliable inspection reports are needed. However, the current practice of infrastructure condition evaluation is primarily based on visual inspection. Such approaches have been identified with several limitations: costly, time consuming, and prone to subjective error. This thesis develops image-based condition assessment tools and techniques, which can be integrated with existing bridge management systems (BMSs) in order to enhance the reliability of current inspection practices.

In the current practice, BMSs store large numbers of digital images; however, the images are used just as a reference to support the inspected documents. This thesis utilizes digital image based inspection of bridges focusing on object detection and quantification of defects in order to augment the information obtained from current inspection practices. Although, remote sensing technologies were used earlier for tracking of Earth objects, their applications in Civil Engineering for condition assessment of bridges has been recognized only recently after recent development in camera and other imaging technologies.

The research encompasses three modules: digital image processing, data processing, and condition assessment modules. The condition assessment module of this research is based

on data processing where the important feature metrics are extracted from digital images using various image-processing technologies. For data acquisition, commercially available digital cameras have been used to acquire digital images from lab experiments during bending test of reinforced concrete beams, as well as from field study of existing bridges in Montreal, Quebec.

The first module of this research develops crack quantification model which evaluates crack properties using digital image processing. The quantified crack properties have been validated by measuring the crack properties manually using crack scales. Further, this module develops relationship between crack width and length, which are essential pieces of information required for condition assessment of concrete structures. The result of this module showed that under the increasing tendencies of loads, the crack width increases, while the crack length may or may not increase.

The second module of this thesis develops an automated prediction algorithm for condition rating of concrete bridge elements using digital images. Under this method, scaling defects are considered as a candidate defect in bridges, and the guideline adopted for developing the algorithm is based on Ontario Structure Inspection Manual (OSIM). Although only scaling defect is considered for demonstration purpose, the method can be easily extended to other types of defects on a concrete surface. The developed automated algorithm for mapping of condition ratings is based on the supervised training of back propagation neural networks. The result of the developed models showed better prediction capability of condition rating over the existing methods: Naïve Bayes Classifiers and Bagged Decision

Tree. The developed model has been validated using validation data sets and presented in the form of statistical data.

Likewise, this research also proposes change detection model defined as change in element condition state over times. The purpose of this model is to track the progression of defects at different inspection intervals. In this method, a set of dimensionless metrics pertinent to spectral and fractal analysis of digital images are generated. The fractal analysis of digital images is described by fractal dimension (FD) using Box Counting algorithms. Similarly, the method of spectral analysis requires digital images to be translated from spatial domain to Fourier domain, and then finds one dimensional signatures of an image to quantify change detection. Such approach avoids image registration process since it doesn't operate in spatial domain. The proposed methods successfully generate unique numbers to represent defect characteristics required for change detection and make them feasible for computer automated applications. To assist visual inspection for condition assessment of bridge components, each of the above discussed modules utilizes 3D visualization of defects to mimic on-site visual inspection.

The developed image-based models in this research can be potentially integrated with any existing automated bridge management system such as PONTIS in order to enhance the reliability of visual inspection or can be integrated in an excel sheet for independent analysis.

7.2 Contributions

1) This research contributed an integrated model consisting of crack quantification model supported by 3D defect visualization, and neural networks models for condition assessment of reinforced concrete beams.

One important contribution of the integrated model is crack length estimation based on crack skeleton itself which considers the tortuosity of the crack alignment. This aspect (tortuosity) has been overlooked in the existing method where the length of a crack is estimated from a bounding box. The existing crack segmentation method is based on searching of crack connectivity which requires input of at least one crack skeleton point to start searching for the crack connectivity. Also, the orientation angle of each crack pixel need to be calculated and checked to know whether the crack pixel can be included in that crack segment or not. The proposed method detects branch points (key marks) in a given image frame and extracts the features automatically. Current approach for 3D visualization requires field survey for defect measurement and then develops 3D models. A fast and easy 3D visualization approach has been proposed based on the digital images. Hence, it does not require field survey for measurements except digital images with high resolution cameras. The area of interest for industry experts are not only the maximum or the minimum crack width, but also the average crack width in a given crack segment. This information is important for billing or contractual purpose. In many cases, the depth of concrete beams is concealed and it is inaccessible for measuring crack lengths. This work

presents a model for crack length estimation given crack widths which are usually visible and can be measured using remote sensing technology.

2) Another contribution of the research is the development of automated prediction of condition rating model using neural networks and digital image processing techniques.

Digital image processing helps to automate the extraction of defect attributes, whereas, the application of neural networks automates the mapping of condition rating. The presented work is useful in enhancing the reliability of current Bridge Management System if integrated with any automated bridge management system such as PONTIS. Recently researchers have started to use Street View Google Images for quantification of civil infrastructure. This research forms a base for automated predication of bridge condition states without going to field visits if integrated with Google Street View models.

3) The third contribution of this research is to present change detection model based on spectral and fractal analysis of digital images to assess defects in reinforced concrete bridges. The proposed spectral method is based on Fourier Transform of digital images. The proposed approach works in the frequency domain, and hence, the method does not require the cumbersome operations in spatial domain such as, pixel-based operations or threshold based operations and image registration. Furthermore, the twisting of cracks can be best described by fractal analysis of crack images. The result of the current work is also compared by evaluating Damage Index (DI) based on fractal dimension obtained from fractal analysis of digital images. Non-Euclidean geometry-based measurement of change in defects for condition assessment of concrete bridge is one of the major contributions of

this thesis. The proposed approach eliminates the limitations of visual inspection and the process can be automated with the computer vision application to enhance the reliability of current inspection practices.

Based on the contribution from the present research a number of papers have produced for peer-reviewed journals and conferences as listed in Appendix-E.

7.3 Limitations of the Current Research and Scope for Future Studies

1) Training and testing of neural networks

The training and testing of neural networks are done with data collected from a particular beam tested in lab. Ideally data shall be collected from various sources with different types of beams, loading, and boundaries conditions. Then only the result of this model can be generalised for practical purpose in different locations. Another problem is the quantification of defects in common units of measurements. So, further automated image pre-processing algorithms need to be developed for automatic tracking of images scale. It is evident that the number of image pixels is different if the images of the same defects are taken at different fields of view. In the current research, either artificial or natural targets have been used to define scale in each image frame. The application of Ground Positioning System (GPS) for automatic tracking of images scale should be explored in the future studies. Also, the developed model needs to be compared with Fuzzy logic to compare the outputs which can accelerate the decision making process.

2) 3D visualization Model

The developed 3D models based on digital images provide additional information about condition of an infrastructure. The model developed for 3D visualization was based on commercially available software. Although this method was efficient in photo projection with texture, human intervention was required for drawing 3D elements on screen. The initial work has demonstrated the detection of defects and structural components using combination of 3D point cloud and digital images, a detailed analysis is required for automated development of 3D visualization model in combination of digital images for large and complex structures.

3) Scaling Problems in Digital Imaging

The current work considered only scaling defects for prediction of element condition ratings. However, an element might consist of several defects and each individual defect (extent and severity) contributes to the element condition rating. So, for the proper element condition assessment of elements, several expert functions need to be developed which can be integrated together to obtain a single condition rating for the element. Different digital image processing algorithms need to be developed to capture the different defects and extracting their feature vector for defect mapping. Also, the depth perception of defects is highly influenced by lighting conditions. The mapping of difference in lighting intensity (ΔI) and defect depths work well when digital images are taken in similar lighting conditions. However, in actual practice it might be difficult to maintain the same lighting conditions during data acquisition. So, it is necessary to acquire digital images in similar environmental conditions so that image pre-processing tasks can be minimized. The thesis

demonstrated the methodology of automated prediction of condition rating for bridges based on 19 data patterns obtained from analyzing digital images for demonstration purpose. However, the output of the models can be updated with additional information if available.

4) Available Time for Inspection

The future study will be able to answer the question of what will be the revised inspection frequency for an element or what is the remaining life of an element by combining fracture mechanics with NDT. Cracking in concrete can cause failure of bridges due to fracture of critical elements, and the two aspects need to be understood to deal with these situations. First, a mechanism is required to capture cracks with the aid of Non Destructive Test (NDT) to access the current condition of elements. Second, a failure assessment of bridge components needs to be evaluated based on element fracture mechanism. The first criterion is discussed to a great extent in this research to capture a crack and its quantification using digital image processing. However, the estimation of the remaining life of a component based on the fracture analysis of elements needs further study. The neural networks model discussed in this work can serve as the starting point towards this study. More tests are required to capture the effects of different materials and their strengths which would ultimately affect the relationship between the crack depth and width. In a future study, finite element models can be helpful to study the effect of fracture mechanism of concrete elements under cyclic loads. From such simulations, it may be possible to establish a relationship among variable of concrete structures useful for condition assessment of civil infrastructure.

5) Selection of Parameter for Change Detection

In engineering practice of bridge inspection, the exact measurement regarding the shape of an object is not always important; rather a comparison of one shape to another is required for decision making purposes. Currently, the comparisons of two objects are performed through routine inspection based on Euclidean distance measurements. Such measurements are unable to describe the characteristics of defects associated with surface properties such as texture and color of digital images. To overcome such limitations, the proposed method based on spectral and fractal analysis of digital images provides unique metrics with respect to surface characteristics of digital images. However, the proposed methods possess the following limitations. There exist a number of spectral parameters that can be derived from spectral analysis of digital images. But it is not always obvious which parameter will better represent a particular type of defect in question. The use of a particular parameter is application-dependent and it needs to be carefully selected for a particular problem in hand. Likewise, for fractal analysis, robust defect quantification algorithms are necessary to estimate fractal dimensions of 2D objects. The result of fractal analysis reveals that the selected defects do not possess fractal properties for the entire box size increments. Hence, only local fractal dimension is estimated for change detection analysis. However, such estimation might have an effect on the performance evaluation of structural elements based on fractal dimension. In terms of operating time, spectral analysis performed faster over fractal analysis of digital images. The future work requires making a correlation between shape descriptors and object's behavior. The following two approaches might be

suitable for establishing such relationships. First, all possible information regarding the shape that controls an object's behavior would be collected. Based on these collected data, statistical analysis could be performed to find out which shape descriptors would be closely correlated to the performance of component by establishing suitable mathematical equations. Second, a series of controlled experiments using finite element software could be performed to study the object's behavior with different surface characteristics. By considering few experiments, it would be possible to study the effect of any variable on the behavior of an object more effectively than only statistical analysis.

References

AASHTO (2001), American Association of State and Highway Transportation Officials, Manual for condition evaluation of bridges, 2nd Ed, 2001 Washington, D.C

AASHTO (2005), Cambridge Systematic, I., Pontis Bridge Management Release 4.4 User Manual, Washington D.C. p. 572

AASHTO (2009), BRIDGEWare Update Newsletter, 3.

AASHTOWare Bridge, Webinar Series, Basic Uses of PONTIS, 2012, <http://www.youtube.com/watch?v=GAUylcxkWTY>

Abdalla J. A. and Hawileh R. A. (2013), Artificial Neural Network Predictions of Fatigue Life of Steel Bars Based on Hysteretic Energy, Journal of Computing in Civil Engineering, 27(5), 489-496.

Abdel-Qader I., Abudayyeh O., Kelly M. E., (2003), Analysis of Edge-detection Techniques for Crack Identification in Bridges, Journal of Computing in Civil Engineering 17 (4) 255–263.

Abdel-Qader I., Pashaie-Rad S., Abudayyeh O., Yehia S., (2006), PCA-based algorithm for Unsupervised Bridge Crack Detection, Advances in Engineering Software 37 (12) 771–778.

Abudayyeh, O., Al Bataineh, M., & Abdel-Qader, I. (2004), An Imaging Data Model for Concrete Bridge Inspection. Advances in Engineering Software, 35(8), 473-480.

ACI 224R-01, (2008), Control of Cracking of Concrete Structures, ACI Committee 224, American Concrete Institute, Farmington Hills, MI.

Adhikari, R. S., Moselhi, O., & Bagchi, A. (2014), Image-based Retrieval of Concrete Crack Properties for Bridge Inspection, *Automation in Construction*, 39, 180-194.

Adhikari, R.S., Moselhi, O. and Bagchi, A., (2013a), Image-based Change Detection for Bridge Inspection, 30th International Symposium on Automation and Robotics in Construction (ISARC 2013), August 11 to 15, 2013 in Montreal, Canada.

Adhikari, R.S., Moselhi, O. and Bagchi, A., (2013b), A Study of Image-Based Element Condition Index for Bridge Inspection, 30th International Symposium on Automation and Robotics in Construction (ISARC 2013), August 11 to 15, 2013 in Montreal, Canada.

Adhikari, R.S., Zhu, Z., Moselhi, O. and Bagchi, A., (2013c), Automated Bridge Condition Assessment with Hybrid Sensing, 30th International Symposium on Automation and Robotics in Construction (ISARC 2013), August 11 to 15, 2013 in Montreal, Canada.

Adhikari, R.S., Bagchi, A. and Moselhi, O., (2013d), Spectral and Fractal Analysis of Digital Images for Evaluating Defects in Bridges, IEMCON2013, 23 August 2013, Science City, Kolkata, India.

Adhikari, R. S., Moselhi, O., & Bagchi, A. (2012a). Automated Prediction of Condition State Rating in Bridge Inspection. *Gerontechnology*, 11(2), 81.

Adhikari, R. S., Moselhi, O., & Bagchi, A. (2012b). Image-based Retrieval of Concrete Crack Properties. *Gerontechnology*, 11(2), 315.

Ahlborn, T. M., Shuchman, R., Sutter, L. L., Brooks, C. N., Harris, D. K., Burns, J. W., & Oats, R. C. (2010). An Evaluation of Commercially Available Remote Sensors for Assessing Highway Bridge Condition, Transportation Research Board.

Akgul, F. (2012), Development of a Bridge Management System Incorporating a Newly Developed Model for Element Condition Evaluation based on Damage Effects, Structure and Infrastructure Engineering.

Aktan, H., Attanayake, U., Mohammed, A. W., & Wiggerhauser, H. (2013). Research on Non-Destructive Evaluation-Workshop (No. RC-1597).

Alan M. L., A (2011), Framework for Object Recognition in Construction Using Building Information Modeling and High Frame Rate 3D Imaging, PhD Thesis, Virginia Polytechnic Institute and State University.

Anderson, J. A., & Davis, J. (1995). An Introduction to Neural Networks (Vol. 1). Cambridge, MA: MIT press.

Aronoff, S. (2005). Remote Sensing for GIS Managers. Redlands, CA, ESRI Press.

ASCE Report Card for America's Infrastructure, 2013

<http://www.infrastructurereportcard.org/a/#p/bridges/conditions-and-capacity>.

Ashley M.L. (1898), Concerning the Significance of Intensity of Light in Visual Estimates of Depth, Psychol. Rev.5:595–615.

Ashkenazy Y., Lewkowicz M., Levitan J., Havlin S., Saermark K., Moelgaard H., & Thomsen P. B., (1999), Discrimination Between Healthy and Sick Cardiac Autonomic Nervous System by Detrended Heart Rate Variability Analysis, Fractals, 7(01), 85-91.

Austroroads, (2002), "Bridge management systems: The State of the Art." Report No. AP-R198, Australian and New Zealand Road Transport and Traffic Authorities, Australia.

Banerjee S., (2009), Online Lecture Series on Chaos, Fractals and Dynamical Systems, Department of Electrical Engineering, IIT Kharagpur.

<http://www.nptel.iitm.ac.in/video.php?subjectId=108105054>

Batchelor B. and Whelan P., (1997), Intelligent Vision Systems for Industry, Cmbridge University Press, Cambridge, England.

Bektas, B. A. (2011). Bridge Management from Data to Policy, Doctoral dissertation, Iowa State University.

Berke J., (2005), Spectral Fractal Dimension, Proceedings of the 7th WSEAS Telecommunications and Information's (TELE-INFO'05), Prague, ISBN 960 845, 11(4), pp.23 -26

Biagini F., (2008), stochastic calculus for fractional Brownian motion and applications, Springer

Bień J., Rewiński S. (1999), "New Generation of the Bridge Management Systems". XLV Scientific Conference: Research Problems in Building Engineering, Krynica, Poland.

Bien, J. (1999). Expert Functions in Bridge Management Systems. Wroclaw University of Technology, Poland.

Bień, J. (2000). Neural Networks in Bridge Management Systems. In Structures Congress of the American Society of Civil Engineers, Advanced Technology in Structural Engineering, Philadelphia

BIRM (2012), Federal Highway Administration, Bridge Inspector's Reference Manual (BIRM). Washington, DC. Publication No. FHWA NHI 12-049

Bisby L. A. and Briglio M. B. (2004), ISIS Canada Educational Module No. 5: An

Introduction to Structural Health Monitoring, Prepared by ISIS Canada, Page 3.

Biswas, P. K., (2008), Online Video Lectures Series on Digital Image Processing by Prof. P.K. Biswas, IIT Khadagpur, Department of Electronics and Communication Engineering, <http://nptel.iitm.ac.in/syllabus/syllabus.php?subjectId=117105079>.

Bjerrum, J. and Jensen, F., (2006), Internet-based Management of Major Bridges and Tunnels using the Danbropsystem, In: P.J.S. Cruz, D.M. Frangopol, and L.C. Neves, eds. Proceedings of IABMAS2006 the 3rd international conference on bridge maintenance, safety, management, life-cycle performance and cost, 16–19 July 2006, Porto, Portugal. London, UK: CRC-Press-Balkema-Taylor & Francis Group, 598–605.

Bosc M., Heitz F., Armspach J. P., Namer I., Gounot D., and Rumbach L., (2003), Automatic Change Detection in Multimodal Serial MRI: Application to Multiple Sclerosis Lesion Evolution, *Neuroimage*, vol. 20, pp. 643–656.

Bridge Condition Indicators, (2002), Guidance Note on Evaluation of Bridge Condition Indicators, Volume 3, published by CSS, July 2002.

Brilakis I. K., Soibelman L., & Shinagawa Y., (2006), Construction Site Image Retrieval based on Material Cluster Recognition, *Advanced Engineering Informatics*, 20(4), 443-452.

Brilakis, I. K., & Soibelman, L. (2008), Shape-based Retrieval of Construction Site Photographs, *Journal of Computing in Civil Engineering*, 22(1), 14-20

BRIM-1, Bridge Inspection's Reference Manual, Federal Highway Administration, National Highway Institute (HNHI-10), 2012, <http://www.fhwa.dot.gov/bridge/nbis/pubs/nhi12049.pdf>.

Brown M., Lowe D., (2007), Automatic Panoramic Image Stitching using Invariant Features, *International Journal of Computer Vision* 74 (1) (2007) 59–73.

Carlotto M. J., (1997), Detection and Analysis of Change in Remotely Sensed Imagery with Application to Wide Area Surveillance, *IEEE Image Processing*, VOL 6, NO 1, January.

Carpinteri A., (1994), Fractal nature of material microstructure and size effects on apparent mechanical properties, *Mech. Mater.*, 18, 89–101

Carpinteri A., Lacidogna G., and Niccolini G., (2009), Fractal Analysis of Damage Detected in Concrete Structural Elements under Loading” *Chaos, Solitons and Fractals* 42 (2009) 2047 – 2056

Carpinteri A., Corrado M., & Lacidogna G., (2012), Three Different Approaches for Damage Domain Characterization in Disordered Materials: Fractal Energy Density, Value Statistics, Renormalization Group Theory. *Mechanics of Materials*, 53, 15-28.

Chen, M. J., & Abraham, D. M. (2001). Neuro-fuzzy Approaches for Sanitary Sewer Pipeline Condition Assessment. *Journal of Computing in Civil engineering*, 15(1), 4-14.

Chen, P. H., & Chang, L. M. (2000). Application of Neuro-fuzzy Thresholding to Bridge Painting Defect Recognition. *Compare*, 6, T7.

Cheng H., Shi X., Glazier C., (2003), Real-time Image Thresholding based on Sample Space Reduction and Interpolation Approach, *Journal of Computing in Civil Engineering* 17 (4) (2003) 264–272.

Commission of Inquiry into the Collapse of a Portion of the de la Concorde Overpass, Report, (2007), http://www.cevc.gouv.qc.ca/UserFiles/File/Rapport/report_eng.pdf, October 3, 2006-October 15, 2007, (Retrieved March 12, 2014).

Coppin P. R., & Bauer M. E., (1996), Digital change detection in forest ecosystems with remote sensing imagery, *Remote sensing reviews*, 13(3-4), 207-234

Coster M., Chermant J. L. (1985). *Précis D'Analse D'Images*. Éditions du Centre National de la Recherche Scientifique, Paris.

Coules J., (1955), Effect of Photometric Brightness on Judgments of Distance, *J Exp Psychol*. 1955; 50:19–25

Curtis R. H., White H., (2007), NYSDOT Bridge Deck Task Force Evaluation of Bridge Deck Cracking on NYSDOT Bridges, New York State Department of Transportation, February 2007. 1–26.

Dougherty E. R., Astola J. (1994). *An Introduction to Nonlinear Image Processing*. SPIE, Bellingham, WA.

Dryden, I. L. and Mardia, K. V., (1998), *Statistical Shape Analysis*, John Wiley & Sons.

El-Omari S., and Moselhi O., (2008), Integrating 3D Laser Scanning and Photogrammetry for Progress Measurement of Construction Work, *Automation in construction*, 18(1), 1-9.

Fadi A. A., (2010), *An Automated Framework for Defect Detection in Concrete Bridge Decks*, PhD Thesis, Western Michigan University.

FANN, (2009), Fast Artificial Neural Network Library, <http://www.leenissen.dk/fann/N> (April 10, 2009)

Farhidzadeh A., Dehghan-Niri E., Moustafa A., Salamone S., & Whittaker A., (2013), Damage Assessment of Reinforced Concrete Structures using Fractal Analysis of Residual Crack Patterns, *Experimental Mechanics*, 1-13.

Frangopol D. M., Strauss A., and Kim S., (2008a), Bridge Reliability Assessment based on Monitoring. *J. Bridge Eng.*, 13(3), 258–270.

Frangopol D. M., Strauss A., and Kim S., (2008b), Use of Monitoring Extreme Data for the Performance Prediction of Structures: General approach. *Eng. Struct.*, 30(12), 3644–3653.

Fausett L., (1994), *Fundamental of Neural Networks*, Florida Institute of Technology, 4.

FHWA, (2006), Administration, Federal Highway, "Bridge inspector's reference manual" Washington, DC.

Fu G., Feng J., Dimaria J., Zhuang Y., (2007), Bridge deck corner cracking on skewed structures, Department of Civil and Environmental Engineering, Wayne State University, Research Report RC-1490, September 2007, pp. 1–153.

FHWA, (1995), *Recording and Coding Guide for the Structure Inventory and Appraisal of the Nation's Bridges*; FHWA-PD-96-001, Federal Highway Administration (U.S. Department of Transportation).

Fryer J. G., (2000), *Introduction in Close Range Photogrammetry and Machine Vision*, Whittles Publishing, Roseleigh House, Latheronwheel, Caithness, KW5 6DW, Scotland, UK.

Ganapuram S., Adams M., Patnaik A., (2012), Quantification of Cracks in Concrete Bridge Decks in Ohio District 3, FHWA/OH-2012/3, Ohio Department of Transportation, 2012.

Ghasemi H., Penrod J., and Hooks J. M., (2009), Developing Advanced Methods of Assessing Bridge Performance. *Public Roads* 73, no.3: 2.

Ghosh P. K., Deguchi K., (2008), *Mathematics of Shape Description*, Wiley, Singapore.

Gilbert R. I., (1992), Shrinkage Cracking in Fully Restrained Concrete Members, *ACI Structural Journal* 89 (2) (1992) 141–149.

Gose E., Johansonbaugh R., Jost S., (1996), *Pattern Recognition and Image Analysis*, Prentice Hall, Inc N. J.

Gonzalez R. C., Woods R. E., & Eddins S. L., (2009), *Digital Image Processing using MATLAB (Vol. 2)*, Knoxville, Gatesmark Publishing.

Google sketch up, 3D for everyone, <http://www.sketchup.com/intl/en/index.html>.

Gruen A., (2000), Development of Digital Methodology and Systems, in *Close Range Photogrammetry and Machine Vision*, Whittles Publishing, Roseleigh House, Latheronwheel, Caithness, KW5 6DW, Scotland, UK, 2000, pp. 78–104.

Gutkowski R. M., & Arenella N. D., (1998), Investigation of PONTIS, A Bridge Management Software (No. MPC Report No. 98-95), Mountain-Plains Consortium.

Haas C., Hendrickson C., McNeil S., Bullock D., A field prototype of a robotic pavement crack sealing, *The 9th International Symposium on Automation and Robotic in Construction*, June 3–5, Tokyo, Japan, 1992.

Hammad A., Yan J., & Mostofi B., (2007), Recent Development of Bridge Management Systems in Canada. In *2007 Annual Conference and Exhibition of the Transportation Association of Canada: Transportation-An Economic Enabler (Les Transports: Un Levier Economique)*.

Hawk H., (1999), BRIDGIT User-friendly Approach to Bridge Management. *Transportation Research Circular*, 498(1).

Hearn G., and Shim H. S., (1998), Integration of Bridge Management Systems and Non-Destructive Evaluations. *Journal of Infrastructure Systems*, 4(2), 49-55.

Heaton Research, (2013), Online Resources, Introduction to Neural Networks using C#, <http://www.jeffheaton.com/ai/>, (accessed October, 2013).

Hinzen K. G., (2013), Support of Macroseismic Documentation by Data from Google Street View. *Seismological Research Letters*, 84(6), 982-990

Houston J. T., Atimay E., Ferguson P. M., (1972), Corrosion of Reinforcing Steel Embedded in Structural Concrete, Re-port CFHR-3-5-68-112-1F, and Center for Highway Research, University of Texas, Austin.

Humar J., Bagchi A., and Xu H., (2006), Performance Analysis of Vibration based Techniques for Structural Damage Identification, *Structural Health Monitoring – An Int. J.*, 5(3):215-227.

Landis E. N., Nagy E. N., Keane D. T., and Nagy G., (1999), Technique to Measure 3d Work-of- Fracture of Concrete in Compression, *Journal of Engineering Mechanics*, Vol. 123, No. 6, June, 1999.123, No. 6, June, 1999.

Lee J. J., Fukuda Y., Shinozuka M., Cho S., and Yun C., (2007), Development and Application of A Vision-based Displacement Measurement System for Structural Health Monitoring of Civil Structures, *Smart Structures and Systems*, 3(3), 373-384.

ImageJ 1.45s, (2013), NIH, Commercial Software for Image Analysis, Online Resources.

National Institutes of Health, USA, <http://rsb.info.nih.gov/ij/>, (accessed October, 2013).

Intelligent Sensing for Innovative Structures, (2001), Design Manual 2, Guidelines for Structural Health Monitoring, Winnipeg, Manitoba, ISIS Canada Corporation.

Iyer S., Sinha S. K., (2006), Segmentation of Pipe for Crack Detection in Buried Sewers, *Computer-Aided Civil and Infrastructure Engineering* 21 (2006) 395–410.

Jáuregui D. V., Tian Y., and Jiang R, (2006), Photogrammetry Applications in Routine Bridge Inspection and Historic Bridge Documentation. *Transportation Research Record: Journal of the Transportation Research Board*, 1958(1), 24-32.

Jiang R, Jáuregui DV, and White K, (2008), Close-range Photogrammetry Applications in Bridge Measurements: Literature Review. *Measurement* 41: 823-834

Khan Z., Zayed T., and Moselhi O., (2009), Structural Condition Assessment of Sewer Pipe Lines, *Journal of performance of constructed facilities*, 24(2), 170-179.

Krauss P. D., Rogalla E. A., (1996), *Transverse Cracking in Newly Constructed Bridge Decks*, NCHRP Report 380, Transportation Research Board, National Research Council, Washington, D. C.

Kulatilake P. H., Fiedler R., and Panda B. B., (1997), Box fractal dimension as a measure of statistical homogeneity of jointed rock masses, *Engineering Geology*, 48(3), 217-229.

Laptev I., Mayer H., Linderberg T., Eckstein W., Steger C., Maumgartner A., (2000), Automatic Extraction of Roads from Aerial Images based on Scale Space and Snakes, *Machine vision and Applications* 12 (1) 23–31.

Lee Y. H., Carr J. R., Barr D. J., and Haas C. J., (1990), The Fractal Dimension as A Measure of the Roughness of Rock Discontinuity Profiles. In *International journal of rock mechanics and mining sciences & geo-mechanics abstracts* (Vol. 27, No. 6, pp. 453-464). Pergamon.

Liao H.K., Yen C.I., and Yau N.J., (2008), Development of A Bridge Maintenance Decision Support Module for Taiwan Bridge Management System. In: H.M. Koh, and

D.M.Frangopol, Proceedings of IABMAS2008 the 4th international conference on bridge maintenance, safety, management, health monitoring and informatics, 13–17 July 2008, Seoul, Korea. London, UK: CRC-Press- Balkema-Taylor & Francis Group, 606–613.

Liaw S. S., & Chiu F. Y., (2009), Fractal Dimensions of Time Sequences, *Physica A: Statistical Mechanics and its Applications*, 388(15), 3100-3106.

Lichtenstein A. G., (1993), The Silver Bridge Collapse Recounted, *Journal of performance of constructed facilities*, 7(4), 249-261.

Liu G.P., (2001), Neural networks, *Nonlinear Identification and Control: A Neural Network Approach*, Springer, London, 210.

Liu W., (2010), Terrestrial LiDAR-based Bridge Evaluation, *Dissertation Abstracts International*, 71(06).

Liu S. W., Sung J. C., Lee C. C., and Huang J. H., Detection of Cracks using Neural Networks and Computational Mechanics, *Computer Methods Applied Mechanics and Engineering* 191 (2002) 2831–2845.

Loncaric S., (1998), A Survey of Shape Analysis Techniques, *Pattern Recognition* 31(8): 983 – 1001.

Luhmann T., Robson S., Kyle S., and Harley I., (2006), *Close-range Photogrammetry: Principles, Methods, and Applications*, Hoboken, NJ Caithness Whittles.

Maini R., and Aggarwal H., (2009), Study and Comparison of Various Image Edge Detection Techniques, *International Journal of Image Processing (IJIP)*, 3(1), 1-11.

Maksymowicz M., Cruz P. J. S., and Bien J., (2011), Load Capacity of Damaged RC Slab Spans of Railway Bridges, *Archives of Civil and Mechanical Engineering* XI (4).

Mandelbrot B., (2008), Fractal Geometry of Nature, Kindel edition.

Maosen C., Qingwen R., and Pizhong Q., (2006), Nondestructive Assessment of Reinforced Concrete Structures Based on Fractal Damage Characteristic Factors, Journal of Engineering Mechanics, 132 : 924-931.

Masri S. F., (2000), Application of Neural Networks for Detection of Changes in Nonlinear Systems, Journal of Engineering Mechanics 126 : 666–676.

MATLAB version R2012a, (2012), The Technical Computing Computer Software, the Math Works Inc.

MacCurdy E., (1938), The Notebooks of Leonardo da Vinci volume I (London: Jonathan Cape).

McRobbie S. G., (2008), Automated Inspection of Highway Structures 2008/09, Published Project Report PPR 412, Transportation Research Laboratory, UK..

McRobbie S., Woodward R., Wright A., (2010), Visualisation and Display of Automated Bridge Inspection Results, Transport Research Laboratory, UK NJDOT, 2009, Bridge Inspection Work Zone, Setup Guide, 2010.

Moore M., Phares B., Graybeal B., Rolander D., and Washer G., (2001), Reliability of Visual Inspection for Highway Bridges, volume I: Final report (No. FHWA-RD-01-020,).

Moselhi O. and Shehab-Eldeen T., (2000), Classification of Defects in Sewer Pipes using Neural Networks, Journal of infrastructure systems, 6(3), 97-104.

Moselhi O., and Shehab-Eldeen T., (1999a), Automated Detection of Surface Defects in Water and Sewer Pipes. Automation in Construction, 8(5), 581-588.

Moselhi O., and Shehab-Eldeen T., (1999b), An AI-based System for Detection and Classification of Defects in Sewers. In Proceedings of INFRA 99 International Conference on Infrastructure Facilities, Montreal, Que (Vol. 1, p. 3B).

Moselhi O., Hegagy T., and Fazio P., (1994), Developing Practical Neural Networks Applications Using Back-Propagation. *Microcomputers in Civil Engineering*, Blackwell, 9 (2), 145 – 159.

NASA, (2013), The Electromagnetic Spectrum, Goddard Space Flight Center http://imagine.gsfc.nasa.gov/docs/science/known_12/emspectrum.html.

National Transportation Safety Board, NTSB, (2008), Collapse of I-35W Highway Bridge, Minneapolis, Minnesota, August 1, 2007. Highway Accident Report NTSB/HAR-08/03, Washington, DC. <http://www.nts.gov/doclib/reports/2008/HAR0803.pdf>.

Navy Bridge Inspection Program, (2008), Bridge Inspection and Reporting Guidelines, Collins Engineers, Inc., User Guide UG-60020-OCN. http://www.wbdg.org/ccb/DOD/UFC/ufc_3_310_08_navy_guidelines.pdf.

NCHRP SYNTESIS 375, (2007), Bridge Inspection Practices A Synthesis of Highway Practice, National Cooperative Highway Research Program.

Neal F. B., and Russ J. C., (2012), *Measuring Shape*, CRC Press, Taylor & Francis Group, 6000 Broken, Sound Parkway NW, Suite 300, Boca Raton, FL 33487 – 2742.

Nishimura S., Kimoto K., Kusuhara S., Kawabata S., Abe A., and Okazawa T., Development of A Hybrid Camera System for Bridge Inspection, 2012, www.krcnet.co.jp/papers/pdf/International/International2012_02.pdf.

Ohio DoT, (2010), Manual of Bridge Inspection, Bridge Inspection Program Requirements,

http://www.dot.state.oh.us/Divisions/Engineering/Structures/News%20Document/Manual%20of%20Bridge%20Inspection_2010.pdf.

Ontario Bridges, (2013), The Ministry of Transportation, Ontario,

<http://www.mto.gov.on.ca/english/bridges/bci.shtml>.

Ontario Structure Inspection Manual (OSIM), (2008), Ontario Ministry of Transportation, Ronen House, Toronto, Canada, 2008,

http://www.elliottlakeinquiry.ca/exhibits/pdf/05162-NL_E000013134.pdf.

Ontario-BMS, (2012), Ontario Bridge Management System, Version.2.5.0, Ministry of Transportation of Ontario,

http://www.xfer.mto.gov.on.ca/PTASapps/Bridge%20Management%20System/BMS_V25_Release_Notes_April_1_12.pdf.

Orcesi A. D., and Frangopol D. M., (2010), Use of Lifetime Functions in the Optimization of Non-destructive Inspection Strategies for Bridges." J. Struct. Eng., 137(4), 531–539.

Otsu N., (1979), A Threshold Selection Method from Gray-Level Histograms, IEEE Transactions on Systems, Man, and Cybernetics, Vol. 9, No. 1, pp. 62-66.

Parker J. R., (1997), Algorithms for Image Processing and Computer Vision. John Wiley & Sons, New York.

Paul M.D., Harry B. H., Clive S. F., Bjorn R., Wolfgang N., (2002), An Operational Application of Automatic Feature Extraction: the Measurement of Crack in Concrete Structures, 17 (99) : 453–464.

Pontis Bridge Inspection Manual, (2009),

http://www.michigan.gov/documents/mdot/MDOT_PontisManual_2007_195365_7.pdf?20140106182922.

Pooled Fund Project Crack Survey Protocol, (2011), Pooled Fund TPF-5(051) Construction of Crack-Free Concrete Bridge Decks, Kansas Department of Transportation.

Project Scoping Manual, Revised June (2013), Michigan Department of Transportation, http://mdotcf.state.mi.us/public/docs/design/files/scopingmanual/Scoping_Manual.pdf.

Radke R. J., Andra S., Al-Kofahi O., and Roysam B., (2005), Image Change Detection Algorithms: A Systematic Survey. *Image Processing, IEEE Transactions on*, 14(3), 294-307

Rahmatian A. (2014), Performance of an Innovative Sensing System for Structural Health Monitoring of FRP-Reinforced Concrete Structures, PhD Thesis, Concordia University.

Recording, FHWA, (1995), Coding Guide for the Structure Inventory and Appraisal of the Nation's Bridges. Federal Highway Administration Report FHWA-PD-96-001.

Remondino F., and El-Hakim S., (2006), Image-based 3d Modelling: A Review, *The Photogrammetric Record* 21 (115): 269–291.

Richard L., Xuemin C., and Min W., (2001), Automatic Crack Monitoring System, Texas DOT 7-3997, Texas Department of Transportation.

Ritchie S. G., Kaseko M., and Bavarian B., (1991), Development of an Intelligent System for Automated Pavement Evaluation (No. 1311).

Rizkalla S. H., Shahawi M. El., and Kwok C. K., (1982), Cracking Behaviour of Reinforced Concrete Members, Canadian Society for Civil Engineering, Annual Conference, Edmonton, Alberta May 27–28.

Roberts J. E., and Shepard R., (2000), Bridge Management for the 21st Century. Transportation Research Record: Journal of the Transportation Research Board, 1696(1), 197-203.

Roy D., (2008), Remote sensing in Engineering Geology, Lecture Series on Engineering Geology, Department of Civil Engineering, I. I. T. Kharagpur, <http://nptel.iitm.ac.in>.

Ryan C. H., (2012), An Evaluation of Surface Defects Detection in Reinforcement Concrete Bridge Decks using LiDAR, (Master thesis) Michigan Technological University.

Ruiz M., Castelli E., and Prato T., (2008), A New Bridge Management System for the National Department of Transportation of Argentina, In: H.M. Koh, and D.M.Frangopol, Proceedings of IABMAS2008 the 4th international conference on bridge maintenance, safety, management, health monitoring and informatics, 13–17 July 2008, Seoul, Korea. London, UK : CRC-Press-Balkema – Taylor & Francis Group, 598–605.

Russ J., (1992), The Image Processing handbook, CRC press, Inc., Florida.

Ryall M. J., (2003), Bridge Management, Butterworth-Heinemann, Newton, Mass.

Ryell J. and B.S. Richardson, (1972), Cracks in Concrete Bridge Decks and Their Contribution to Corrosion of Reinforcing Steel and Pre-stressing Cables, Report IR51, Ontario Ministry of Transportation and Communications, Downs view, ON, Canada.

Samonds J. M., Potetz B. R., and Lee T. S., (2012), Relative Luminance and Binocular Disparity Preferences are Correlated in Macaque Primary Visual Cortex, Matching Natural Scene Statistics. Proceedings of the National Academy of Sciences, 109(16), 6313-6318.

Scheffy C., Coetze N., and Diaz E., (1999), Asphalt Concrete Fatigue Crack Monitoring and Analysis using Digital Image Analysis Techniques, Accelerated Pavement Testing - International Conference October 18–20, Reno, Nevada, October 18–20.

Sezgin M., and Sankur B., (2004), Survey over Image Thresholding Techniques and Quantitative Performance Evaluation. *J. Electronic Imaging* 13: 146–165.

Shehab-Eldeen T., (2001), An Automated System for Detection, Classification and Rehabilitation of Defects in Sewer Pipes, Doctoral dissertation, Concordia University.

Sinha S. K., Fieguth P. W., and Polak M. A., (2003), Computer Vision Techniques for Automatic Structural Assessment of Underground Pipes, *Computer Aided Civil and Infrastructure Engineering*, 18(2), 95-112.

Singh A., (1989), Digital Change Detection Techniques using Remotely-sensed Data, *International Journal of Remote Sensing* 10 (6) 989–1002

Sinha, and Fieguth, (2006), Segmentation of Buried Concrete Pipe Images, *Automation in Construction* 15: 47–57.

Schmitt T. R., and Darwin D., (1995), Cracking in Concrete Bridge Decks, SM Report No. 39, University of Kansas Center for Research, Inc., Lawrence, 1995. (152 pp).

EL Shehaby A. R., AL Semyary H. H., Salah M., and Ibrahim S. M., (2012), Assessment of Spread Range of Urban Development in the West Delta by Utilizing High Resolution Satellite Images, *Journal of Civil Engineering Research*, 2(6): 57-63 DOI: 10.5923/j.jce.20120206.02

Soderqvist M., (2004), Experience in the Finnish Bridge Management System Development. In: E. Watanabe, D.M. Frangopol, and T. Utsunomiya, eds. *Proceedings of IABMAS2004, 2nd international conference on bridge maintenance, safety, management and cost*, 18–22, Kyoto, Japan. London, UK: A. A., 165–166.

Solomon C., and Breckon T., (2011), *Fundamentals of Digital Image Processing: A Practical Approach with Examples in Matlab*. John Wiley & Sons.

Sun H. Q., Ding J., Guo J., and Fu D. L., (2011), Fractal Research on Cracks of Reinforced Concrete Beams with Different Aggregates Sizes, *Advanced Materials Research*, 250, 1818-1822.

Tamura S. I., and Tateishi M., (1997), Capabilities of A Four-layered Feed Forward Neural Network: Four Layers versus Three. *Neural Networks, IEEE Transactions on*, 8(2), 251-255.

Thompson P. D., and Shepard R. W., (1994), Pontis, *Transportation Research Circular*, (423).

Tonias D.E. and Zhao J.J., (2007), *Bridge Engineering*, New York: McGraw-Hill, 463.

Townshend J. R. G., Justice C. O., and Gurney C., (1992), The Impact of Misregistration on Change Detection,” *IEEE Trans. Geosci, Remote Sensing*, vol. 30, pp. 1054–1060, Sept

Turner M. J., Blackledge J. J. M., and Andrews P. R., (1998), *Fractal geometry in Digital Imaging*, Access Online via Elsevier.

Vaysburd A., and Benoit B., (2007), *Commission d’enquête sur le Viaduc de la Concorde – Inspection*”, May 2007, <http://collections.banq.qc.ca/ark:/52327/bs1563917>, (Retrieved March 12, 2014).

Wakchaure S. S., and Jha K. N., (2012), Determination of Bridge Health Index using Analytical Hierarchy Process, *Construction Management and Economics* (2012) 30, 133–149.

Ward Systems, (2013), *Neuroshell 2, Release 4, (1993-2000)*, Online Documentation. <http://www.wardsystems.com/manuals/neuroshell2/index.html?idxhowuse.htm>, (accessed October, 2013).

Weil G., (1998), Detecting the Defects, *Civil Engineering, ASCE*, 59(9), 72-77.

Woodward et al., (2001), Bridge Management in Europe (BRIME)-Deliverable D14 Final Report. Technical report, European Commission under the Transport RTD Programs of the 4th Framework Program PL97-2220. <http://www.trl.co.uk/brime>.

Xu H., and Humar J., (2006), Damage Detection in A Girder Bridge by Artificial Neural Network Technique, *Computer-Aided Civil and Infrastructure Engineering* 21: 450–464.

Xu G.B., Zhou M.J, Xiong Z. G, and Yin Y. X, (2012), An Improved Adaptive Fusion Edge Detection Algorithm for Road Images, *AISS*, vol. 4, no. 4, pp. 129-137.

Yamaguchi T., and Hashimoto S., (2009), Fast Crack Detection Method for Large-size Concrete Surface Images using Percolation-based Image Processing, *Machine Vision and Applications* 11 (5) 797–809.

Yehia S., Abudayyeh O., Nabulsi S., and Abdelqader I., (2007), Detection of Common Defects in Concrete Bridge Decks using Non-destructive Evaluation Techniques. *Journal of Bridge Engineering*, 12(2), 215-225.

Yunping et al., (2003), Assessment of the Cracking Problems in Newly Constructed Bridge Decks in Colorado, Department of Transportation — Research, Colorado, 2003.

Zhou H. W., and Xie H., (2003), Direct Estimation of the Fractal Dimensions of A Fracture Surface of Rock, *Worlds Scientific Publishing Company*, Vol. 10, No. 5, 571-762, 2003.

Zhu Z., (2012), Automated As-built Modeling with Spatial and Visual Data Fusion, 12th International Conference on Construction Applications of Virtual Reality, Nov. 1–2, Taipei, Taiwan.

Zhu Z., German S., and Brilakis I., (2010), Detection of Large-scale Concrete Columns for Automated Bridge Inspection, *Automation in construction* 19 (2010) 1047-1055

Zhu Z., German S., and Brilakis I., (2011), Visual Retrieval of Concrete Crack Properties for Automated Post-earthquake Structural Safety Evaluation, *Automation in Construction* 20, 2011, 874-883.

Appendix A: Sample images of spalling defect

The first part of this Appendix shows the real spalled defects of a reinforced concrete bridges in Montreal as shown in the following figures.



Figure: A.1 Spalled Defects in a Reinforced Concrete Structures with exposed reinforcement in a bridge in Montreal, Quebec

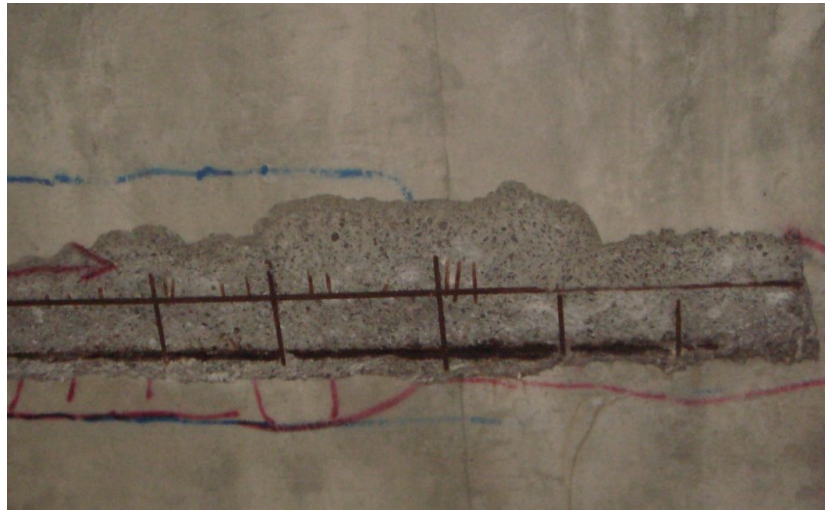


Figure: A.2 Spalled Defects in a Reinforced Concrete Structures with exposed reinforcement in a bridge in Montreal, Quebec

Appendix B: Condition rating charts and figures

| Location | Challenges | Indicator | Rating Based, in Part, on Theoretical Sensitivity for Measurement Technologies | | | | | | | | | | | | |
|-------------------|------------|------------------------------------|--|---------|--------------------|-------------------------------|------------------------|-------|------------|-----------|-----|------------------------------|-------|------------------------------|----|
| | | | GPR | Spectra | 3D Photo-grammetry | EO Airborne/Satellite Imagery | Optical Interferometry | LIDAR | Thermal IR | Acoustics | DIC | Radar (Backscatter/ Speckle) | INSAR | StreetView-Style Photography | |
| Deck Surface | | Tom/Missing Seal | 0 | 8 | 14 | 12 | 11 | 13 | 11 | 0 | 0 | 0 | 9 | 0 | 13 |
| | | Armored Plated Damage | 0 | 0 | 14 | 12 | 11 | 13 | 11 | 0 | 0 | 0 | 0 | 0 | 13 |
| | | Cracks within 2 Feet | 0 | 8 | 14 | 0 | 12 | 12 | 11 | 0 | 0 | 0 | 9 | 0 | 13 |
| | | Spalls within 2 Feet | 0 | 8 | 14 | 12 | 12 | 12 | 11 | 0 | 0 | 0 | 9 | 0 | 13 |
| | | Chemical Leaching on Bottom | 0 | 11 | 0 | 0 | 0 | 0 | 0 | 0 | 0 | 0 | 0 | 0 | 0 |
| | | Surface Cracks | 0 | 8 | 14 | 12 | 12 | 12 | 11 | 8 | 0 | 0 | 9 | 0 | 13 |
| | | Depression in Surface | 0 | 8 | 14 | 12 | 12 | 12 | 11 | 0 | 0 | 0 | 9 | 0 | 13 |
| | | Spalling | 0 | 8 | 14 | 12 | 12 | 12 | 11 | 0 | 0 | 0 | 9 | 0 | 13 |
| | | Expansion Joint | 0 | 0 | 0 | 0 | 11 | 0 | 0 | 0 | 0 | 0 | 0 | 0 | 0 |
| | | Material in Joint | 0 | 0 | 0 | 0 | 0 | 0 | 0 | 0 | 0 | 0 | 0 | 0 | 0 |
| Deck Subsurface | | Moisture in Cracks | 11 | 0 | 0 | 0 | 0 | 0 | 11 | 0 | 0 | 0 | 0 | 0 | 0 |
| | | Internal Horizontal Crack | 0 | 0 | 0 | 0 | 0 | 0 | 11 | 8 | 0 | 0 | 0 | 0 | 0 |
| | | Hollow Sound | 0 | 0 | 0 | 0 | 0 | 0 | 0 | 8 | 0 | 0 | 0 | 0 | 0 |
| | | Fracture Planes / Open Spaces | 12 | 0 | 0 | 0 | 0 | 0 | 0 | 8 | 0 | 12 | 0 | 0 | 0 |
| | | Depression in Surface | 12 | 0 | 0 | 0 | 0 | 0 | 11 | 0 | 0 | 0 | 0 | 0 | 0 |
| | | Depression with Parallel Fracture | 12 | 0 | 0 | 0 | 0 | 0 | 11 | 0 | 0 | 0 | 0 | 0 | 0 |
| | | Corrosion Rate (Resistivity) | 0 | 0 | 0 | 0 | 0 | 0 | 0 | 0 | 0 | 0 | 0 | 0 | 0 |
| | | Corrosion | 0 | 0 | 0 | 0 | 0 | 0 | 0 | 0 | 0 | 0 | 0 | 0 | 0 |
| | | Change in Cross-Sectional Area | 13 | 0 | 0 | 0 | 0 | 0 | 0 | 8 | 0 | 13 | 0 | 0 | 0 |
| | | Chloride Content through the Depth | 12 | 0 | 0 | 0 | 0 | 0 | 0 | 0 | 0 | 12 | 0 | 0 | 0 |
| Girder Surface | | Surface Cracks | 0 | 8 | 11 | 0 | 12 | 0 | 11 | 0 | 0 | 0 | 0 | 0 | 0 |
| | | Steel Structural Cracking | 0 | 8 | 11 | 0 | 12 | 0 | 11 | 8 | 0 | 0 | 0 | 0 | 0 |
| | | Concr. Structural Cracking | 0 | 0 | 11 | 12 | 0 | 13 | 0 | 11 | 0 | 0 | 11 | 0 | 0 |
| | | Steel Section Loss | 0 | 0 | 0 | 0 | 0 | 0 | 0 | 0 | 0 | 0 | 0 | 0 | 0 |
| | | Paint Condition | 0 | 9 | 0 | 0 | 0 | 0 | 0 | 11 | 7 | 0 | 0 | 0 | 0 |
| | | Change in Cross-Sectional Area | 0 | 0 | 11 | 12 | 0 | 13 | 11 | 7 | 0 | 0 | 11 | 0 | 0 |
| | | Concrete Section Loss | 0 | 0 | 0 | 0 | 0 | 0 | 0 | 11 | 8 | 0 | 0 | 0 | 0 |
| | | Concr. Structural Cracking | 0 | 0 | 0 | 0 | 0 | 0 | 0 | 7 | 0 | 11 | 0 | 0 | 0 |
| | | Concrete Section Loss | 0 | 0 | 0 | 0 | 0 | 0 | 0 | 8 | 0 | 9 | 0 | 0 | 0 |
| | | Prestress Strand Breakage | 9 | 0 | 0 | 0 | 0 | 0 | 0 | 0 | 0 | 0 | 0 | 0 | 0 |
| Girder Subsurface | | Corrosion Rate (Resistivity) | 0 | 0 | 0 | 0 | 0 | 0 | 0 | 0 | 0 | 0 | 0 | 0 | 0 |
| | | Corrosion | 0 | 0 | 0 | 0 | 0 | 0 | 0 | 0 | 0 | 0 | 0 | 0 | 0 |
| | | Change in Cross-Sectional Area | 8 | 0 | 0 | 0 | 0 | 0 | 0 | 8 | 0 | 13 | 0 | 0 | 0 |
| | | Chloride Content through the Depth | 10 | 0 | 0 | 0 | 0 | 0 | 0 | 0 | 0 | 11 | 0 | 0 | 0 |
| | | Chloride Ingress | 0 | 0 | 15 | 13 | 0 | 0 | 0 | 9 | 0 | 12 | 0 | 0 | 0 |
| | | Bridge Length | 0 | 0 | 12 | 0 | 0 | 12 | 0 | 0 | 9 | 0 | 12 | 0 | 0 |
| | | Bridge Settlement | 0 | 0 | 12 | 0 | 0 | 12 | 0 | 0 | 9 | 0 | 12 | 0 | 0 |
| | | Vertical Movement of Bridge | 0 | 0 | 12 | 0 | 0 | 12 | 0 | 0 | 9 | 0 | 12 | 0 | 0 |
| | | Transverse Directions | 0 | 0 | 12 | 0 | 0 | 12 | 0 | 0 | 9 | 0 | 12 | 0 | 0 |
| | | Surface Roughness | 0 | 9 | 14 | 13 | 12 | 12 | 0 | 0 | 11 | 13 | 13 | 13 | 0 |
| Global Metrics | | Surface Roughness | 0 | 9 | 14 | 13 | 12 | 12 | 0 | 0 | 10 | 12 | 12 | 12 | 0 |
| | | Vibration | 0 | 0 | 0 | 0 | 12 | 0 | 0 | 0 | 10 | 12 | 12 | 12 | 0 |

Figure B.1: Comparison of Remote Sensing Technologies (Ahlborn et al. 2010)

PHOTO LOG FORM

INSPECTORS GRL (WB) PHOTO LOG NO. _____
 BRIDGE NO. MP-056-0064-B00293 DATE: 7.9.11 (Photos 1-11)
 BRIDGE NAME 7th Street to 13th Street Unit 7.10.11

| PHOTO # | LOCATION | DESCRIPTION |
|---------|---------------------------------|--|
| 1 | Pier 46WB from parking level | General View Sta Abd at end of Ramp (left) beg. at Pier 47WB |
| 2 | Pier 49WB | Crack at end weld at Girder Conn (S9-Span 48WB) |
| 3-7 | Pier 49W Span 49W | Gen View of end weld crack w/ close-ups |
| 8 | North side Pier 50WB | Gen View of Fascia Girder (S19) w/ full length long stiffeners |
| 9 | Pier 55WB | torn strip seal over cross girder and pin & hanger assembly |
| 10 | Pier 55WB (north side) | Top view of Deck Looking Bk Stations |
| 11 | Pier 55WB | Pin & Hanger Assembly w/ Bol support (Looking North) |
| 12 | Span 48WB Girder S5 | 2 nd Diaph (Cross Bracing) Top Conn to end weld cracking and toe weld cracking on Girder web to Flg (Previously reported - no change) opposite end of bow stainer condition |

Figure B.2: Photo Log (BRIM 2012)

| | | | | | | |
|--------------------------|--------------------------------|------------------------|-----------------------------|-----------------------|-----------------------------|----------------------------|
| Approaches (4%) | Substructures (18%) | Waterways (5%) | Foundations (33%) | Superstructures (22%) | Auxiliary Works (4%) | Bearings (14%) |
| Alignment (16%) | Abutment (18%) | River Bed (4%) | Foundations (66%) | Girders (35%) | Wearing Surfaces (8%) | Bearings (50%) |
| Signage (6%) | Dirt Wall (5%) | Guide Bunds (13%) | Apron (14%) | Cross beams (14%) | Footpaths (7%) | Bearing Seats (25%) |
| Embankment/Cutting (13%) | Weep Holes (4%) | Spurs (8%) | Foundation Protection (20%) | Articulation (13%) | Expansion Joints (18%) | Restraint Earthquake (25%) |
| Railing (15%) | Wing Walls (7%) | Retaining Walls (15%) | | Deck Slabs (15%) | Pre-stressing Element (19%) | |
| Approach Slab (10%) | Abutment Protection Works (9%) | Toe Walls (8%) | | Cantilever Slab (13%) | Medians (5%) | |
| Approach Joint (10%) | Pier (26%) | Floor Protection (12%) | | Joints (10%) | Kerbs (5%) | |
| Side Drain (10%) | Pier Caps (16%) | Apron (11%) | | | Light Posts (4%) | |
| Slope Protection (20%) | Pier Protection Works (16%) | Cutoff Walls (15%) | | | Drainage Spouts (7%) | |
| | | Ground Anchors (14%) | | | Parapet Barriers (12%) | |
| | | | | | Waterproofing (8%) | |
| | | | | | Painting System (4%) | |
| | | | | | Utilities (4%) | |

Figure B.4: Element Importance Factors (Wakchaure and Jha, 2012)

Appendix C: Back Propagation Algorithm

Consider a neuron j at the output layer and C is the set of all neurons in output layer. At the n^{th} iteration (i.e. the presentation of n^{th} pattern in an epoch, where a complete set of patterns is called epoch), the error signal is given by Eq. (5.1),

$$e_j(n) = d_j(n) - y_j(n) \quad (5.1)$$

where, d_j is the desired output of neuron j & and $y_j =$ is the actual output of neuron j .

Then, instantaneous value of error energy is given by Eq. (5.2),

$$E(n) = \frac{1}{2} \sum_{j \in C} e_j^2(n) \quad (5.2)$$

If N is the total numbers of training patterns which makes one epoch; and then average squared error energy can be calculated as in Eq. (5.3),

$$E_{av}(n) = \frac{1}{N} \sum_{n=1}^N E(n) \quad (5.3)$$

The energy calculated from Equations (2)-(3) will not be same. Then the induced local field at the input neuron j was evaluated. The input to the activation function of neuron j will be given by Eq. (4),

$$v_j(n) = \sum_i^m w_{ji}(n) y_i(n) \quad (5.4)$$

where, w_{ji} is the synaptic weight connection from nodes i to j ; m is the number of neurons in the previous layer i.e., the hidden layer; and y_i is the actual output in the previous layer.

And actual output of neuron j is defined by Eq. (5.5),

$$y_j(n) = \phi(v_j(n)) \quad (5.5)$$

Now, to find the change in weight $\Delta w_{ji}(n)$ to update the actual weight $w_{ji}(n)$, it is necessary to find this term, $\frac{\delta E(n)}{\delta w_{ji}(n)}$, which can be obtained by applying the chain rule as below.

$$\frac{\delta E(n)}{\delta w_{ji}(n)} = \frac{\delta E(n)}{\delta e_j(n)} \cdot \frac{\delta e_j(n)}{\delta y_j(n)} \cdot \frac{\delta e_j(n)}{\delta v_j(n)} \cdot \frac{\delta v_j(n)}{\delta w_{ji}(n)} \quad (5.6)$$

By substituting the respective values from the above equation, and after taking partial derivatives, it can be found that

$$\frac{\delta E(n)}{\delta w_{ji}(n)} = -e_j(n) \phi' (v_j(n)) y_i(n) \quad (5.7)$$

The correction applied to $w_{ji}(n)$ is proportional to the learning rate “ η ”,

$$\Delta w_{ji}(n) = -\eta \frac{\delta E(n)}{\delta w_{ji}(n)} = \eta e_j(n) \phi' (v_j(n)) y_i(n) \quad (5.8)$$

We substitute, $\delta_j(n) = e_j(n) \phi' (v_j(n))$ in the above equation; the local gradient can be defined as

$$\delta_j(n) = -\frac{\delta E(n)}{\delta v_j(n)} \quad (5.9)$$

The final form of the change in synaptic weight is given by Eq. (5.10),

$$\Delta w_{ji}(n) = \eta \delta_j(n) y_i(n) \quad (5.10)$$

The only underlying problem in the above Eq. (5.10) is to calculate the local gradient. The problem can be divided into the following two cases.

Case 1: Neuron j belongs to output layer, in which case, $\delta_j(n)$ can be calculated from Eq. (9) because this is the supervised learning and the output is known in advance.

Case 2: Neuron j belongs to a hidden layer. In this case, since the error in hidden layer is known yet, it is difficult to determine $\delta_j(n)$. But, with the similar formulation as shown above, the local gradient in hidden layers can be estimated by using the Equation (5.10) for weight adjustment. These algorithms do not have any restriction on their input data. The only underlying assumption in back propagation algorithm is that the input parameters shall not be changed during the forward and backward pass.

Appendix D: Sample MATLAB Code for Spectral and Fractal Analysis

Spectral Analysis of digital images

```
ff = imread('face1.tif');
imshow(ff);
f=rgb2gray(ff);
% imshow(f);
S = fftshift(fft2(f));
S = log(1+abs(S));
%figure;
%imshow(S,[]);
[d, e, g] = specxtexture(f);
%figure;
% plot(d)
%axis tight
%axis([0 240 1400 2200])
% axis([0 500 1200 5000])
%figure;
%plot(b)
%axis tight
subplot(2,2,1); imshow(ff)
subplot(2,2,2); imshow(S,[])
subplot(2,2,3); plot(d), axis tight, axis([0 240 1600 2300])
subplot(2,2,4); plot(e), axis tight
%%
subplot(3,1,1); imshow(ff)
subplot(3,1,2); imshow(S,[])
subplot(3,1,3); plot(d), axis tight, axis([0 240 1600 2300])
%subplot(2,2,4); plot(e), axis tight
function [srad, sang, S] = specxtexture(f)
%SPECXTURE Computes spectral texture of an image.
% [SRAD, SANG, S] = SPECXTURE(F) computes SRAD, the spectral energy
% distribution as a function of radius from the center of the
% spectrum, SANG, the spectral energy distribution as a function of
% angle for 0 to 180 degrees in increments of 1 degree, and S =
% log(1 + spectrum of f), normalized to the range [0, 1]. The
% maximum value of radius is min(M,N), where M and N are the number
% of rows and columns of image (region) f. Thus, SRAD is a row
% vector of length = (min(M, N)/2) - 1; and SANG is a row vector of
% length 180.
% Copyright 2002-2004 R. C. Gonzalez, R. E. Woods, & S. L. Eddins
% Digital Image Processing Using MATLAB, Prentice-Hall, 2004
% $Revision: 1.7 $ $Date: 2003/11/21 14:48:47 $
% Obtain the centered spectrum, S, of f. The variables of S are
% (u, v), running from 1:M and 1:N, with the center (zero frequency)
% at [M/2 + 1, N/2 + 1] (see Chapter 4).
S = fftshift(fft2(f));
S = log(1+abs(S));
[M, N] = size(S);
x0 = round(M/2 + 1);
y0 = round(N/2 + 1);
% Maximum radius that guarantees a circle centered at (x0, y0) that
% does not exceed the boundaries of S.
```



```

rmax = min(M, N)/2 - 1;
% Compute srاد.
srاد = zeros(1, rmax);
srاد(1) = S(x0, y0);
for r = 2:rmax
[xc, yc] = halfcircle(r, x0, y0);
srاد(r) = sum(S(sub2ind(size(S), xc, yc)));
end
% Compute sang.
[xc, yc] = halfcircle(rmax, x0, y0);
sang = zeros(1, length(xc));
for a = 1:length(xc)
[xr, yr] = radial(x0, y0, xc(a), yc(a));
sang(a) = sum(S(sub2ind(size(S), xr, yr)));
end
% Output the log of the spectrum for easier viewing, scaled to the
% range [0, 1].
S = mat2gray(log(1 + S));
%-----%
function [xc, yc] = halfcircle(r, x0, y0)
% Computes the integer coordinates of a half circle of radius r and
% center at (x0,y0) using one degree increments.
%
% Goes from 91 to 270 because we want the half circle to be in the
% region defined by top right and top left quadrants, in the
% standard image coordinates.
theta=91:270;
theta = theta*pi/180;
[xc, yc] = pol2cart(theta, r);
xc = round(xc)' + x0; % Column vector.
yc = round(yc)' + y0;
%-----%

function [xr, yr] = radial(x0, y0, x, y)
% Computes the coordinates of a straight line segment extending
% from (x0, y0) to (x, y).
%
% Based on function intline.m. xr and yr are returned as column
% vectors.
[xr, yr] = intline(x0, x, y0, y);

```

Fractal Analysis of Digital Images

```

subplot(2,2,1), FraktalT(1,01,[pi/9,-pi/9],[0,0],[0,0.5])
set(gca,'FontSize', 14);
xlabel('a) Initial Crack, n= 1', 'FontSize', 14); ylabel('Crack Depth', 'FontSize', 14) ;
subplot(2,2,2), FraktalT(2,01,[pi/9,-pi/9],[0,0],[0,0.5])
set(gca,'FontSize', 14);
xlabel('b) Crack, n= 2', 'FontSize', 14); ylabel('Crack Depth', 'FontSize', 14) ;

subplot(2,2,3), FraktalT(4,01,[pi/9,-pi/9],[0,0],[0,0.5])
set(gca,'FontSize', 14);
xlabel('c) Crack, n= 4', 'FontSize', 14); ylabel('Crack Depth', 'FontSize', 14) ;

subplot(2,2,4), FraktalT(3,01,[pi/9,-pi/9],[0,0],[0,0.5])

```

```

set(gca,'FontSize', 14);
xlabel('d) Crack, n= 3', 'FontSize', 14); ylabel('Crack Depth', 'FontSize', 14) ;

set(gcf,'Color',[1,1,1])
[ax,h3]=suplabel('Crack Propagation by Fractal Analysis' , 't');
set(h3,'FontSize',18)
function A = FraktalT(n,r,phi,xb,yb)
% This function allow you to bild fractal trees
% by using modified algorithms based on the so-called Kantor`s array
% and method of inverse trace
% These methods allow you to economise time and computer memory
% considerably
% It`s arguments:
% Fraktal(n,r,phi,xb,yb)
% n - number of iterations
% r - scale factor
% in case of nonuniform fractals where different scale-factors take
% place, r may be vector (in this case the lengths of r and phi must be equal)
% phi - vector of angles in fractal generator that are calculated
% relative to the horizontal axis connecting end points of generator
% xb and yb - coordinates of trunk
%
% For example for famous Pifagorus`s tree in it`s vertical position the call of this function is
% so:
% FraktalT(n,0.5,[pi/4,-pi/4],[0,0],[0,1])
% n is recommended to be in range 1..12 not to call the overloaded of stack

%h=figure;
%axes('Parent',h);

mN=length(phi);
if length(r)==1
rM=ones(1,mN)*r;
elseif length(r)==mN
rM=r;
else
warndlg('The sizes of scale vector and vector of angles in fraktal`s generator don`t equal');
end
The adress to the system to ignore warnings as divide by zero
warning off MATLAB:divideByZero

% ksi - angle of trunk with vertical axes
% it`s calculated on the basis of coordinates xb and yb of trunk
% by using the line-equation:
%  $y=k*x+d$ , here
%  $k=(yb(2)-yb(1))/(xb(2)-xb(1))$ ;
%  $d=(yb(1)*xb(2)-xb(1)*yb(2))/(xb(2)-xb(1))$ ;
a=sqrt((xb(1)-xb(2))^2+(yb(1)-yb(2))^2); % scale factor
b=1;
c=sqrt((1-xb(2))^2+(yb(2))^2);
alpha=acos((a^2+b^2-c^2)/(2*a*b));
k=(yb(2)-yb(1))/(xb(2)-xb(1)); % define the tangent
d=(yb(1)*xb(2)-xb(1)*yb(2))/(xb(2)-xb(1)); % define the free member
if yb(2)>=yb(1)
ksi=alpha;
else

```

```

ksi=-alpha;
end

% auxiliary vectors for theta and rD (see below their definition)
psi=zeros(n,mN^n);
ralt=ones(n,mN^n);
% psi and ralt have Kantor array's structur !!!

for i=1:1:n
z=1;
for j=1:1:mN^(i-1)
for k=1:1:mN
for m=1:1:mN^(n-i)
psi(i,z)=phi(k); % define psi on the base of phi
ralt(i,z)=rM(k); % define ralt on the base of rM
z=z+1;
end
end
end
end

theta=zeros(n,mN^n); % vector of angles between each branch of fractal and vertical axes
rD=ones(n,mN^n); % lengths of branches
for i=1:1:mN^n
for j=1:1:n
for k=1:1:j
theta(j,i)=theta(j,i)+psi(k,i); % define theta on the base of psi
rD(j,i)=rD(j,i)*ralt(k,i); % define rD on the base of rD
end
end
end
theta=theta+ksi;
% ----Matrix for coordinates-----
A=ones(n+1,mN^n,2);
% initial coordinates
A(1,:,1)=ones(1,mN^n)*xb(2); % x-coordinate
A(1,:,2)=ones(1,mN^n)*yb(2); % y-coordinate
for j=1:1:mN^n
for i=1:1:n
% define following coordinates
A(i+1,j,1)=A(i,j,1)+a*rD(i,j)*cos(theta(i,j));
A(i+1,j,2)=A(i,j,2)+a*rD(i,j)*sin(theta(i,j));
end
end

% By visualisation the method of inverse trace is used
tau=1;
for i=1:mN:mN^n
z=1;
for k=1:1:mN-1
for j=z:1:n-1
line([A(j,i,1),A(j+1,i,1)],[A(j,i,2),A(j+1,i,2)],'LineWidth',3, 'color', 'r');
end
z=z+1;
end
end

```

```

% ----- end branches -----
for i=1:mN^n
line([A(n,i,1),A(n+1,i,1)],[A(n,i,2),A(n+1,i,2)],'LineWidth',3, 'color', 'r');
end
% ----- Trunk -----
line([xb(1),xb(2)],[yb(1),yb(2)],'LineWidth',3, 'color', 'r');
d1 = imread('crackmap3.tif');
figure
image(d1)
axis image
%%
d2 = ~im2bw(d1, 0.5);
%
% i = c(1:230,1:1551, 3);
% bi = (i<80);
figure
imshow(d2);
% imagesc(bi)
% colormap gray
% axis image

%% Dilate
% %togglefig('Dilated Image Segments');
%
% d = imdilate (d2, strel ('disk', 2));
% imshow (d2)
%%
d = bwareaopen (d2,20);
%togglefig('Vessel Segments Exclude Small Length');
imshow (d)
%%
figure
[n,r] = boxcount(d,'slope');
%%
boxcount(d)
figure
boxcount(d)
%%
df = -diff(log(n))./diff(log(r));
disp(['Fractal dimension, Df = ' num2str(mean(df(3:5))) ' +/- ' num2str(std(df(3:5)))]);
%%
subplot (1,3,1), image(imrotate (d1,90)), axis image
subplot (1,3,2), boxcount(d);
subplot (1,3,3), [n,r] = boxcount(d,'slope');

```